

THE FORMATION OF SMOKE IN FLAMES.

Peter Alan Bott.

Doctor of Philosophy.

The University of Aston in Birmingham.

September 1980.

SUMMARY

The setting-up and operation of a quadrupole mass spectrometer for studying the natural ionisation in flames is described. Results are presented for a simple oxygen / hydrogen flame to which two hydrocarbon fuels, ethylene and acetylene were added. The ethylene flame contained forty-two negative flame ion species, whereas the acetylene flame contained thirty-two. These ions are discussed in parallel, due consideration being given to the differences between the flames and to ions formed by the sampling process. In both flames many ions can be attributed to hydrated species of oxygenated parent ions, formed mainly on the sampling nozzle of the apparatus. Some of these hydrated species evidently help to stabilise the parent ion. Ring structures for some of these as a possible explanation of this stabilisation are envisaged. Ions containing C and H only are identified as acetylides and polyacetylides. This formation is favoured in the acetylene flame because more reactions are thermodynamically possible for the formation of the precursor ions C^- , CH^- , C_2^- and C_2H^- .

Peter Alan Bott, Ph.D. Thesis, 1980.

Key words: Flames, Mass Spectrometry, Negative Ions.

CONTENTS.

	Acknowledgement	1.
I	Introduction.	2.
I.1.	Aim of Work.	2.
I.2.	Ionisation in Flames; Positive Ions.	3.
I.3.	Ionisation in Flames; Negative Ions	5.
I.4.	Soot Formation.	16.
I.5..	A Brief Survey of Different Experimental Methods.	21.
I.6.	Theoretical Consideration of Quadrupole Design.	23.
II.	Description of Apparatus and Experimental Procedure.	30.
II.1.	Brief Description of Apparatus.	30.
II.2.	Detailed Description of Apparatus.	32.
II.3.	A Critique of the Experimental Technique.	57.
III.	Results.	64.
III.1.	Results, Introduction.	64.
III.2.	Ethylene, Flame F1.	68.
III.3.	Acetylene, Flame F2.	79.
IV.	Discussion.	88.
IV.1.	Discussion, Introduction.	88.
IV.2.	The Presence of Chlorine in the Ethylene Flame.	93.
IV.3.	The Difference Between the Ion Intensities of the Two Flames.	95.

IV.4.	O_2^- Formation.	97.
IV.5.	Ions Formed by Charge Transfer of Neutrals with O_2^-	103.
IV.6.	Ions Formed from O_2^- by Processes not Involving Charge Transfer.	134.
IV.7.	Other Oxygenated Species Observed in the Flames.	144.
IV.8.	Carbonaceous Species.	147.
IV.9.	Unassigned Ion Profiles.	158.
V.	Conclusions.	164.
VI.	Suggestions for Further Work.	165.
	References.	167.

LIST OF FIGURES.

Figure		Page.
1.	Potential Energy Curves Illustrating the Formation of a Negative Ion From a Diatomic Molecule by Dissociative Resonance Capture.	9.
2.	Potential Energy Curves Illustrating the Formation of a Negative Ion From a Diatomic Molecule by Resonance Capture.	11.
3.	Potential Energy Curves Illustrating the Formation of a Negative Ion From a Diatomic Molecule by Ion-Pair Production.	13.
4.	Electrical Connections to Quadrupole Mass Filter.	24.
5.	Schematic of Apparatus.	31.
6.	Vacuum System.	33.
7.	Burner and Flame Carriage.	35.
8.	Schematic Showing Connections of Gas Lines to the Flowmeters and Burner.	36.
9.	Flow Meter Calibration for Hydrogen at S.T.P.	37.
10.	Flow Meter Calibration for Oxygen at S.T.P.	38.
11.	Flow Meter Calibration for Argon at S.T.P.	39.
12.	Flow Meter Calibration for Ethylene at S.T.P.	40.
13.	Flow Meter Calibration for Acetylene at S.T.P.	41.
14.	Inlet Nozzle.	43.
15.	Schematic of Ion Lens.	47.
16.	Connection of Multiplier for Positive Ion Detection.	50

Figure 17.	Connection of Multiplier for Negative Ion Detection.	51.
18.	Reproduction of a Typical Backing Pressure Recording.	56.
19.	Reproduction of Five Runs for One Ion Profile.	66.
20.	Reconstructed Averaged Ion Profile From Figure 19.	67.
21.	Stick Spectrum of the Negative Ions Found in the Ethylene Flame.	72.
22.	Stick Spectrum of the Negative Ions Found in the Acetylene Flame.	82.
23.	Ion Profiles for 35 a.m.u. and 37 a.m.u. in Flame F1.	94.
24.	Ion Profiles for 32 a.m.u., 50 a.m.u. and 68 a.m.u. in Flame F1.	98.
25.	Ion Profiles for 32 a.m.u. and 50 a.m.u. in Flame F2.	99.
26.	Ion Profiles for 16 a.m.u. and 34 a.m.u.	108.
27.	Ion Profiles for 17 a.m.u., 35 a.m.u., 53 a.m.u., 53 a.m.u. and 71 a.m.u.	110.
28.	Ion Profiles for 32 a.m.u., 51 a.m.u. and 69 a.m.u.	115.
29.	Ion Profiles for 41 a.m.u.	119.
30.	Ion Profiles for 43 a.m.u.	122.
31.	Ion Profiles for 45 a.m.u., 46 a.m.u., and 63 a.m.u. in Flame F1.	125.
32.	Ion Profiles for 45 a.m.u., 46 a.m.u. and 63 a.m.u. in Flame F2.	126.

Figure 33.	Ion Profiles for 66 a.m.u. and 84 a.m.u. in Flame F1.	130.
34.	Ion Profiles for 60 a.m.u., 78 a.m.u. and 96 a,m,u. in Flame F1.	137
35.	Ion Profiles for 60 a.m.u., 78 a.m.u. and 96 a.m.u. in Flame F2	138.
36.	Ion Profiles for 61 a.m.u., 79 a.m.u. and 97 a.m.u. in Flame F1	140.
37.	Ion Profiles for 61 a.m.u., 79 a.m.u. and 97 a,m,u. in Flame F2	141.
38.	Ion Profiles for 76 a.m.u. and 94 a.m.u.	143.
39.	Ion Profiles for 87 a.m.u. and 105 a.m.u.	146.
40.	Ion Profiles for 24 a.m.u., 25 a.m.u., 36 a.m.u., 49 a.m.u., 60 a.m.u. and 61 a.m.u. in Flame F1.	154.
41.	Ion Profiles for 72 a.m.u., 73 a.m.u., 84 a.m.u., 85 a.m.u., 96 a.m.u. and 97 a.m.u. in Flame F1.	155.
42.	Ion Profiles for 24 a.m.u., 25 a.m.u., 36 a.m.u., 37 a.m.u. and 73 a.m.u. in Flame F2.	156.
43.	Ion Profiles for 60 a.m.u., 61 a.m.u., 96 a.m.u. and 97 a.m.u. in Flame F2	157.
44.	Ion Profiles for 64 a.m.u.	161.
45.	Ion Profiles for 73 a.m.u., 74 a.m.u., 75 a.m.u. and 91 a.m.u. in Flame F2.	162.
46.	Ion Profiles for 90 a.m.u. and 92 a.m.u.	163.

LIST OF TABLES.

Table		Page.
1.	Intensities and Positions of Negative Ions Observed in the Flame with Ethylene as Additive.	70.
2.	Experimental Data for the Ion Profiles in the Ethylene Flame.	78.
3.	Intensities and Positions of Negative Ions Observed in the Flame with Acetylene as Additive.	81.
4.	Experimental Data for the Ion Profiles in the Acetylene Flame.	87.
5.	Assignment of Ions in the Ethylene Flame.	90.
6.	Assignment of Ions in the Acetylene Flame.	92.
7.	Modes of Formation of Negative Flame Ions with O_2^- as the Primary Ion.	102.
8.	Electron Affinities and Heats of Formation of Possible Flame Neutrals.	132.
9.	Proton Affinities of Negative Flame Ions in Order of Decreasing Base Strength.	133.

ACKNOWLEDGEMENT.

I would like to thank Professor F.M. Page and the staff of the Chemistry Department, The University of Aston in Birmingham for their help and encouragement; Thornton Research Centre, Shell Ltd., Ellesmere Port, Cheshire for the mass spectrometer; A.E.I. Ltd., Barton Dock Estate, Manchester for the loan of the rotary pump; the Physics Department at Aston for help with the electronic circuitry and vacuum system; finally British Gas for a research studentship.

I. INTRODUCTION.

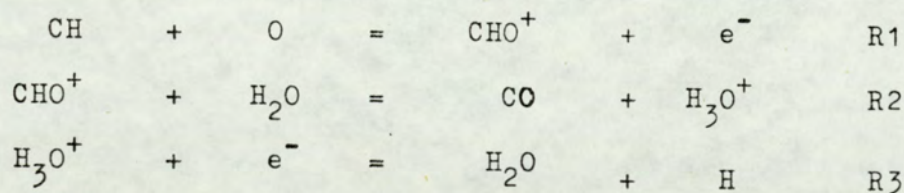
I.1. AIM OF WORK.

The major part of the experimental work was to rebuild and set up an existing flame ionisation mass spectrometer, with due consideration to some of the more recent developments. The main differences and improvements will be discussed.

The second part was to obtain results for a simple hydrogen/oxygen flame, using argon as a diluent containing small measurable quantities of a hydrocarbon fuel. Since most of the preceding work has been confined to positive ions, the experiments were largely devoted to the study of negative ions, and in particular, to quantifying a complete mass spectrum and obtaining ion profiles of each particular ion. These ion profiles will be discussed in an attempt to provide more detailed information about the formation of reactive intermediates in the flame, with due consideration to the results of previous workers in this field.

I.2. IONISATION IN FLAMES; POSITIVE IONS.

The past twenty-five years has seen an enormous amount of work on ionisation in flames. Eltenton in 1947 (1) showed that several radical intermediates were formed in the reaction zones of low pressure flames. Furthermore, different radicals formed at different places in the reaction zone. This method employed a mass spectrometer with its own ionisation source, thus only radicals, rather than flame ions formed in the flame could be discussed. Mass spectrometers which analysed the natural ionisation in flames were developed, notably by three separate groups, Calcote (2), Deckers and van Tiggelen (3), and Sugden and co-workers (4). All the instruments sampled ionised gas directly, the essential difference being the pressures at which the flames were burnt. From these studies many ions were found to form in flames, none however being negative. Both Calcote and Sugden suggested the same primary ionisation reaction and this is generally accepted as the principal mechanism for the production of ions:-



The primary ion, CHO^+ , is formed early in the reaction zone and will undergo proton transfer reactions with those neutral species having a proton affinity higher than CO. Subsequent proton transfer reactions will favour neutrals of

increasing proton affinity. Many reactions of this type have been measured at 300K, and are generally known to be fast ($k \approx 10^{-9} \text{cm}^3 \text{molecule}^{-1} \text{sec}^{-1}$) (5). In general, the ions that have been observed in flames are consistent with a reaction scheme which is dominated by proton transfer processes (6).

1.3. IONISATION IN FLAMES; NEGATIVE IONS.

The high electrical conductivity of the reaction zones of hydrocarbon flames, and its association with free electrons in amounts of the order of 10^{12} cm^{-3} , has been known for many years (7). Up until 1964, negative ions had not been found in pure hydrocarbon flames; the positive ion chemistry was explained without recourse to atomic or molecular negative ions. A wide variety of negative ions had been observed in seeded flames containing alkali halides, but only well downstream of the flame front (8). These ions are probably due to direct electron attachment processes in the cool equilibrated combustion products.

Miller and Fontijn (9) detected measurable quantities of several ions when studying the reactions of atomic oxygen and acetylene in a low pressure flow tube. The ions were found mainly in the region surrounding the reaction zone, suggesting that they are formed predominantly by attachment processes. Miller and Calcote (10) studied a low pressure flame, (1 to 10 mbar) mass spectrometrically and found several ions. The most intense peak, (O^-) was two orders of magnitude smaller than the largest observed positive ion peak, (H_3O^+), and the ions all peaked at a position further downstream in the reaction zone. A possible anomaly in much flame chemistry work is the position of the flame front, and hence the reaction zone; from this the various discussions about where the ions peak are derived. In this work, the method of Bohme et al (6) has been adopted; this will be discussed later.

Negative ions are not as stable as positive ions, and this may be shown by consideration of the forces encountered on a species containing an extra electron. In a neutral atom or positive ion the valence electron moves in an attractive coulombic field modified by the charge distribution of the other electrons at small radii. For negative ions there is an extra electron, and the force exerted on this electron by the parent neutral is different in character, being short range and non-coulombic. The approximate calculations on the hydrogen atom, performed by Massey illustrate this point (11).

Neglecting polarization effects, the probability that the atomic electron of hydrogen is found at a distance between r and dr from the nucleus is $4\pi r^2 \psi^2 dr$, where ψ is the wave function of the ground state of the hydrogen atom. The potential energy, $V(r_1)$, due to the atomic electron at point r_1 from the nucleus is given by:-

$$V(r_1) = \frac{4\pi e^2}{r_1} \int_0^{r_1} \psi^2 r^2 dr + 4\pi e^2 \int_{r_1}^{\infty} \frac{\psi^2 r^2 dr}{r} \quad E1$$

where e is the electronic charge. The first term on the right hand side arises from the charge within the radius r_1 , and the second term from the remainder outside r_1 . The wave function ψ , is given by:-

$$\psi = (\pi a_0^3)^{-\frac{1}{2}} \exp(-r/a_0) \quad E2$$

a_0 is written for $h^2/4\pi e^2 \mu$, where h is Planck's constant, and μ is the reduced mass of the electron-proton system.

Integration of this expression and inclusion of the term $-e^2/r_1$ which arises from the interaction of the extra electron with the hydrogen nucleus, results in the potential energy at r_1 becoming $V(r_1)$, where

$$V(r_1) = -e^2(1/r_1 + 1/a_0) \exp(-2r_1) \quad E3$$

This gives a field of force decreasing exponentially with distance and not as the inverse square of the distance as the coulombic field does. By including the effects of polarisation this force may be altered to one falling off as the inverse fifth power of the distance, but this is still decidedly short range.

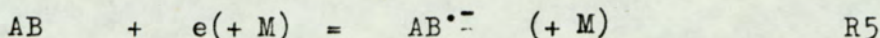
These short range forces differ from coulombic forces in their properties and, in particular, they give rise to only a finite number of stationary states. This result when combined with the Pauli exclusion principle, makes it possible to understand the behaviour of different atoms to electron attachment. In the hydrogen atom with one electron, for example, no states are forbidden to the extra electron by the Pauli exclusion principle and a stable negative ion can be formed if the effective attractive field is strong enough. For helium, since the one-quantum state is already filled an extra electron can only attach in a two-quantum state. However, since the effective attractive field is unlikely to be strong enough to give rise to two stationary states, helium would not be expected to form a stable negative ion.

Primary negative ions may be produced by three processes:-

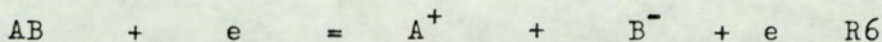
1. Dissociative Resonance Capture:-



2. Resonance Capture, or Three-body Attachment:-



3. Ion pair Production:-



A basic idea of these mechanisms can be obtained by consideration of the transitions between the potential energy curves representing the ground states of the molecule AB and the molecular ion $AB^{\bullet-}$. For a stable state diatomic molecule the potential energy is at a minimum at the equilibrium separation of the nuclei. As the atoms approach each other the potential energy rapidly increases because of the repulsion of the charged nuclei, and when the atoms separate, the potential energy increases due to the work done against the electronic binding within the molecule, although as the nuclear distance increases the potential energy tends to a limiting value representing dissociation of the molecule.

The Franck-Condon principle is used in conjunction with the potential energy curves. This states that in electronic transition, because of the large ratio of nuclear to electronic mass, the time taken for the transition is negligible when compared with the nuclear vibration period and hence the nuclear separation does not change significantly, i.e. in the potential energy diagrams the transition may be represented by a vertical line. In Fig.1. the shaded region is known as the Franck-Condon region and the most probable transition occurs from the centre of the region requiring an energy, E.

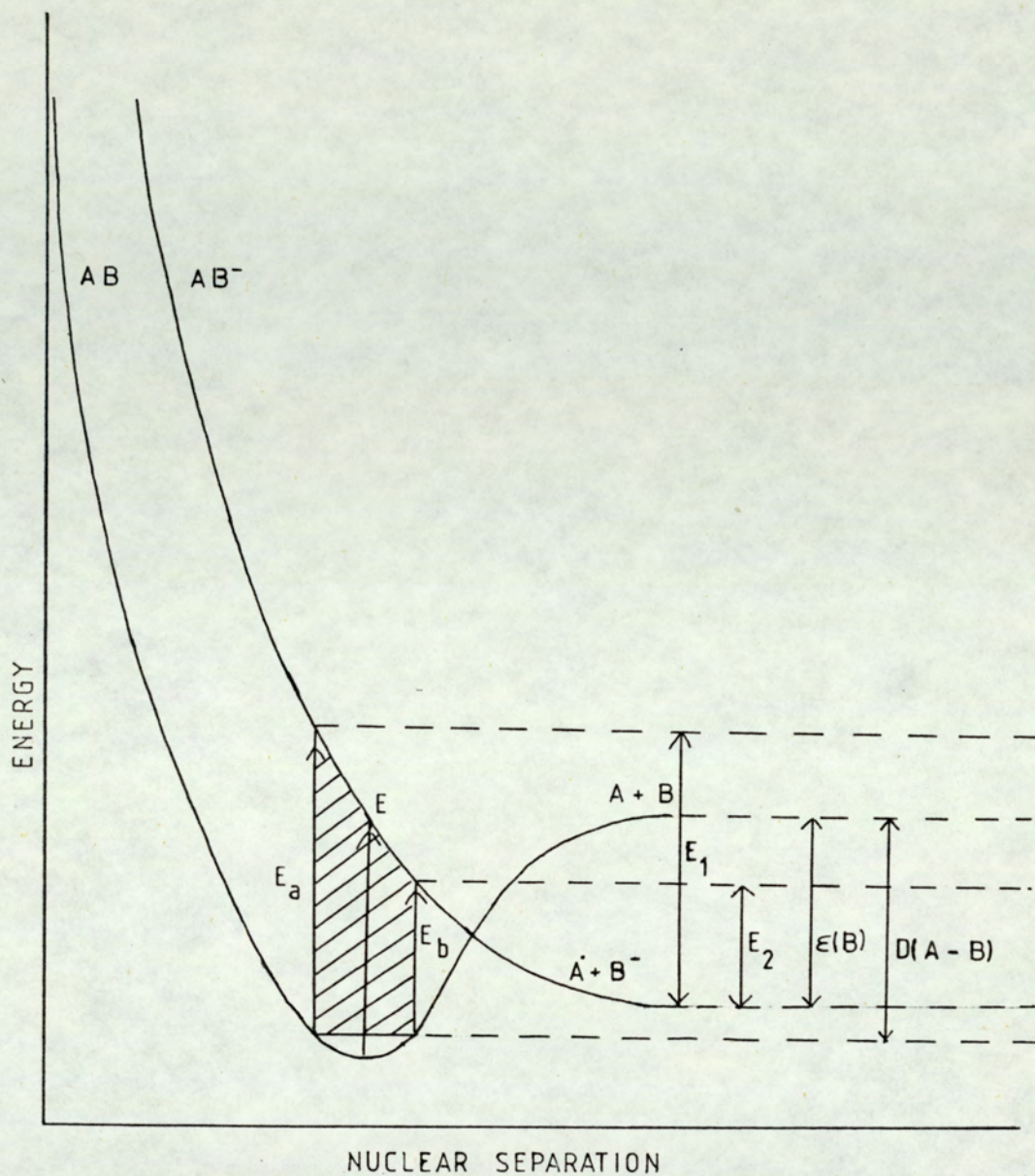


Figure 1. Potential Energy Curves Illustrating the Formation of a Negative Ion From a Diatomic Molecule by Dissociative Resonance Capture.

AB^- represents the negative ion, which is formed in an unstable excited state shown by the upper repulsive curve. The ion has an energy greater than at infinite nuclear separation and breaks up into a radical, A^\cdot and a negative ion, B^- . Electron capture occurs in the limited range of the electron energies, E_a to E_b , and the resulting radical and negative ion possess kinetic energy totalling between E_1 and E_2 and distributed between them, according to the principles of momentum conservation, as

$$\frac{KE(A^\cdot)}{KE(B^-)} = \frac{M(B^-)}{M(A^\cdot)} \quad E4$$

where KE represents kinetic energy, and $M(A^\cdot)$ and $M(B^-)$ are the masses of A^\cdot and B^- .

The appearance potential, $P(B^-)$ of the negative ion, i.e. the energy at which the ion first appears in the mass spectrum is given by:-

$$P(B^-) = D(A-B) - \epsilon(B) + \sum W \quad E5$$

where $D(A-B)$ is the dissociation energy of AB^\cdot , $\epsilon(B)$ the electron affinity of atom B, and $\sum W$ is the total kinetic and electronic excitation energies of the species A^\cdot and B^- .

This is a dissociative resonance capture process, and usually occurs for electron energies up to 15 eV.

In Fig.2. some of the possible states of the ion AB^- have an energy less than that at infinite separation.

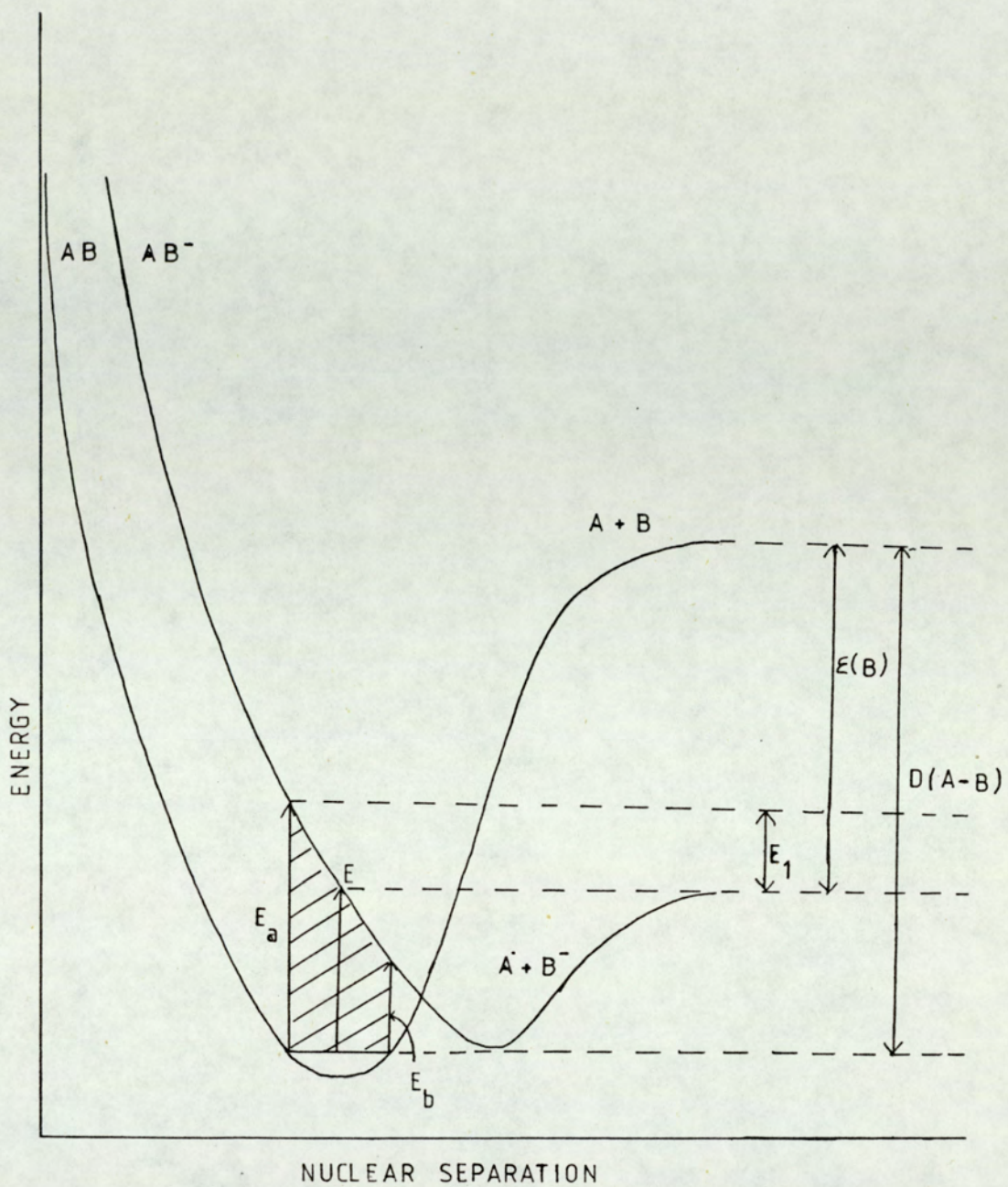


Figure 2. Potential Energy Curves Illustrating the Formation of a Negative Ion From a Diatomic Molecule by Resonance Capture.

Dissociation will only occur if the electron energy is greater than E and the kinetic energy to be shared between the two species is between 0 and E_1 . If the electron is captured and the resulting transition has an energy between E_b and E , then a vibrationally excited ion $(AB^-)^*$ is formed. This excited ion may release the captured electron and return to its neutral state by the reverse process, or it may be stabilised as AB^- by losing its energy as radiation or collision with a third body.

The appearance potential is given by:-

$$P(AB^-) = \Sigma W - \xi(AB) \quad E6$$

where ΣW is the excitation energy of AB , and $\xi(AB)$ is the electron affinity. Negative ions formed by resonance capture usually appear at low potentials ($\approx 0eV$), but at higher pressures in the presence of a third body it may be an important process.

Ion-pair production is shown in Fig.3. The molecule AB after suffering electron impact makes an electronic transition into a state which dissociates to give a positive ion and a negative ion, $(A^+$ and $B^-)$, either of which may be in an excited or ground state. The electron is not captured but acts as a source of energy. This mechanism can occur over a wide range of electron energies. The kinetic energy to be shared lies in the region E_1 to E_2 and the appearance potential $P(B^-)$ of the ion B^- is such that

$$P(B^-) = P(A^+) = D(A-B) + I(A) - \xi(B^*) + \Sigma W \quad E7$$

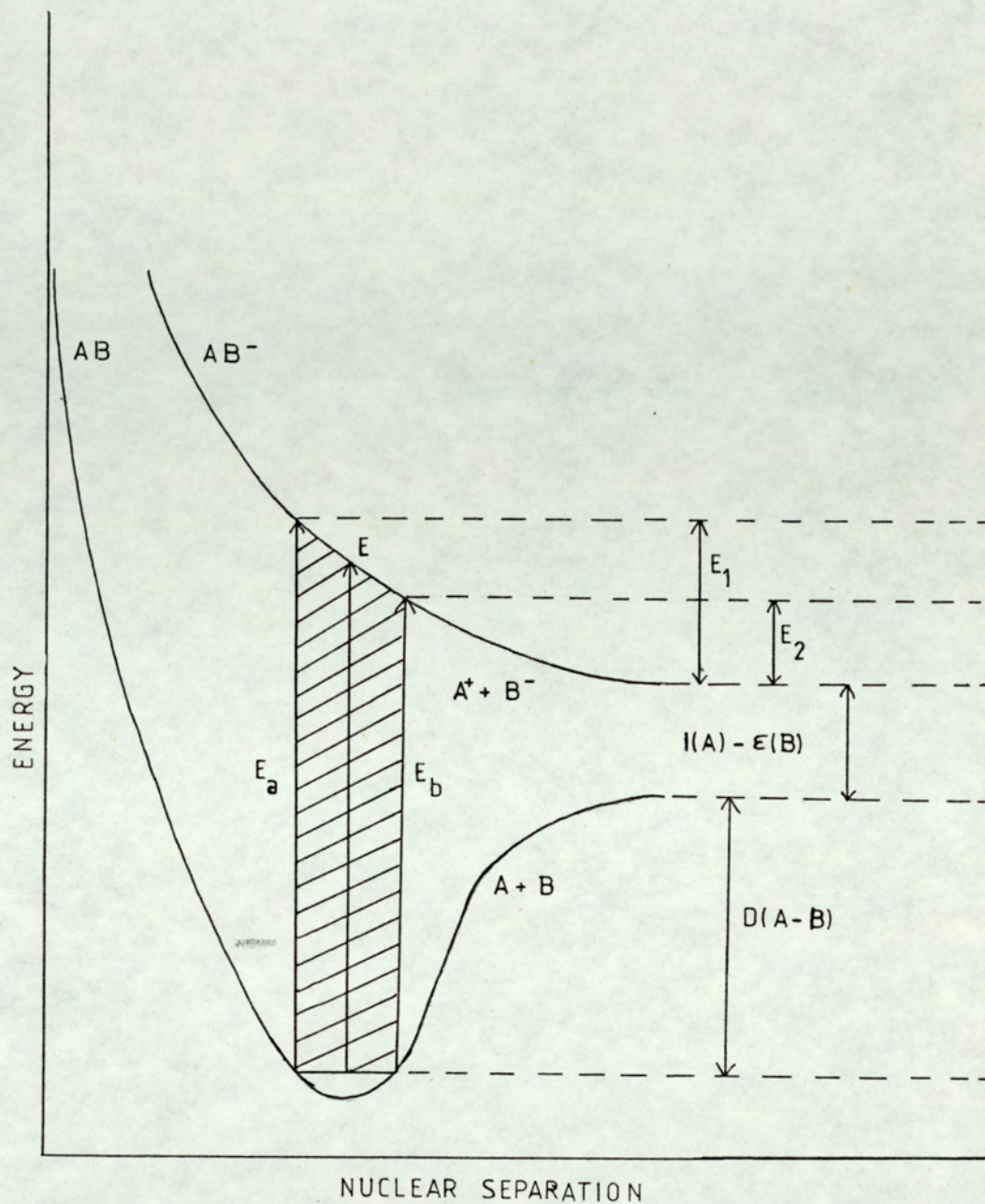


Figure 3. Potential Energy Curves Illustrating the Formation of a Negative Ion From a Diatomic Molecule by Ion-Pair Production.

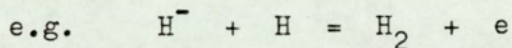
where $I(A)$ is the ionization potential of the atom A.

Due to the participation of the $I(A)$ term, the appearance potential of this process usually occurs at energies above 10eV.

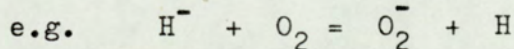
This picture is approximately applicable to polyatomic molecules in which only one bond is broken by electron impact. Although for negative atomic ions, the force exerted on the extra electron by the parent neutral is short range and gives rise only to a finite number of stationary states, and so makes it improbable that any excited electronic states exist, this is not the case for molecules. There may be a number of electronic states for the molecular ion which do not autoionize rapidly and each of these states has the same assembly of vibrational and rotational levels found in the neutral molecule.

It has been suggested that the negative ion chemistry of flames originates with O_2^- ions formed early in the reaction zone, but it is complicated by the fact that several types of reaction are possible (6). These can be listed:-

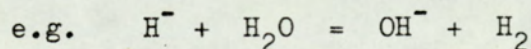
1. Associative detachment.



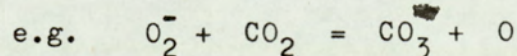
2. Charge transfer.



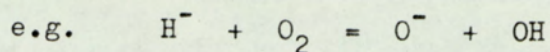
3. Atom transfer.



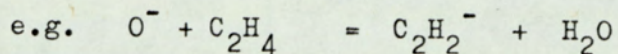
4. Transfer of negative atomic ions.



5. Transfer of positive atomic ions.



6. Displacement and rearrangement reactions.

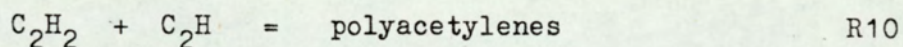


Charge transfer of electrons will favour neutrals of increasing electron affinity. Proton transfer reactions are possible for negative ions which have sufficiently high base strength to abstract protons from neutral 'acids'. A negative ion is energetically capable of proton removal from the neutral whose corresponding negative ion has a lower proton affinity. Some ions may undergo three-body association reactions to form cluster ions. This may be the case for some of the heavier ions observed in flames. In some instances cluster ions may undergo fast switching reactions such that the neutral clustered to the ion is replaced by a different neutral. Since all of these reactions are fast, it may not be possible to detect every single ion formed, even with the most sensitive equipment.

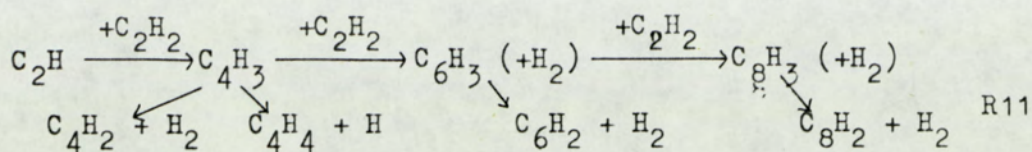
I.4. SOOT FORMATION.

A study of the constituents of soot shows that many species are present (12). In the burnt gas region of fuel rich flames many higher hydrocarbons can be detected, these being attributable to polyacetylenes and aromatic species containing several aromatic rings (13). These aromatic species then dehydrogenate to give graphitic carbon structures as the final step of soot formation. Soot particles have a compact structure, their density being 2.0 g cm^{-3} , which is 10% less than that of three dimensionally ordered graphite (14).

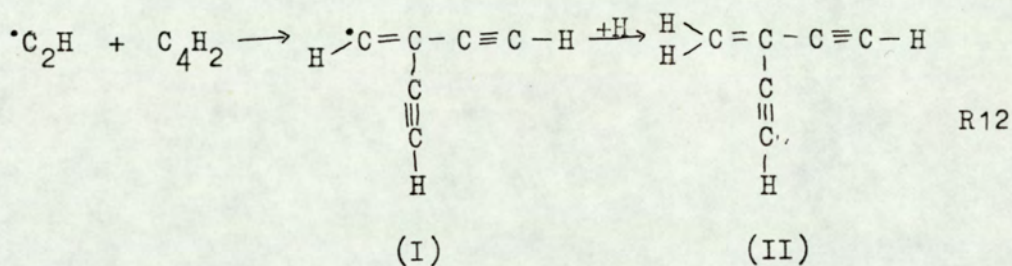
The process of soot formation is not well enough known to allow a complete reaction mechanism. However, Homann (15) has attempted to interpret the course of soot formation in premixed flames of lower hydrocarbons. In the upstream, cooler part of the reaction zone, free radicals lead to hydrocarbons containing more carbon atoms than the starting fuel, e.g.:-



Acetylenes and the polyacetylenes predominate in the hotter, central region of the reaction zone. Polyacetylenes reach a maximum concentration when the oxygen supply has been consumed: at the downstream end of the reaction zone. They are probably formed by free radical reactions:-



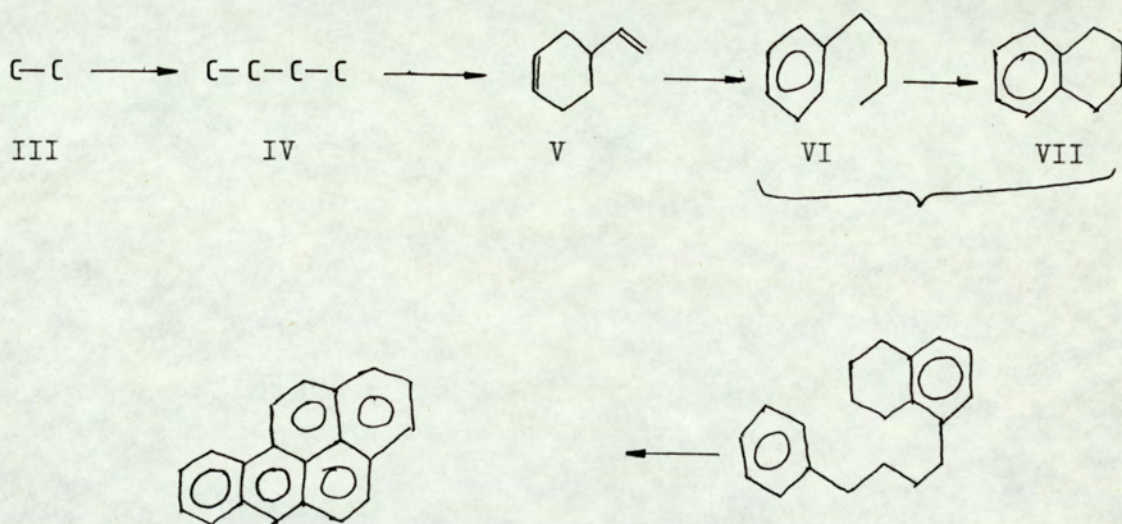
This mechanism for polyacetylene formation is sufficiently fast only in the reaction zone, which is rich in free radicals. Continuing growth of polyacetylenes does not lead directly to soot particles, since these are by no means enormous chain molecules. When C_2H or other hydrocarbon radicals attack a polyacetylene, the probability of attack at other positions apart from the end carbon increases with increasing chain length. However, addition of this type leads either to cleavage or a larger molecule, which will not be a polyacetylene, since these cannot be branched, e.g.:-



The radical, (I), can attain stability at lower temperatures by formation of (II), but at flame temperatures, it would be highly unstable. Therefore it is probable that a radical such as (I) may add on further acetylene and polyacetylenes without loss of its free radical character. The products of these additions are branched radicals, which may then undergo cyclisation to form five-membered and six-membered rings.

Furthermore, this leads to the formation of comparatively hydrogen-rich hydrocarbons with side chains of up to 500 atomic mass units. These species probably retain their free radical nature at flame temperatures (16) and add on further polyacetylenes and combine with each other. As these soot particles grow the free-radical nature and hydrogen content decrease, partly due to the fact that more reactive higher polyacetylenes add more readily as the free radical nature decreases.

Badger et al (17) have postulated a step-wise synthesis for the formation of benz(a)pyrene from an initial two-carbon species:-



Compound (IV) is likely to be diacetylene or vinylacetylene; 1,3-butadiene is unlikely since this is characteristically absent in the products of acetylene pyrolysis. However, some compounds are formed, such as pyrene and phenanthrene which are relatively inert (18). These are regarded as by-products rather than reactive intermediates since, unlike the majority of

the reactive polycyclic compounds, they continue to form in the burnt gases; their concentrations rise whilst the rate of soot formation declines. It is thus possible that they are formed by heterogeneous reactions on the surface of soot particles and evaporate off because of their relatively high vapour pressures.

It has been suggested (19) that a series of stepwise free radical reactions occur involving chain lengthening of acetylene, followed by cyclisation to some apparently primary monocyclic species which may in part, be stabilised by the formation of intermediates such as phenylacetylene, styrene and indene. As can be seen, the mechanism of soot formation is by no means fully understood.

The formation of soot particles is limited by nucleation. Nuclei may be of two types, either complex unsaturated polymeric molecules or simple radicals (20). The properties of the primary nucleus define the process of its further growth and the properties of the resultant soot. The 'molecular nucleus' is obtained as a result of condensation, aromatization and dehydrogenation reactions. The final product will be a particle having no uniformity, being X-ray amorphous, and containing many volatiles.

A 'radical nucleus' initiates a different set of processes to produce soot particles that are compact and regular. The first stage of the process should involve the conversion of the radical nucleus into a nucleus having a physical surface. This formation is most difficult to investigate but may be visualised to a certain extent. As mentioned above, heavier and less active

radicals are formed, and the propagation rate will slow down. At a certain stage the radical nucleus will lose its radical properties, attain the properties of a physical surface, and become a soot particle of minimum size.

The chain-type scheme of nucleation and growth of soot is not strictly proved. The scheme does not take into account the coagulation of the growing particles which actually takes place and results at late stages of particle formation in the chain-like structure.

1.5. A BRIEF SURVEY OF DIFFERENT EXPERIMENTAL METHODS.

The principal methods of detection and concentration measurement for reactive species in flames utilize optical or mass spectrometry. Optical methods include visible, ultra-violet, infra-red and microwave spectroscopy, and laser scattering techniques.

For the study of flame species, the selection of either an optical or mass spectrometric technique is influenced by a comparison of general capabilities. Optical spectroscopy will detect most atoms and diatomic species, whereas mass spectrometry will detect species including polyatomics. Radical detection is limited to OH by direct means by optical methods but all radicals can be detected using a mass spectrometer. Although spatial resolution is better using mass spectrometry, the necessity for probe sampling affects the flame, and secondary reactions may occur which may be difficult to distinguish from pure flame reactions.

Mass spectrometric studies may be divided into two classes: natural ionisation, and secondary ionisation before mass analysis. In the first case the mass spectrometer has no source for ion production, the naturally produced flame ions being collimated and directly focussed into the analyser region of the mass spectrometer. The method of electron impact, (E.I.) at the entrance of the mass spectrometer is useful, since it enables molecular beams to be used, derived from a skimmer electrode behind the sampling probe. This technique produces a better collimated beam (and thus improved resolution and reproducibility)

but it is more difficult to distinguish between the ions which occur naturally in the flame, and those which arise from ionisation of neutrals by the ionising source. Also, unless a low ionising potential is used, spurious ions and fragmentation ions will result.

All types of mass spectrometer have been used for flame studies. Nowadays however, the commonest type is the quadrupole mass filter. Although electronically this is more difficult to design and operate, it can be used in vacuum systems of higher pressure than in conventional mass spectrometers. Also, the ion energies of species entering the quadrupole do not have to be so well defined, thus the path length can be much shorter, (typically 5 - 10 cm from probe to filter) and the focusing lens does not have to be so complex and voltages are much lower.

Flames are usually studied either at atmospheric pressure or at reduced pressure (1 - 20 mbar). The advantage of atmospheric pressure flames is that the vacuum system is fairly simple, but the reaction zone is very small and the measurements of ions may be difficult in this small zone. Flames of lower pressure have longer reaction zones, so that they can be characterized better, but the problems of fabrication of the vacuum system and alignment and movement of the burner makes this method rather complicated. In this work a quadrupole mass filter has been used to study atmospheric pressure flames.

I.6. THEORETICAL CONSIDERATIONS OF QUADRUPOLE DESIGN.

The quadrupole mass filter is ideally constructed of four electrically conducting hyperbolic cylindrical surfaces described by the equation:-

$$x^2 - y^2 = \pm C \quad \text{E8}$$

where C is a constant. Opposite electrodes of the filter are connected together, (Fig.4.) and to one pair is applied a potential

$$\phi(t) = U + V \cos(2\pi ft) \quad \text{E9}$$

where U is a d.c. voltage, V is the peak amplitude of a radiofrequency voltage of frequency f, and t is the time. To the other pair of electrodes is applied the same potential, but of opposite sign. Under these circumstances, the equipotential surfaces are symmetric hyperbolic cylinders, and the potential on the z-axis is zero. In the x-direction, the ions have natural oscillation frequencies close to the hyperbolic surface which are considerably lower than the applied frequency, but highest for the lighter ions. The forced oscillation reaches a maximum amplitude which is higher the lighter the ion, and hence light ions tend to strike the positive rods and be lost. On the y-axis, the behaviour is more complicated, but whilst the d.c. field tends to drive the ions out, the r.f. field tends to focus them in. The focusing ^S_λ

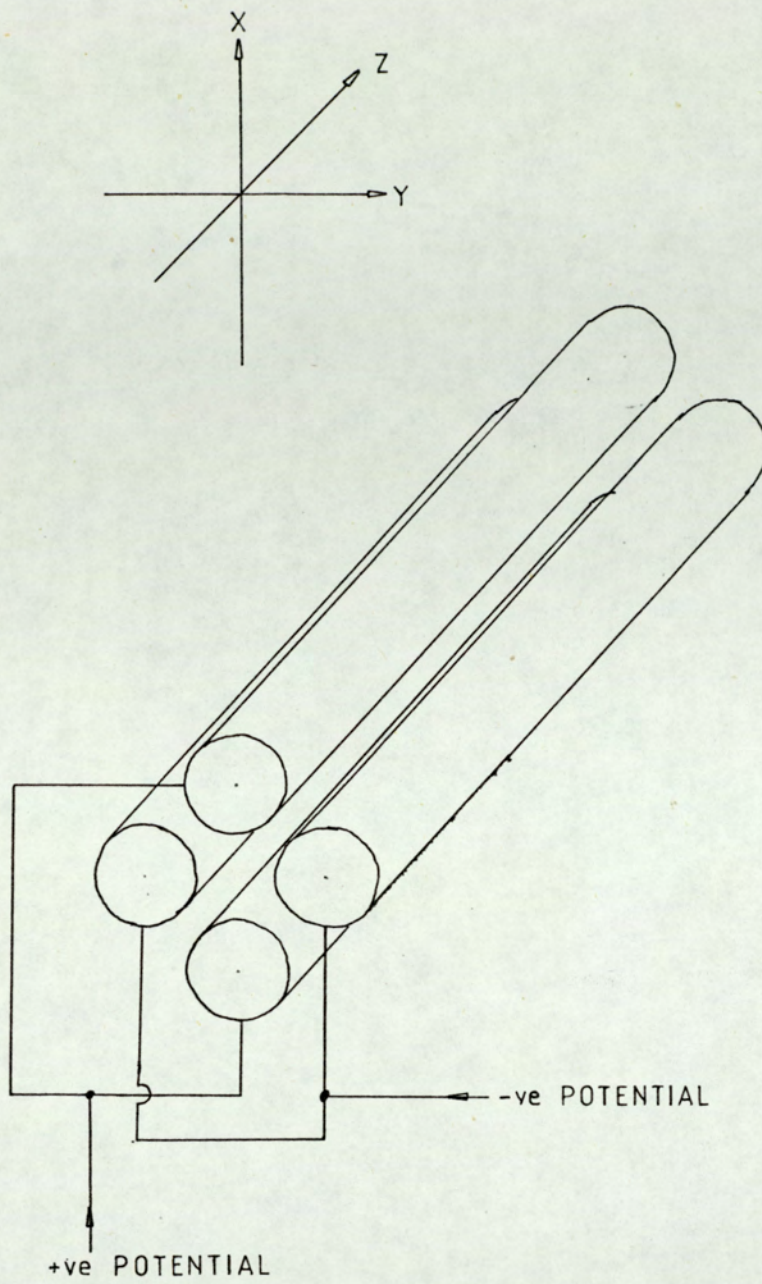


Figure 4. Electrical Connections to Quadrupole Mass Filter.

is more effective the lighter the ion, so that on this axis the heavy ions tend to be lost. Therefore it can be arranged so that the two conditions of stability stand with only a narrow gap between, through which only ions of the desired mass can have some chance of passing. The differential equations of motion in the x-y plane are Mathieu equations (21) the solutions for which depend on the value of m/e of the ion. With proper selection of U and V, ions of a given m/e will have stable trajectories, i.e. the ions will oscillate about the z-axis and ultimately emerge from the other end of the assembly.

The mass resolution of a quadrupole mass filter is given by:-

$$\frac{m}{\Delta m} = \frac{0.126}{0.16784 - U/V} \quad \text{E10}$$

By making $U/V = 0.16784$, a theoretical infinite resolution may be obtained. The resolution can be changed by varying the ratio U/V . For infinite resolution the values of U and V are given by

$$U(\text{volts}) = 1.212mf^2r_0^2 \quad \text{E11}$$

$$V(\text{volts}) = 7.219mf^2r_0^2 \quad \text{E12}$$

where m is the mass in a.m.u., f is the r.f. frequency in MHz, and r_0 is the radius of the circle which is tangential to the four hyperbolic electrodes.

For mass separation to occur, any ion of the incorrect m/e must remain in the transverse fields long enough so that it

will be rejected, and this requires that a maximum axial ion energy exists for a filter of length, L. The approximate relationship is that

$$E_{\text{ion}} < \frac{1}{25} f^2 L^2 \left(\frac{\Delta m}{m}\right) \cdot m \quad \text{E13}$$

E_{ion} is the longitudinal ion energy in eV.

In a real situation, the ions are injected into the system off-axis or with a transverse velocity component, and the position becomes more complicated. Although the mass sensitivity of the filter does not change, the transmission becomes a function of the resolution. The maximum distance of an ion's trajectory from the axis depends on its initial position and transverse energy, as the resolution is increased. If the maximum distance from the axis becomes too large, the ions will strike the electrodes and be removed, even though its m/e value is correct for transmission. For ions injected parallel to the axis, the maximum entrance aperture to ensure that none of the ions will strike the electrodes is given by:-

$$a \approx \frac{2r_0}{3} \left(\frac{\Delta m}{m}\right)^{\frac{1}{2}} \quad \text{E14}$$

where a is the radius of the aperture. Similarly, the maximum transverse energy, E_t , that an ion injected on the axis can have if its transmission is to be ensured is given by:-

$$E_t \approx \frac{1}{2} m f^2 r_0^2 \frac{2\Delta m}{m} \quad \text{E15}$$

Thus as the resolution is increased, i.e. $\Delta m/m$ decreased the transmission will diminish until finally only the ions that are injected exactly on axis and travelling parallel to it will emerge from the mass filter.

From equations E11 and E12, the mass variation to be transmitted can be accomplished through the variation of U and V, or the variation of f. Equation E10 indicates that constant resolution $m/\Delta m$ is maintained if the ratio U/V remains constant. In this system, the frequency, f, is held constant and U and V are varied simultaneously.

If the quadrupole is operated in a constant resolution mode, equation E14 shows that the maximum aperture for entrance of ions is dependant^e of mass, but equation E15 indicates that the maximum transverse energy of ions to be transmitted increases with mass. Thus, in this mode, heavy ions might be transmitted whilst light ions may not be. The mass filter should show a mass-dependant transmission, discriminating against lighter ions.

If Δm were to be held constant (by careful variation of U and V), all ions of a given transverse energy E_t' would be transmitted equally well, (equation E15). However in this resolution mode, equation E14 shows that the maximum radius of injection of ions to be transmitted will diminish with ion mass. Injecting a uniform ion current density, it would be expected that the transmitted ion signal, which would be the product of the current density and the area of acceptance aperture would diminish as the inverse power of the mass. This resolution mode would also give a mass-dependant^e ion transmission but would

discriminate against the high masses.

The resolution mode and the transmission of the filter can be varied by letting:-

$$U = \gamma V - \zeta \quad \text{E16}$$

γ, ζ are constants. Substituting into equation E10

$$\frac{m}{\Delta m} = \frac{0.126}{(0.16784 - \gamma) + \zeta/V} \quad \text{E17}$$

If $\zeta = 0$, the constant $m/\Delta m$ resolution mode is operative. If γ is equal to 0.16784, $m/\Delta m$ becomes proportional to V which is (equation 12) proportional to m , this being the condition for having the constant Δm resolution mode.

To avoid mass discrimination, values of γ and ζ can be found which provide a hybrid resolution mode, but little mass discrimination. Since the operation of the mass filter depends on precise electrical fields along the entire length of the filter, the achievement of good resolution requires both high dimensional precision and stability of the applied voltages. The required dimensional precision is more easily achieved if cylindrical rods instead of hyperbolic rods are used. The fields near the z-axis closely approximate those of the hyperbolic quadrupole, when the radius of the cylindrical rods is 1.6 times that of the inscribed circle. However, the trajectories far off-axis are no longer ideal, and equations E14 and E15 become

complex.

To approximate the ideal hyperbolic fields, the value of r_0 can be increased, and this in turn allows r_1 , the entrance aperture to be larger, hence increasing sensitivity for a given mass resolution. In order to have a mass filter of small length, L , a high frequency is desirable. To achieve the best operating conditions, the prime requirement is that high power be available from the power system.

The power, P , is given by:-

$$P \propto m^2 f^5 r_0^4$$

E18

II. DESCRIPTION OF APPARATUS AND EXPERIMENTAL PROCEDURE.

II.1. BRIEF DESCRIPTION OF APPARATUS.

The apparatus was kindly loaned by Shell Ltd. and has been previously used to study flames and flame additives. Although references ^{ve} have been made to its description (22), none has been complete and a detailed description will be given here. Briefly, the flame was burnt horizontally and sampled through an orifice into a chamber at 6×10^{-4} mbar, where most of the gas was pumped away, Fig.5. The ions were formed into a beam by an electrostatic lens and focused through a 2 mm hole into a second chamber which was maintained at 10^{-7} mbar. The ions were mass selected in a quadrupole mass filter and detected either by a particle multiplier or a Faraday cup. Both positive and negative ions could be detected by reversal of the various voltages on the inlet, ion lens and multiplier.

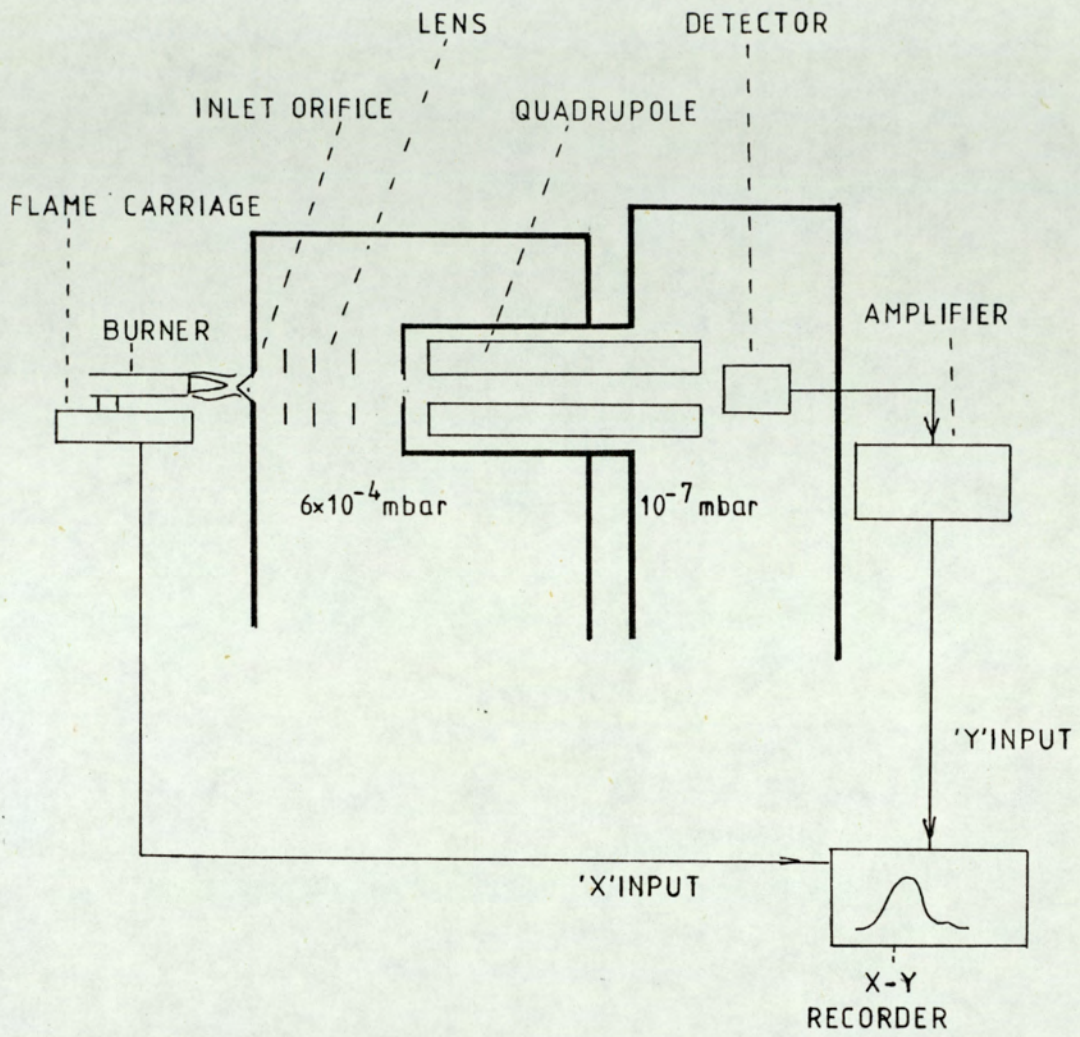


Figure 5. Schematic of Apparatus.

II.2. DETAILED DESCRIPTION OF APPARATUS.

II.2.i Vacuum System.

The vacuum system comprised the two vacuum chambers, their respective oil vapour diffusion pumps, and a single backing pump, (Fig.6.). The chambers were fabricated from austenitic stainless steel, and lead gaskets were used to seal the various flanges. The use of lead seals precluded any sort of baking to improve the cleanliness and high vacuum of the system. The first chamber, which was 0.3m diameter, and 0.34m high, was maintained at a vacuum of 10^{-4} mbar by a vapour booster pump, (Edwards 9B4) capable of a pumping speed of 3800lsec^{-1} for air. The second vacuum chamber, which was 0.2m diameter and 0.31m high, was maintained at 10^{-7} mbar by a liquid nitrogen trapped (Edwards NTM6A) oil diffusion pump, (Edwards EO6) capable of a pumping speed of 1300lsec^{-1} for air.

The diffusion pumps were connected by sweated joint copper pipeline to a single stage Kinney pump, (GKS47, kindly loaned by AEI Ltd., Manchester) which pumped at $80\text{m}^3\text{hr}^{-1}$ for air. This pump was adequate to back both diffusion pumps, and a pumpdown time (to 10^{-7} mbar in the second chamber) of 30 minutes was achievable.

Pressure measurement was by Pirani gauge (VG PIR1A) for the backing pressure; by Penning gauge (BirVac) for the first vacuum chamber, and by ionisation gauge (VG VIG21) for the second chamber. The output from the Pirani Gauge Control Unit was fed

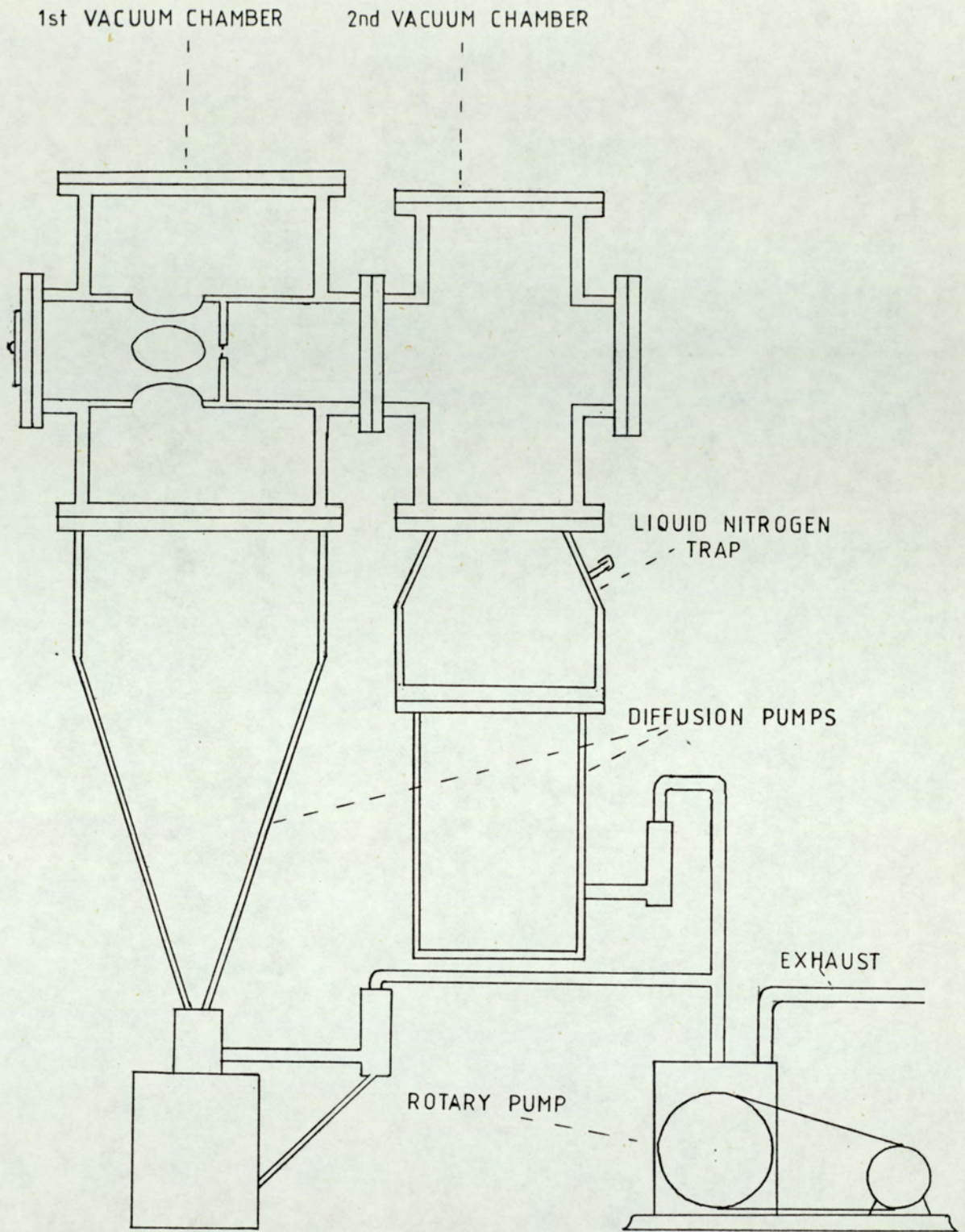


Figure 6. Vacuum System.

into a chart recorder (Honeywell) for pressure monitoring.

II.2.ii Burner, Flame Carriage and Gas Supplies.

The burner was a simple quartz capillary, (i.d. 1.5 mm) surrounded by a glass cylinder, (i.d. 20 mm). This was mounted horizontally onto a screw driven carriage such that the burner could move against the inlet of the first vacuum chamber. To the screw was fitted a series of pulleys such that an a.c. motor could drive the flame carriage. A speed of 1 mm min^{-1} was used for negative ions, and 10 mm min^{-1} for positive ions. On the screw, a gear was fitted, which connected to a ten-turn potentiometer; a voltage applied to this provided the 'x' input signal to an 'x-y' recorder, Fig.7.

The flame was a simple hydrogen/oxygen flame to which argon was added as diluent. A flowing sheath of oxygen and argon surrounded the flame, so that the flame was stabilised, and nitrogen excluded. The exclusion of nitrogen is beneficial, since it greatly simplified the interpretation of the mass spectra. Hydrocarbon fuel (acetylene or ethylene) was added in known quantities up to 10 % by volume. The gases were fed from standard cylinders (BOC) via copper tubing to flow meters, (Meterate). The hydrocarbon gas was fed via seamless mild steel tubing to a flow meter. Copper tubing cannot be used for acetylene because copper acts as a catalyst converting acetylene exothermically to benzene. The gases were premixed after the ~~the~~ flowmeters and then burnt at the burner, Fig.8.

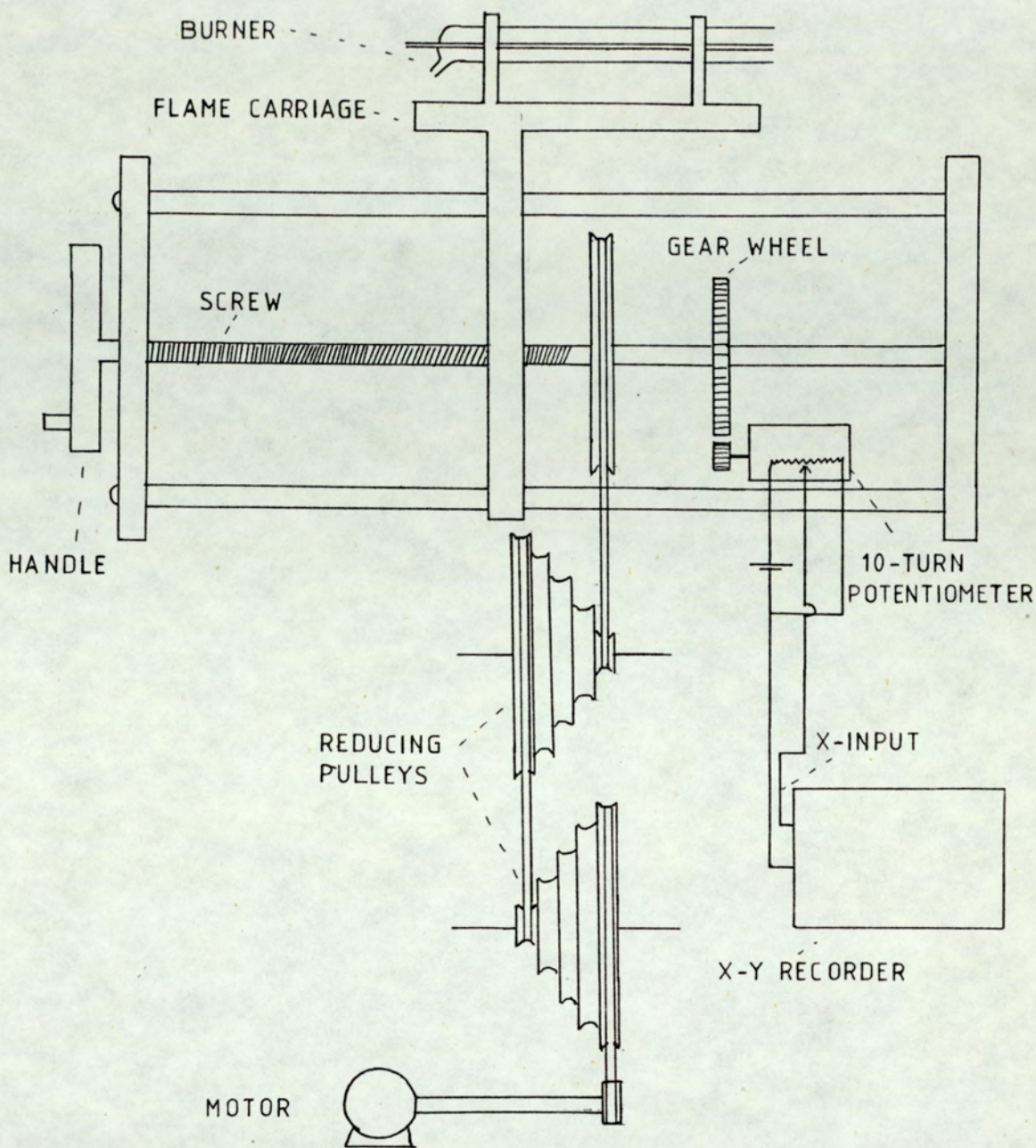


Figure 7. Burner and Flame Carriage.

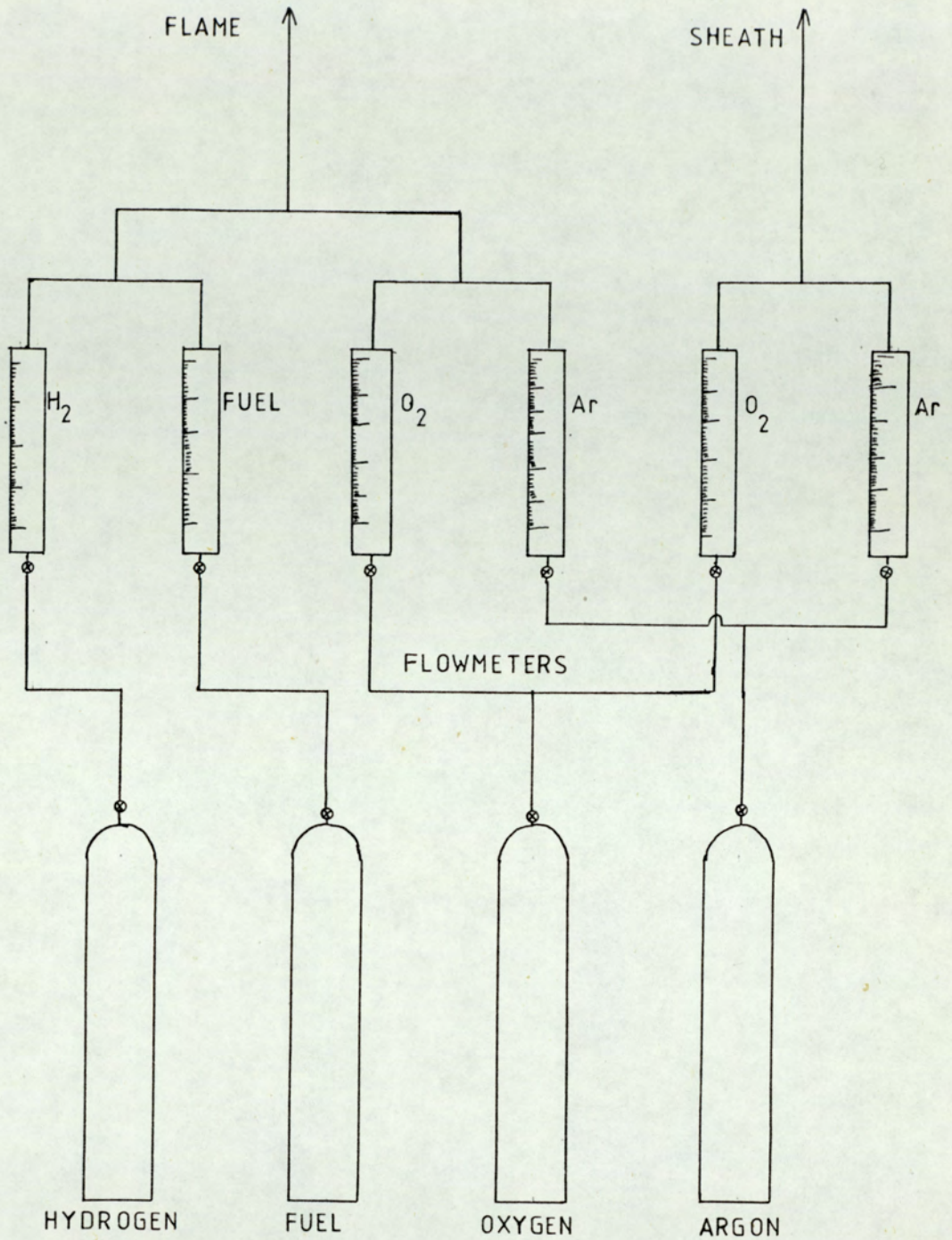


Figure 8. Schematic Showing Connexions of Gas Lines to the Flowmeters and Burner.

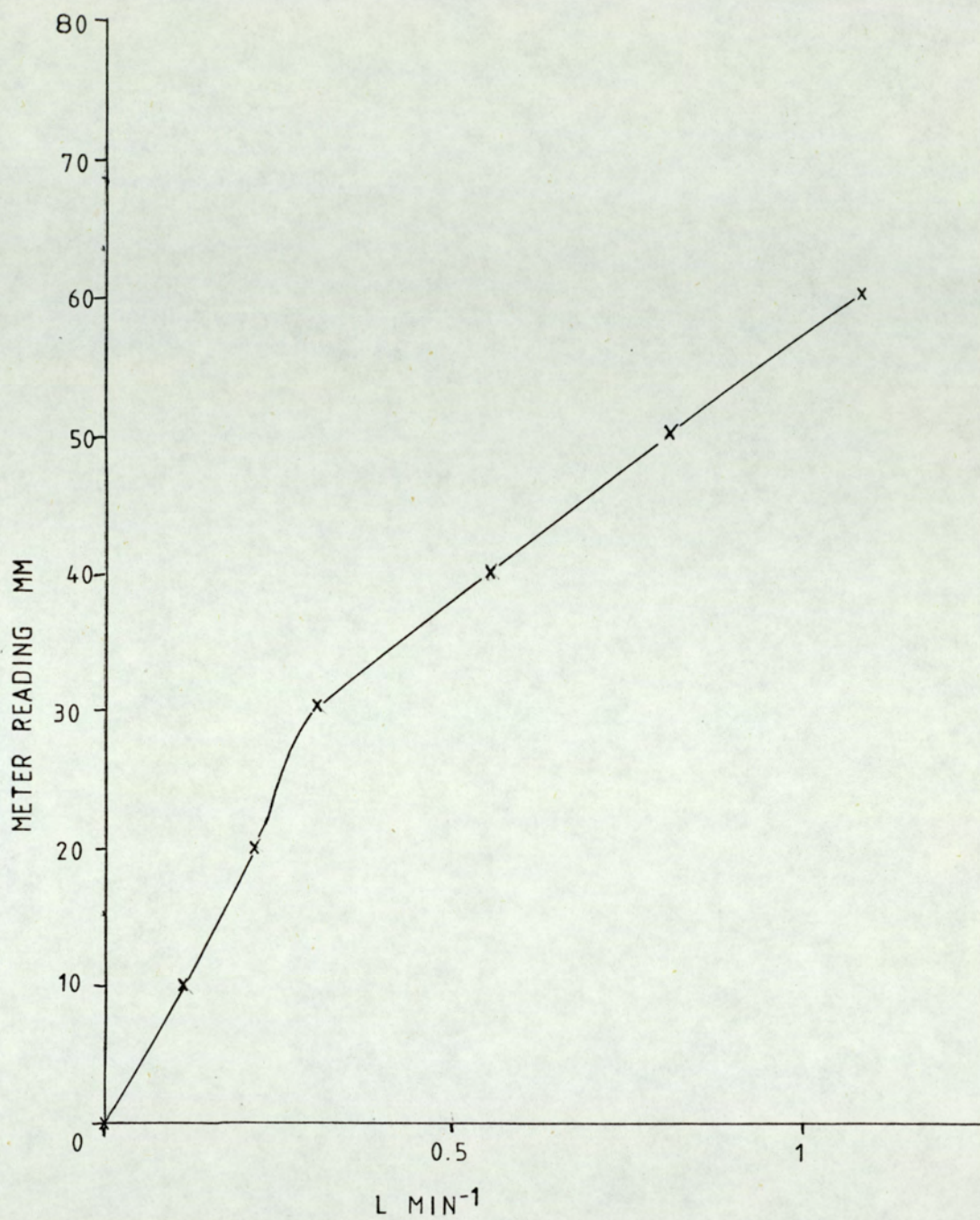


Figure 9. Flow Meter Calibration for Hydrogen at S.T.P.

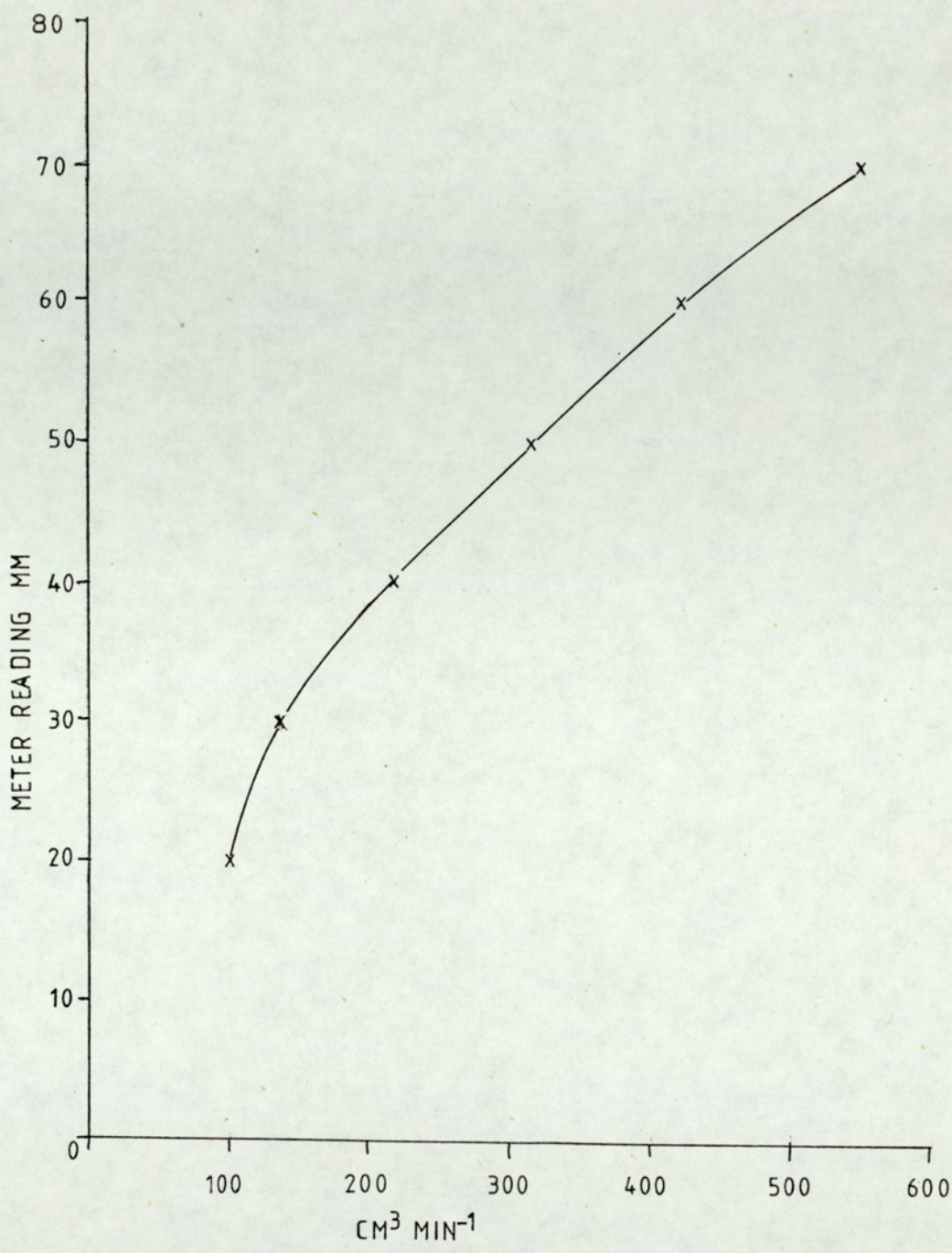


Figure 10. Flow Meter Calibration for Oxygen at S.T.P.

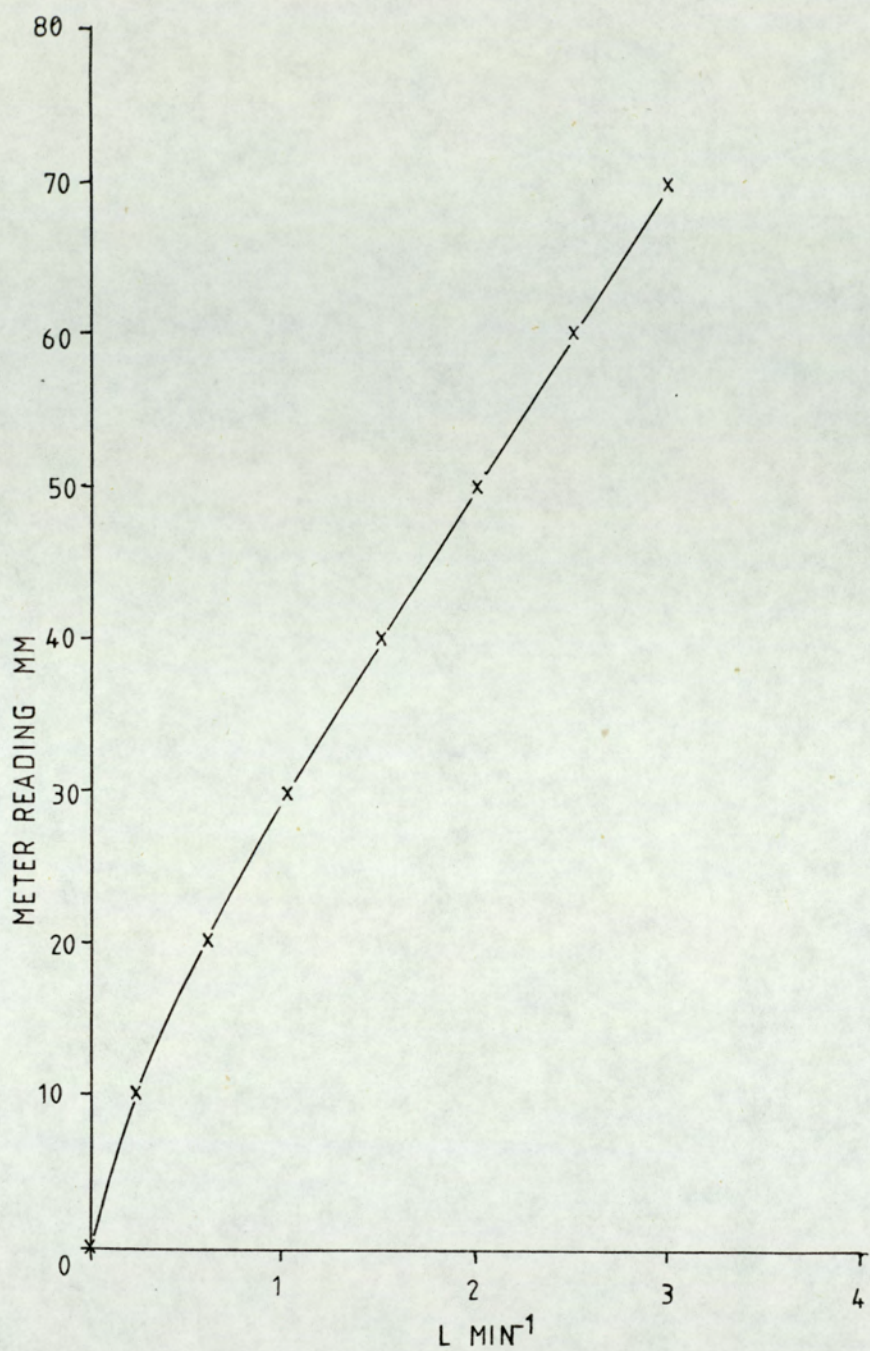


Figure 11. Flow Meter Calibration for Argon at S.T.P.

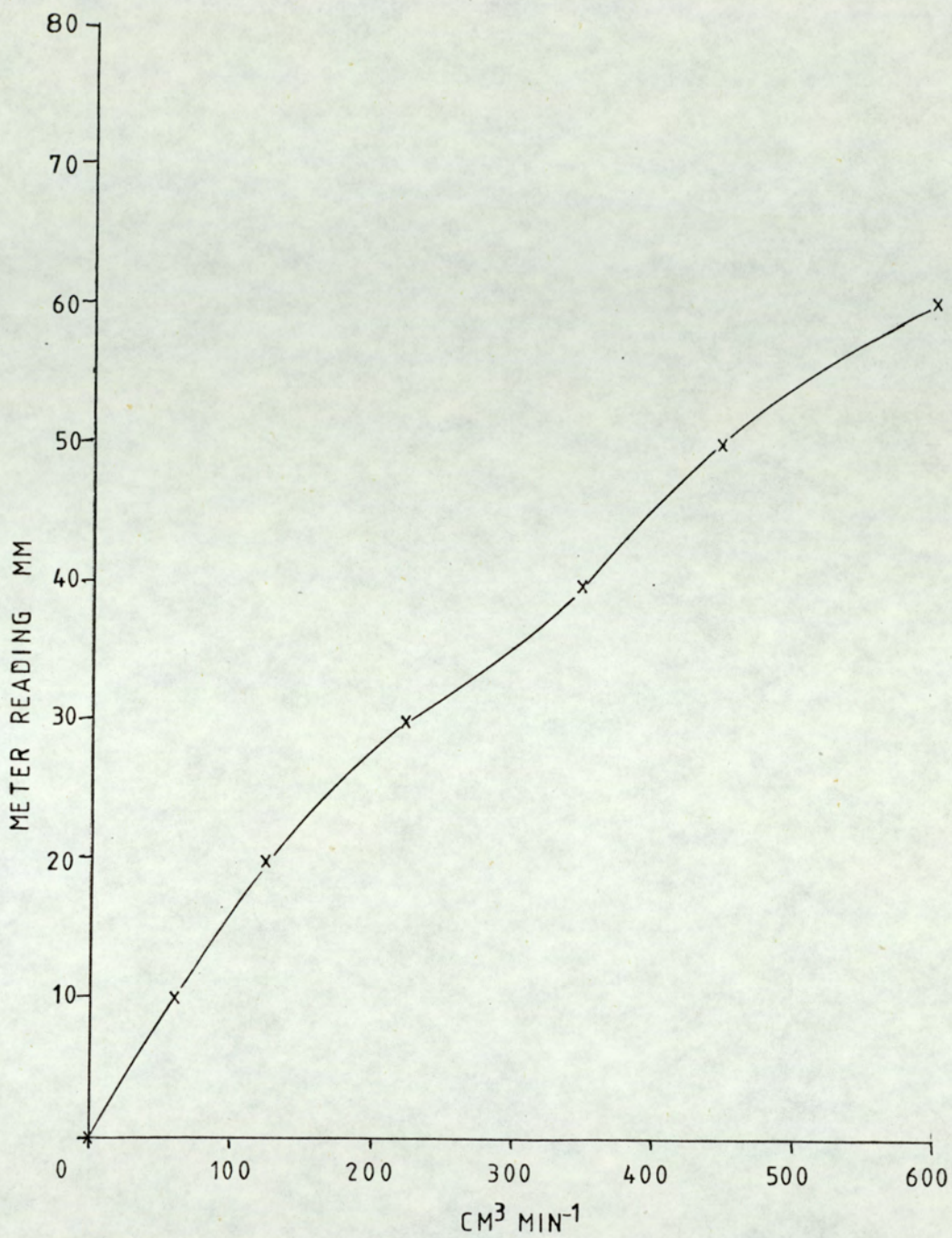


Figure 12. Flow Meter Calibration for Ethylene at S.T.P.

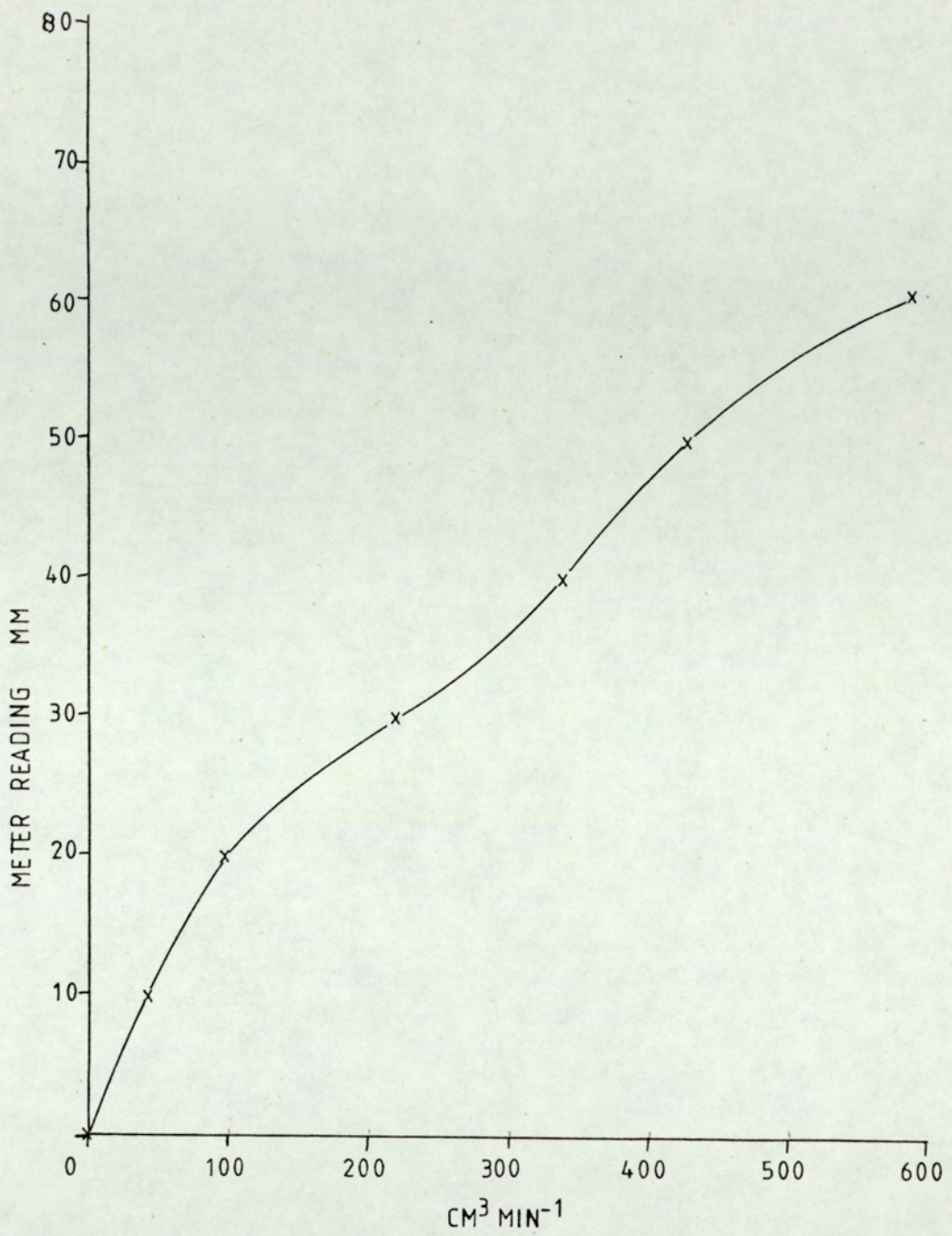


Figure 13. Flow Meter Calibration for Acetylene at S.T.P.

The flow meters were calibrated, by using a gas flow meter and stopwatch, so that the flow in $\text{cm}^3\text{min}^{-1}$ could be directly measured on the meters (Figs. 9, 10, 11, 12, 13). These graphs were in good agreement with the manufacturers calibrations after conversion to S.T.P. Since the prevailing conditions, (temperature and pressure) could result in up to a 10% error on the various flow rates, the gas flow rates were corrected on a day to day basis.

The flame was approximately 10cm long, the reaction zone being typically 2cm long when the hydrocarbon fuel was added. The reaction zone was in the shape of a cone, and coloured blue. This zone was approximately 0.5^mcm thick.

II.2.iii. The Inlet Nozzle.

The inlet nozzle, which was attached to the first vacuum chamber wall, provided a means by which the flame could be sampled. An electroformed nickel cone was clamped to a water cooled stainless steel flange which was bolted onto the wall of the first chamber, a rubber O-ring providing a vacuum seal, (Fig. 14).

There are several theoretical considerations as to the size of the inlet. For the sampling of ions from atmospheric pressure, the most commonly used system is that of a pinhole in a thin wall dividing the flame system, at atmospheric pressure, from the analysing apparatus. Many workers in this field (e.g. 23), have used a system whereby the

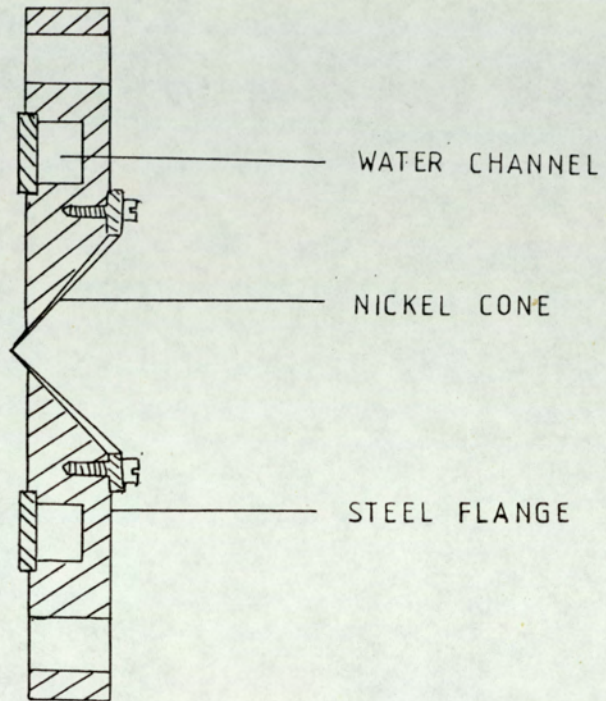


Figure 14. Inlet Nozzle.

flame is burnt at a lower pressure; the gas flow can then be collimated into a molecular beam, with a larger inlet, but a more complex system of focusing^s lenses. An aperture much longer than its diameter is to be avoided since ions are lost to the wall and unwanted secondary reactions may also occur. Thus, it is generally more advantageous to have as large a pinhole as possible (in the thinnest possible wall), an upper limit being set for a particular situation, by the capacity of the first chamber diffusion pump to maintain an adequate vacuum. Experiment showed that for this particular system, an inlet nozzle larger than 0.2mm caused the first vacuum chamber diffusion pump to stall. For this work an inlet nozzle of 0.12mm was used.

The nickel sampling orifice was fabricated by electroforming nickel onto brass. A brass former was made
Onto this was electroplated nickel to a thickness of 0.1mm. The tip of the cone was then carefully filed away until the brass was exposed. Measurements were made by travelling microscope to ensure that the hole in the nickel was of the correct size. The brass was dissolved away by placing the cone into a solution of chromic acid (chromium oxide, 3.20g dissolved in sulphuric acid, 0.025M, 1l). The brass dissolved away rapidly at first, but took up to three days to completely^o dissolve. The chromic acid solution was changed twice a day, as older solutions tended to attack the nickel (24).

II.2.iv. The Ion Lens.

The ion lens comprised the inlet flange, the second chamber wall, two ring electrodes and a beam shift assembly in the first chamber and a narrower ring electrode in the second vacuum chamber prior to the entrance aperture of the quadrupole (Fig.15.). The lens was mounted onto the second chamber housing using glass rods located in nylon bolts, which screwed into the wall. The final element was attached to the rear of this wall by thin ceramic rods fastened with 'Araldite' glue. The second chamber wall was electrically insulated from the other vacuum housing using a teflon flange (which also served as a vacuum seal), and nylon locating bolts. The beam shift assembly consisted of a cylinder cut into quarters longitudinally and held together (as a split cylinder) by ceramic rods and 'Araldite' glue.

Electrical supplies provided for the lens were connected via a 9-pin feedthrough in the top of the first chamber. The inlet flange, (which was isolated from ground potential using a fat rubber O-ring), was supplied by its own separate 350V d.c. power supply, (Farnell). The remainder of the lens was supplied by a 2.5kV d.c. power supply, (VG), and the beam shift electrode ⁴ supplied by a 90V battery. The different voltages on each electrode, and the varying voltages on the four elements on the beam shift electrode were obtained using simple circuitry and potentiometers.

The original lens had an extra set of electrodes between the first and second electrodes of the modified lens.

The power supplies involved impressing voltages of different polarities onto the electrodes (25). This original arrangement was difficult to set up, and the simpler system chosen. The modified lens was more efficient at focusing ions into the quadrupole than the original. For optimum signal the lens elements were moved physically with respect to each other so that the largest ion signal could be obtained.

For negative ion operation, the first flange was floated at between -10 and -50 V, (with respect to earth). The second chamber wall was held at +350 V, and the other lens elements adjusted accordingly to obtain the largest ion signal. It was found that a voltage of greater than 350 V on the second chamber wall made no difference to the ion signal: it was concluded that the lens transmits nearly all ions which enter the system via the sampling orifice.

Positive ions could be detected by a reversal of the various voltages on the lens and inlet flange. The Faraday detector was held at zero volts, since this produced simpler amplification techniques. However, it is then necessary to place a voltage of the same polarity as the ions on the inlet flange so that there is a net voltage change from sampling to detection, otherwise no ions would be focussed into the quadrupole, and detection would not be possible.

The theoretical design of ion lenses is complicated -no attempt was made to derive a theoretically perfect lens. The lens that was used appeared to be of a reasonable design and good

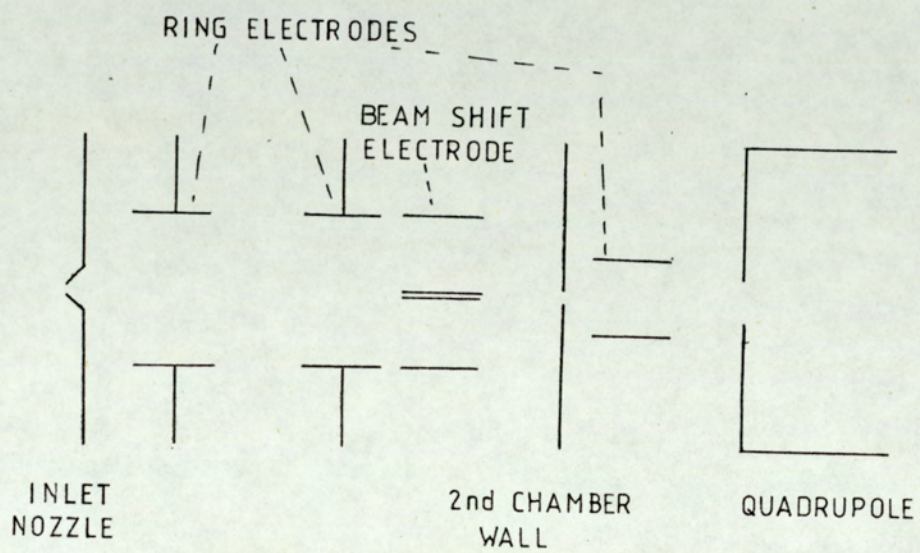


Figure 15. Schematic of the Ion Lens.

focusing^S_λ was obtained

II.2.v. The Quadrupole.

The quadrupole filter was supplied by Extranuclear, Inc. The poles were 0.228m long and 0.019m in diameter. The inscribed radius, r_0 thus being 0.00822m. The rods were held in a stainless steel case, insulation being provided by ceramic discs at each end. The quadrupole was fitted into the second chamber via a steel bracket. The assembly was aligned visually through the second chamber wall orifice (0.002m diameter), and through the front flange (using a larger 0.002m diameter orifice). The power supplies were connected through a feedthrough on the second chamber wall and were carefully screened to ensure r.f. stability.

The power supply and control unit for the quadrupole were also supplied by Extranuclear Inc. After the careful tuning procedure, a maximum mass of 400 a.m.u. could be obtained at an approximate frequency of 1.3MHz. The mass spectrometer could then be calibrated on two ranges, such that an integral reading on the mass meter on the control unit corresponded to an actual integral mass. Thus full scale on the lower range corresponded to 200 a.m.u. (actual reading 20), and 400 a.m.u. (actual reading 20) on the upper range. Calibration was carried out for positive ion detection by seeding the flame with potassium chloride solution, via an aspirator. Potassium is particularly useful since its two most abundant

isotopes (39 and 41 a.m.u.) could be detected, and hence provided a useful check on calibration. This calibration was also valid for negative ion operation, but was checked by detecting $^{35}\text{Cl}^-$ and $^{37}\text{Cl}^-$ in the correct isotopic amounts. Since the mass spectrometer range is linear, a single calibration at a low mass calibrated the complete mass range of the instrument.

II.2.vi. Ion Detection.

(a). The Particle Multiplier.

The original multiplier as supplied with the instrument was found to have outlived its useful life and therefore was replaced. A plot of ion current versus applied voltage for positive ion detection showed no characteristic plateau. The new multiplier (EMI EM140) was of a similar design; viz., a copper/beryllium box and grid type of multiplier, although it had 15 rather than 14 stages.

The multiplier was attached to a stainless steel plate, the complete assembly being bolted to the quadrupole housing, such that the multiplier was parallel but off-axis to the axis of the quadrupole. For positive ion detection the set up is quite straightforward. A negative voltage, (2.5 kV) is applied to the first dynode and the final dynode was earthed, multiplication occurring, (by as much as 10^6) and the resultant signal being taken from the collector electrode, (Fig.16.). Neutrals passed out of the detection system, since they could

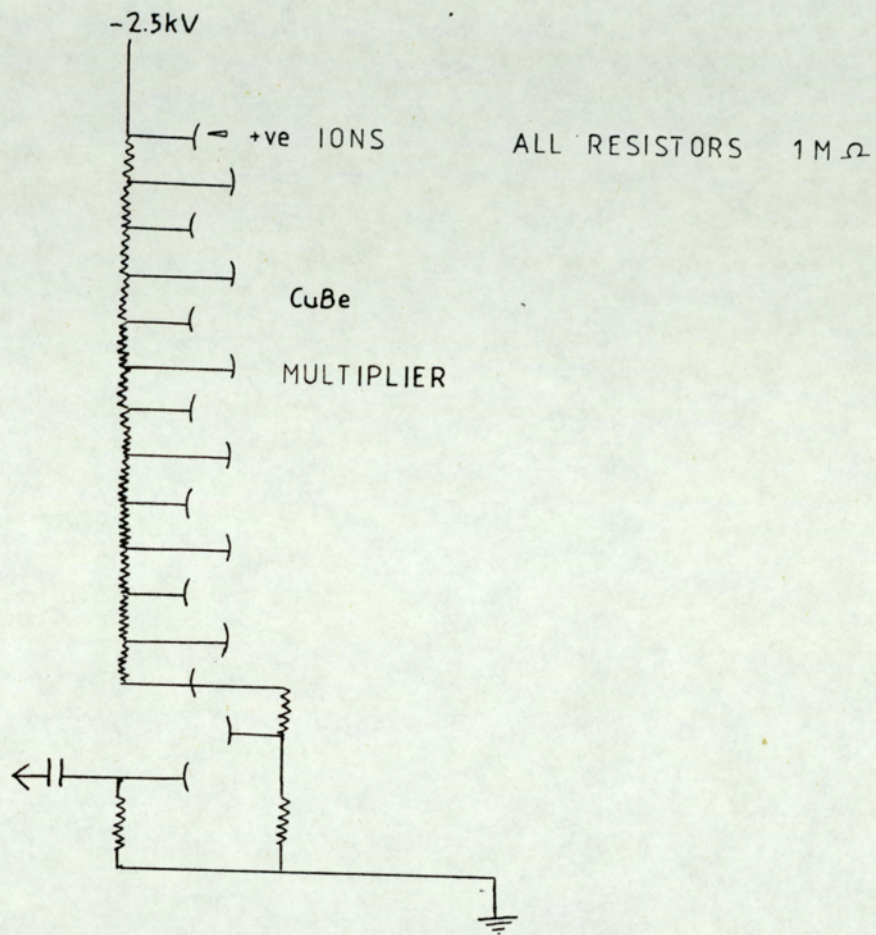


Figure 16. Connection of Multiplier for Positive Ion Detection.

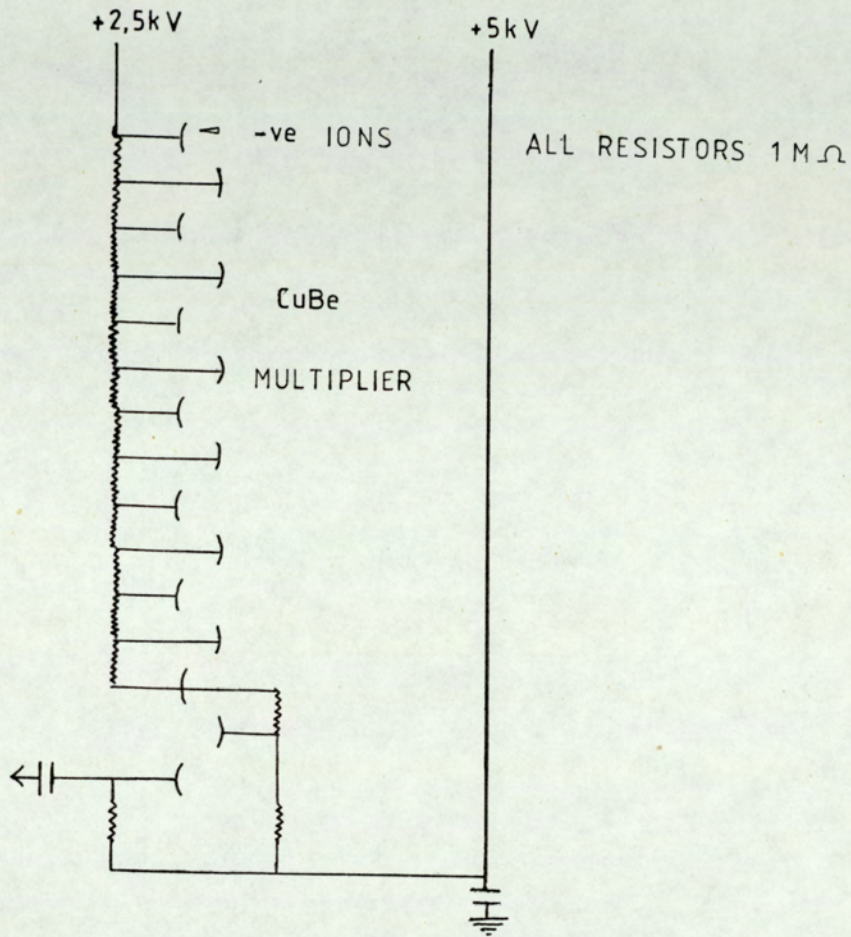


Figure 17. Connection of Multiplier for Negative Ion Detection.

not be deflected down toward the first dynode of the multiplier. However, negative ion detection is somewhat more complicated, since to attract negative ions a high positive potential must be applied to the first dynode. The last dynode must have a correspondingly higher positive voltage applied to it to allow multiplication to occur, and this presents several problems, (Fig. 17). The potentials applied in this case were + 2.5 kV to the first dynode and + 5 kV to the last dynode. A somewhat simpler, safer and cheaper design has been reported by Goodings et al (22); a + 5 kV voltage is applied to the last dynode, and the first dynode is earthed by a large resistor, (c.a. 2 Mohm) so that the resulting potential on the first dynode is approximately + 2.5 kV. This method was tried and found to be reasonably successful.

The output signal was fed via a large capacitor, (1000 pF, 10 kV d.c. working) so that the amplifier was protected from the large d.c. potential. In this mode, d.c. ion signals cannot be detected, the ion signal being a.c. coupled. Because of this the output had to be detected by a phase sensitive technique, brought about by modulating the ion beam before it entered the quadrupole.

To protect the multiplier from accidental short circuits smaller resistors were placed in the H.T. circuit (680 kohm); these failed if a large voltage breakdown occurred. Large paper capacitors were also connected between the H.T. supplies and earth to act as filters, providing extra high voltage

stabilization.

b). The Faraday Cup.

For optimising focusing^S and for most negative ion work, (since it was far simpler), a Faraday cup was used. This consisted simply of a solid brass cylinder, bored out into the shape of a cone. This was fixed immediately behind the exit aperture of the quadrupole so that no ions were lost before hitting the cup. The depth of the cup was about 3 cm long ensuring that most of the ions were discharged in the cup, and that secondary emission did not occur to an appreciable extent. The output signal was connected via a co-axial cable through a feed through to the amplifier. The signal was screened by earthing the co-axial cable onto the quadrupole filter casing, (which was at ground potential).

II.2.vii. Amplification.

(a). Phase Sensitive Detection.

When the multiplier was in use the signal was amplified with a lock-in amplifier, (Brookdeal 9503). The a.c. signal was derived by impressing a square wave voltage of 200 Hz onto the front flange of the first vacuum chamber. The amplitude of this was set up so that the voltage corresponded to the voltage required for optimum transmission. A pre-amp preceded the lock-in amplifier to amplify the signal. The resultant

signal was fed into the 'y' input of the 'x-y' chart recorder (Bryans 20001).

(b). The D.C. Amplifier.

For Faraday cup detection the d.c. signal was fed into a d.c. amplifier (Avo 305). The resultant signal from this was used as the input to the 'x-y' recorder. The maximum signal that was obtained was 10^{-10} amps for positive ion operation and 10^{-12} amps for negative ions.

II.2.viii. Record of Ion Profile.

As previously mentioned the amplified signal was used as the 'y' input of the 'x-y' recorder. The 'x' input was derived from the moving flame carriage; a ten-turn potentiometer providing linear movement of the chart recorder pen. Thus, with the flame reaction zone set a few millimetres away from the inlet nozzle, the flame carriage was moved against this, the pen moving proportionally to the burner, and a profile of a particular ion was recorded.

To eliminate errors when setting up the burner carriage, and to provide a suitable zero point on the 'x'-axis, a second chart recorder was used (Honeywell). This recorded the pressure change in the vacuum system as the flame entered the inlet. At the reaction zone tip, the pressure is at a minimum, steadily increasing as the reaction zone enters the inlet nozzle. Thus by setting both chart recorders to run simultaneously, the zero

point for the ion profile could be found, from the minimum point on the pressure profile (Fig. 18). The pressure readings were taken from the backing pressure change, as monitored by the Pirani gauge on the backing piping to the first vacuum chamber diffusion pump.

To obtain a complete mass spectrum of a particular flame, the burner was positioned so that the reaction tip just entered the inlet nozzle. The 'x'-axis of the chart recorder was connected to the output of the quadrupole control unit so that by varying the mass (manually) on the control, a complete mass spectrum could be obtained. Of course, manual operation could not provide an accurate measurement of peak height, but this procedure was useful in finding particular ions, as a quick simple method.

It was possible to attach a d.c. ramp voltage to the mass spectrometer control, so that a spectrum could be automatically obtained. Difficulties in finding, or making a suitable ramp voltage signal (which needed to peak at 150V) precluded the use of this.

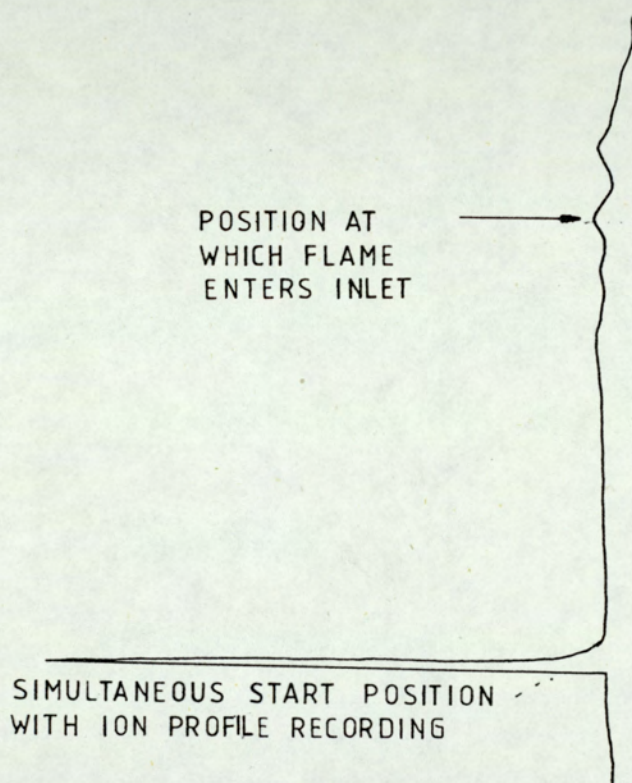


Figure 18. Reproduction of a Typical Backing Pressure Recording.

II.3. A CRITIQUE OF THE EXPERIMENTAL TECHNIQUE.

Several problems arose with the experimental technique and these will be considered in detail, as they are of relevance to the system.

II.3.i. Vacuum System.

Generally the vacuum system required little attention after initial setting up. The lead gaskets which sealed the various flanges on the high vacuum chambers needed care in fabrication and occasional replacement. The oil in the diffusion pumps decomposed slowly with time, its break-up being accelerated if it was not allowed to cool down under a rough vacuum. It was found on shut-down that the pumps needed to cool down for at least an hour after the heaters to them had been switched off. However oil contamination still occurred, all parts of the high vacuum chambers suffering some deposition of pump oil, especially in the first chamber. A remedy would have been to baffle the top of the diffusion pump, and provide some sort of cooling for this, to enable the oil to condense more efficiently.

II.3.ii. The Burner.

It was difficult to stop the flow meters on the gas lines from fluctuating whilst the flame was burning. In some cases, this represented a 10% error in the quantities

of gas flow. However, the position of a particular ion in the reaction zone of the flame could be found accurately because of the simultaneous acquisition of the pressure profile. Thus for experiments where the identification and position of the ions in the flame was required, as long as the error in measurement of the gas flow was fairly small the results did not deviate to a great extent.

The burner itself needed careful alignment against the inlet nozzle, so that sampling occurred on a single axis perpendicular to the burner mouth, and through its centre. Although the burner assembly was fairly crude compared to other workers (e.g. 26) axial alignment could be accurately adjusted by gently moving the burner and aligning it visually. If the burner was not aligned properly, the ion profiles were considerably altered: flat jittery peaks resulted, the profile peaked at a different position and the ion signal intensity was considerably lowered.

II.3.iii. The Inlet Nozzle.

The inlet nozzle is probably the source of most of the unavoidable errors in this type of sampling. Anything placed into a flame will necessarily disturb the flow characteristics, and these effects need to be minimised. At the cone tip of the nozzle, much of the flame flows past the inlet and comes into contact with the cooled outer surface and cold flange of the sampling system. It is here that secondary reactions may

occur, and some work has been done to show what type of secondary reactions may occur (27). Unfortunately, some of these secondary products can become entrained back into the main flow by virtue of the turbulence characteristics of the sampling system

As the flame enters the inlet nozzle, ideally the flame reactions should be quenched. However this is not generally the case, and it has been shown (4) that for positive ions and an inlet of small diameter, (less than 0.1mm) secondary ions, notably hydrates of oxygenated species, occur in some cases exceeding the parent ion signal. For example, H_3O^+ (m/e 19) is known to be a true flame ion but hydrates, $H_3O^+ \cdot nH_2O$ ($m/e=19 + n18$, $n = 1,2,3,4$) can occur, and the first hydrate is often larger than H_3O^+ . Hayhurst and Telford, (28) have done some mathematical modelling of these types of reactions.

For larger inlet orifices, (greater than 0.1mm), the effects of hydrates can be reduced. A change in the angle size of the inlet cone can also have a marked effect on the suppression of secondary ion formation, (29).

For negative ions, there appears to be no correlation between inlet size and secondary reaction processes (27). With the inlet in use in these experiments hydrates did form to an appreciable extent, and these will be discussed in the results.

The inlet hole tended to become clogged up after prolonged sampling, this probably being due to the build up of carbonaceous species. A simple remedy was to remove the front

flange (containing the inlet) and cleaning the orifice on a day to day basis.

Another problem with negative ion experiments was the tendency of the ion signal to gradually decrease with time: this was especially prominent for ions of low mass and therefore of high mobility. It is thought (30) to arise from the oxidation of the cone tip by the flame reactions. A negative charge tends to build up, the resulting electric field opposing the tendency for the ion to be carried into the orifice by the gas flow. The cone was regularly cleaned to avoid excess errors from this source.

The cone was made from nickel: this metal is a good catalyst, and it may be possible that some sort of catalytic effects can produce secondary reactions. No work has been recorded to investigate this type of behaviour but nickel may be used to hydrogenate unsaturated hydrocarbons such as ethylene to ethane, and acetylene to benzene, and at the temperatures of flames this type of behaviour is quite possible.

II.3.iv. The Ion Lens.

The ion lens suffered mainly from oxidation and oil contamination from the diffusion pump. The lens elements were regularly removed and carefully cleaned. Over a period of time the ion signal decreased, due to the build up of contamination.

II.3.v. The Quadrupole.

The connecting leads and feedthroughs to the quadrupole were prone to failure because of the high voltage impressed on them. The ceramic lead-throughs which carried the r.f. power were cleaned using a saturated sodium hydroxide solution to remove carbon traces on the ceramic pillars of the lead-throughs. The ceramic insulators in the quadrupole also needed replacing, and due to the unavailability of parts, they were replaced with teflon insulators: these had an adequate resistivity, and were not liable to mechanical failure. The quadrupole needed occasional removal and cleaning, due to slight oil contamination. This was done by brushing the poles with mild detergent, after decontaminating the stainless steel with trichloroethylene.

II.3.vi. Ion Detection.

(a). The Multiplier.

For positive ion detection no problems were encountered except slight oil contamination, which was removed by washing in a polar solvent. For negative ion operation the main problem was with electronic noise brought about mainly by the two floating high potentials. The multiplier acts as an effective microphone converting mechanical noise and electronic imperfections into signal noise. Also stray electrons in the vacuum system are efficiently collected at the cathode of the multiplier. Typically, a multiplier connected for negative

ion detection is thirty times noisier due to stray electrons than a conventional multiplier connected for positive ion detection, (31). In fact, a large amount of noise was seen in the negative ion mode, and meaningful interpretations of the signal were almost impossible, even with beam modulation. A possible solution, suggested by these workers (31) and now in general commercial use, is to convert the negative ion beam into a positive ion beam by the use of a conversion dynode operating at 2 kV.

(b). The Faraday Cup.

Although this was of simple design, it was felt that improvements to suppress secondary ions would not be worthwhile, since it appeared reasonably efficient at ion detection. It was a deep brass cone, so that ions would be discharged completely. The performance of the cup was improved by polishing it with a proprietary cleaner.

II.3.vii. Amplification.

The ion signal was of the order of 10^{-10} amps for positive ions, and 10^{-12} amps for negative ions. At these low currents, the d.c. amplifier necessarily had a long time constant (7 secs). For accurate representation of the ion profile, therefore, the burner carriage needed to move slowly so that a faithful record could be obtained. A movement of 1mm min^{-1} was satisfactory for these low currents. With the particle

multiplier and lock-in amplifier in operation, the time constant was sufficiently large, (0.5 secs), to allow a flame movement of 10 mm min^{-1} .

III. RESULTS.

III.1. INTRODUCTION.

The experimental work involved the collection of ion profiles in a simple flame to which a hydrocarbon had been added. The ion profiles were recorded on an 'x-y' chart recorder, Fig.19. Five runs were taken, and an average found to produce one profile, Fig.20. For each run, the zero point (i.e. that point at which the downstream edge of the reaction zone occurred) was taken as the minimum position on the backing pressure profile, which was taken simultaneously with the acquisition of the ion profile, as described in Chapter II, Fig.18. The intensities of the ion profiles were corrected for zero before averaging them, by subtracting the height of the profile downstream of the flame front. With the flame moved well back from the inlet nozzle the ion signal diminished to a constant current - it was assumed that no ion current was detected here, and the offset on the plots was due to zero error on the d.c. amplifier. The ion profiles were averaged by taking the profile height at 0.025 mm intervals. This procedure eliminated most of the errors due to signal noise and produced a more accurate position for the profiles.

The flame had a composition of $H_2:O_2:Ar$ of 3.8:1.0:7.1 by volume, the flow rate being about 2.5 l min^{-1} . The temperature of the flame, as measured by the sodium reversal technique, was 2150 K, (32). The hydrocarbon fuel was added

in small amounts not exceeding 10% by volume. This preserved the common flame background, so that comparisons between different hydrocarbons could be made.

The results and discussion will be confined to the negative ion experiments, since the few experiments with positive ions only served to gain experience and practice in setting up the experimental apparatus. Positive ion flame chemistry has also been well documented, (e.g. 7).

The ion currents measured were of the order of 10^{-14} amps for negative ions. No attempt has been made to calibrate the ion signal to the actual number of ions. The relative count was taken by simply measuring the heights of each profile. Measurements taken by the d.c. amplifier on the second chamber wall and the electrode directly prior to the entrance aperture of the quadrupole showed that 40% of the ions in the first chamber reached the quadrupole. The resolving power of the mass spectrometer was approximately 100, measured at 45 a.m.u.

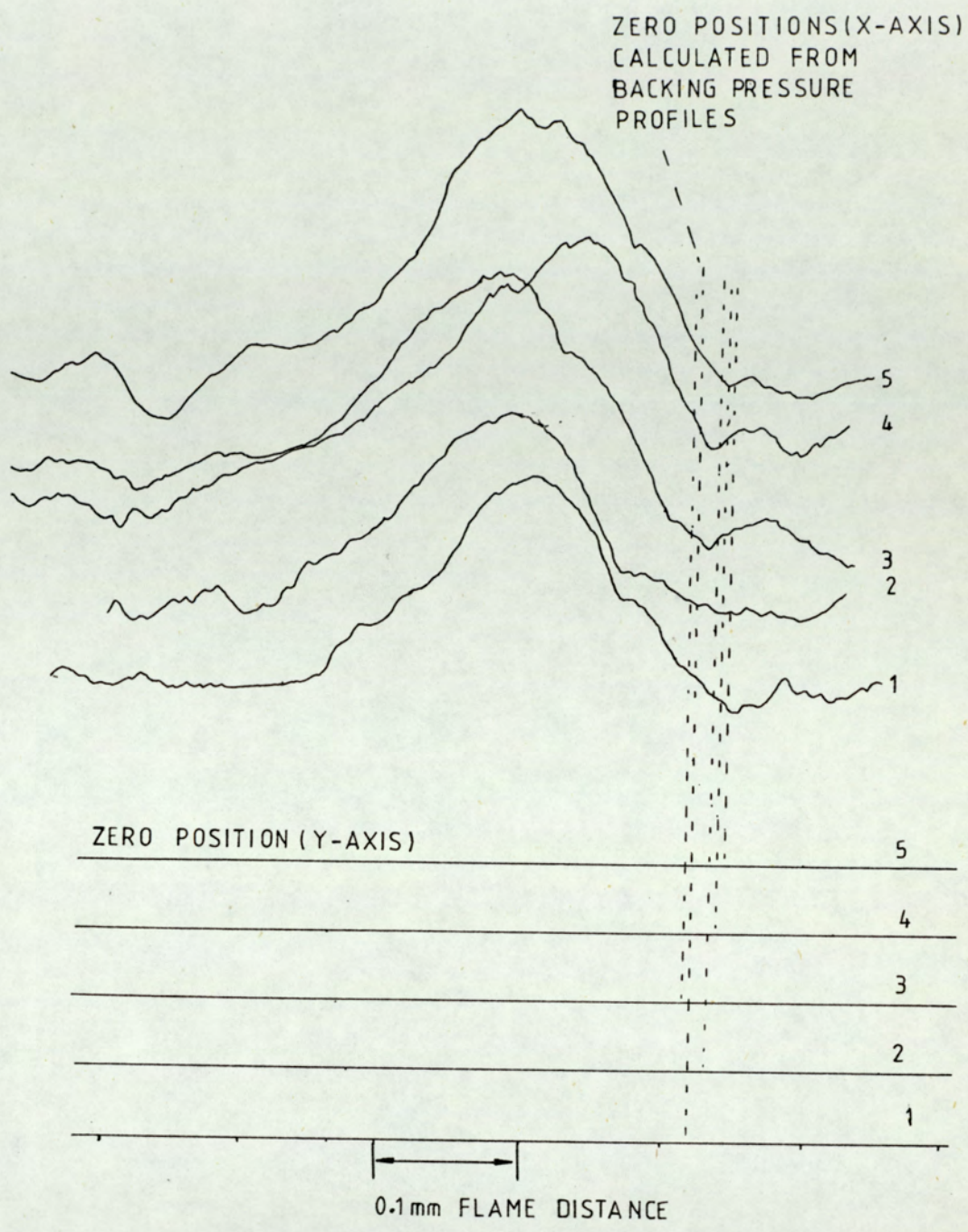


Figure 19. Reproduction of Five Runs for One Ion Profile.

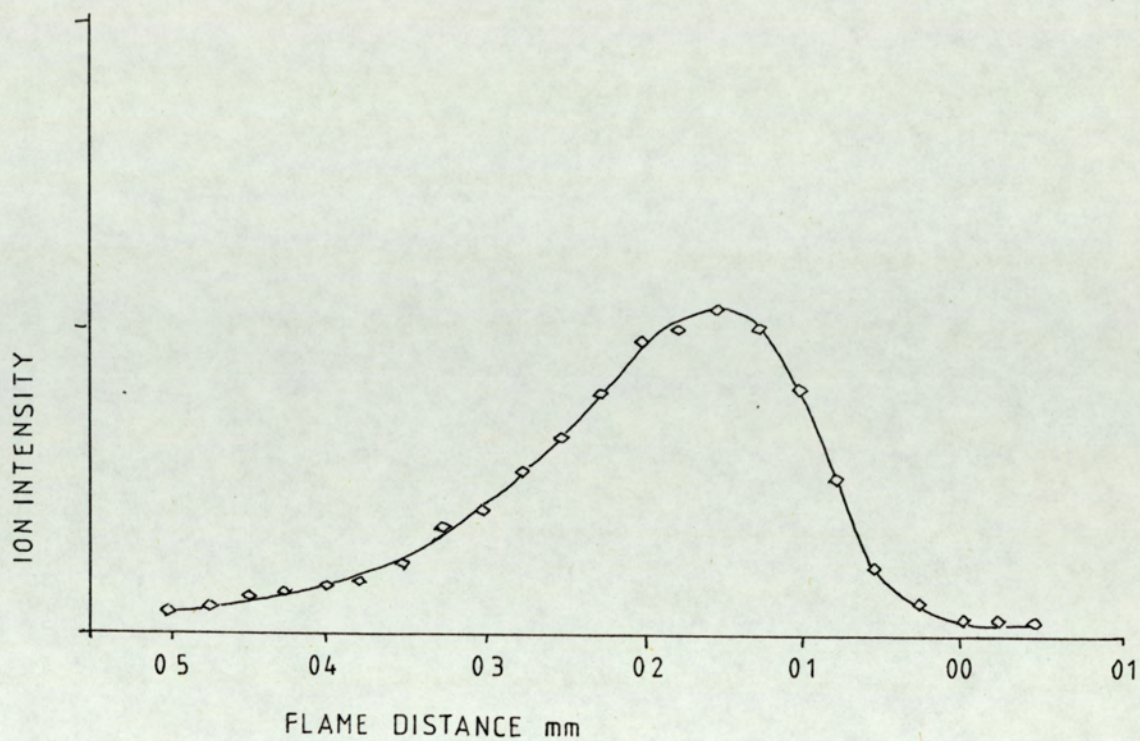


Figure 20. Reconstructed Averaged Ion Profile From Figure 19.



III.2. ETHYLENE, FLAME F1.

When 2% ethylene (by volume) was added to the flame, 42 negative ions were detected, ranging from 16 a.m.u. to 105 a.m.u. The positions and intensities of each ion are given in Table 1., a 'stick spectrum' of the relative intensities of these (at their individual peak heights) is given in Fig.21. In Table 2., the experimental data for each ion is presented.

III.2.i. General Features.

1. All the ion profiles peaked upstream of the reaction zone front.
2. Some ion profiles (notably those containing oxygen and hydrated species) have a considerable extension upstream of the flame front.
3. No ions have more than one peak in their ion profile.
4. Most ion profiles drop off sharply after they have peaked.
5. A few ions have extensions of their profiles through the reaction zone into the burnt gas region.
6. The ions at 35 a.m.u. and 37 a.m.u. are anom^galous, these can be attributed to $^{35}\text{Cl}^-$ and $^{37}\text{Cl}^-$.

Mass, a.m.u.	Intensity ^a	% of Total Ion Current	Position in Flame, mm ^b
16	36.40	0.30	-0.125
17	61.00	0.50	-0.2
24	38.80	0.32	-0.05
25	162.8	1.34	-0.125
32	372.0	3.06	-0.175
33	48.00	0.40	-0.15
35	1680	-	-0.15 ^c
36	598.8	4.93	-0.175
37	709.2	-	-0.175 ^c
41	93.40	0.77	-0.10
43	134.4	1.11	-0.05
45	3240	26.79	-0.10
46	86.20	0.71	-0.15
49	40.80	0.34	-0.025
50	367.0	3.02	-0.15
51	7.40	0.06	-0.10
53	677.0	5.58	-0.175
60	355.0	2.92	-0.10
61	456.0	3.76	-0.10
62	178.4	1.50	-0.125
63	856.0	7.05	-0.125
64	677.5	5.58	-0.10
65	55.20	0.45	-0.125

/contd.

Mass, a.m.u.	Intensity ^a	% of Total Ion Current	Position in Flame, mm ^b
66	117.0	0.96	-0.20
68	270.8	2.23	-0.20
69	158.4	1.30	-0.175
71	98.60	0.81	-0.20
72	444.0	3.66	-0.15
73	32.80	0.23	-0.10
76	102.6	0.85	-0.125
78	292.0	2.91	-0.175
79	776.0	6.39	-0.175
84	63.60	0.52	-0.20
85	88.80	0.73	-0.20
87	362.0	2.99	-0.25
88	57.60	0.47	-0.225
90	77.20	0.64	-0.20
92	244.8	2.02	-0.20
94	18.60	0.15	-0.20
96	94.20	0.78	-0.25
97	204.8	1.41	-0.25
105	94.00	0.77	-0.375

Table 1. Intensities and Positions of Negative Ions
Observed in the Flame with Ethylene as Additive.

/contd.

Notes for Table 1.

- a) Intensity is in arbitrary units only.
- b) Position in flame has been taken with 0.00 being the downstream edge of the reaction zone, thus a negative figure implies that the profile peaked upstream of this point.
- c) The two ions at 35 a.m.u. and 37 a.m.u. are due to $^{35}\text{Cl}^-$ and $^{37}\text{Cl}^-$; they were discounted from the total ion current measurements.

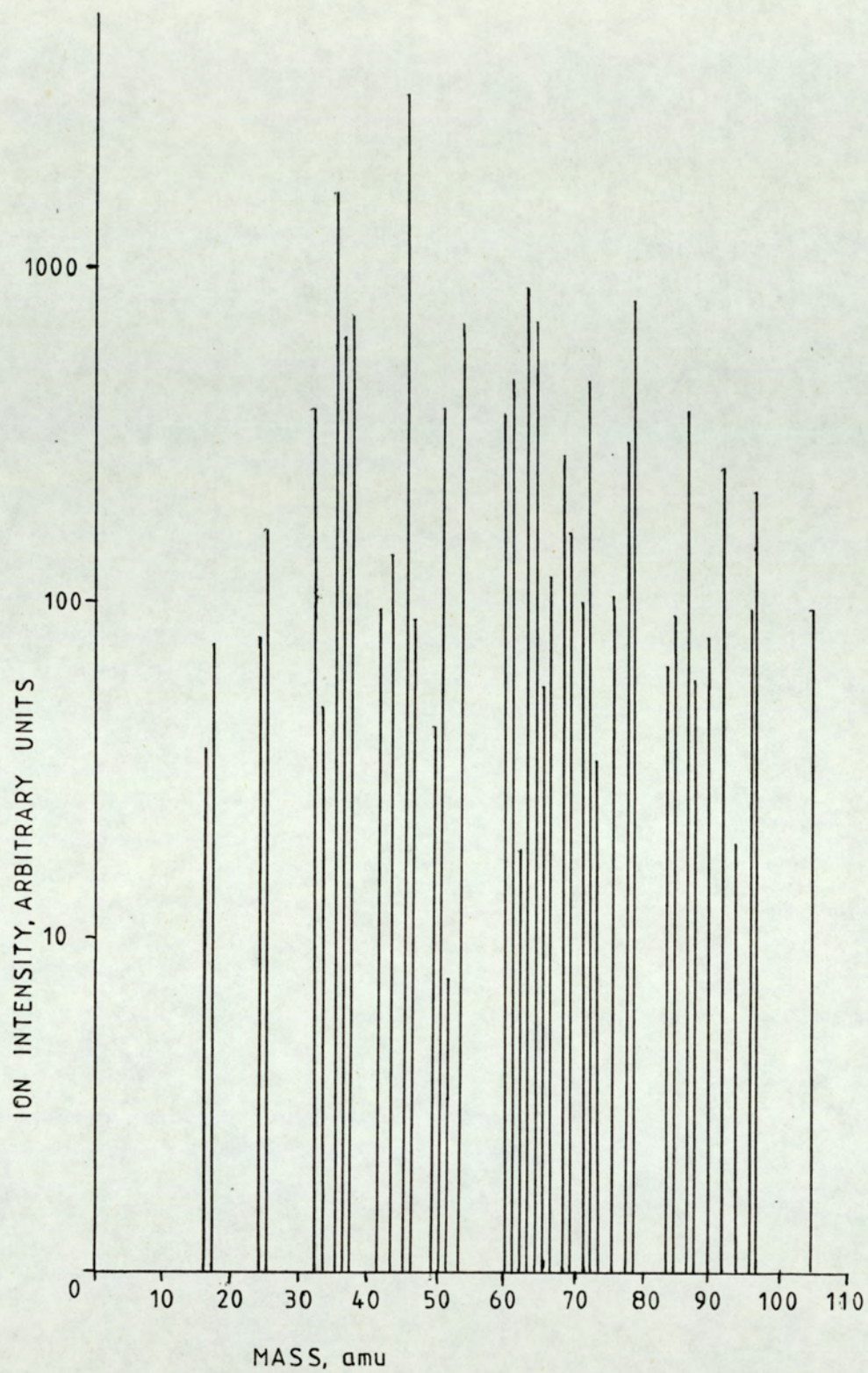


Figure 21. Stick Spectrum of the Negative Ions Found in the Ethylene Flame.

Flame	Ion Intensity, Arbitrary Units, for Each Mass.								
Distance, mm.	16	17	24	25	32	33	35	36	37
0.10		3							
0.075		3	0						0
0.05		3	3						6
0.025		5	8	0				0	10
0.00	0	18	15	18	0	0	0	37	17
-0.025	0	26	31	57	76	8	300	58	25
-0.05	4	35	39	81	204	17	740	85	76
-0.075	16	42	36	138	284	26	1180	160	230
-0.10	30	43	34	163	348	35	1500	274	396
-0.125	36	48	32	144	372	42	1640	470	607
-0.15	25	51	23	115	372	47	1680	564	694
-0.175	16	58	6	62	324	48	1480	599	709
-0.20	10	61	2	40	272	48	1140	598	691
-0.225	9	49	0	17	220	45	860	586	632
-0.25	1	36		0	196	44	660	527	538
-0.275	0	30			172	41	480	466	410
-0.300		27			124	33	300	373	314
-0.325		23			96	28	120	310	244
-0.35		18			68	23	60	254	197
-0.375		13			52	23	20	196	132
-0.40		7			48	20	0	154	96
-0.425		6			28	19		114	52
-0.45		4			16	16		74	41
-0.475		5			4	12		50	28
-0.50		0			0	7		38	0

Table 2. Continued

Flame	Ion Intensity, Arbitrary Units, for each Mass.								
Distance, mm.	41	43	45	46	49	50	51	53	60
0.10					9				
0.075		0			14				
0.05		2			19			0	
0.025		30	0		27			1	0
0.00	0	68	753	0	36	0	0	3	6
-0.025	8	105	2287	8	41	85	0	49	91
-0.05	38	134	2740	15	30	187	0	220	187
-0.075	66	121	3160	35	11	276	6	311	310
-0.10	93	92	3240	51	1	326	7	421	355
-0.125	74	67	3240	71	0	359	6	560	309
-0.15	50	53	3213	80		367	4	639	227
-0.175	19	34	3127	76		340	1	657	159
-0.20	6	20	3073	71		282	0	611	102
-0.225	0	7	2813	55		235		529	65
-0.25		3	2373	44		196		409	36
-0.275		0	1680	20		163		339	29
-0.30			1127	1		133		272	7
-0.325			713	0		104		215	1
-0.35			453			85		156	0
-0.375			273			70		114	
-0.40			140			62		91	
-0.425			93			52		88	
-0.45			60			48		48	
-0.475			47			45		35	
-0.50			0					38	

Table 2. Continued

Flame	Ion Intensity, Arbitrary Units, for Each Mass.								
Distance, mm.	61	62	63	64	65	66	68	69	71
0.10	17	19		23					
0.075	14	19	0	23					
0.05	16	22	6	24					
0.025	28	22	12	35	0				
0.00	79	34	18	45	0	0	0	0	0
-0.025	200	61	169	188	9	2	0	7	7
-0.05	338	111	466	379	18	15	3	17	9
-0.075	440	154	703	568	35	33	16	58	14
-0.10	456	167	854	678	50	48	59	92	31
-0.125	382	178	856	655	55	75	128	131	60
-0.15	271	168	780	601	55	99	197	150	82
-0.175	213	130	628	489	51	110	248	158	97
-0.20	157	93	455	395	46	117	271	136	99
-0.225	109	65	329	279	39	113	252	104	84
-0.25	70	43	246	200	31	103	213	76	71
-0.275	37	32	176	155	22	93	176	63	50
-0.30	21	23	126	119	18	82	141	51	35
-0.325	12	16	89	88	14	65	116	40	23
-0.35	5	10	61	69	13	56	72	27	13
-0.375	4	8	40	50	14	52	70	19	7
-0.40	1	8	20	38	11	45	51	12	5
-0.425	0	0	12	0	10	34	42	6	3
-0.45			6		10	29	34	4	2
-0.475			0		9	23	29	2	1
-0.50					8	18	20	3	0

Table 2. Continued

Flame	Ion Intensity, Arbitrary Units, for Each Mass.								
Distance, mm.	72	73	76	78	79	84	85	87	88
0.10					14				
0.075					14				
0.05					10				
0.025	0			0	24	0			
0.00	10	0	0	6	46	1	0	0	0
-0.025	85	7	16	41	94	1	3	4	0
-0.05	175	18	48	85	270	5	13	15	0
-0.075	300	33	71	155	392	14	28	46	0
-0.10	393	33	98	224	574	23	37	88	4
-0.125	438	23	103	259	688	34	51	133	15
-0.15	444	11	97	285	774	44	66	203	29
-0.175	414	6	79	292	776	61	77	283	43
-0.20	385	5	53	286	584	64	89	331	52
-0.225	301	3	32	274	570	63	87	351	58
-0.25	216	0	17	254	528	60	82	362	56
-0.275	163		3	215	450	52	79	340	60
-0.30	122		1	175	358	46	73	301	62
-0.325	84		0	147	284	46	66	255	66
-0.35	62			122	198	38	55	200	58
-0.375	40			96	136	31	44	166	50
-0.40	29			80	92	24	40	132	38
-0.425	15			65	56	20	32	103	30
-0.45	9			53	36	15	29	92	21
-0.475	5			43	44	6	24	74	16
-0.50	3			31	30	4	18	57	9

Table 2. Continued

Flame Distance, mm.	Ion Intensity, Arbitrary Units, for Each Mass.					
	90	92	94	96	97	105
0.10						
0.075						
0.05						
0.025		0				
0.00	0	4	0	0	0	0
-0.025	0	10	0	0	0	0
-0.05	2	16	0	5	0	0
-0.075	11	41	3	11	0	0
-0.10	20	68	8	17	2	0
-0.125	36	144	12	31	21	0
-0.15	57	195	16	52	58	0
-0.175	71	228	16	72	106	2
-0.20	77	245	19	84	138	0
-0.225	76	238	14	92	180	3
-0.25	70	216	12	94	205	19
-0.275	62	199	7	91	205	47
-0.30	48	163	3	82	201	66
-0.325	37	129	0	73	187	82
-0.35	24	104		65	179	94
-0.375	17	76		57	176	94
-0.40	12	61		49	155	87
-0.425	6	43		42	132	74
-0.45	3	30		37	111	62
-0.475	3	21		24	91	54
-0.50	1	17		16	72	48

Table 2. Continued

Table.2. Experimental Data for the Ion Profiles in the Ethylene
Flame.

III.3. ACETYLENE, FLAME F2

When 3% by volume of acetylene was added to the flame, 32 negative ions were found, from 16 a.m.u. to 97 a.m.u. The positions and intensities of each ion are given in Table 3., a 'stick spectrum' of the relative intensities of these (at their individual peak heights) is given in Fig.22. In Table 4., the experimental data for each ion is presented.

III.3.i. General Features.

1. With a few exceptions, the intensities of the ions were much lower than the corresponding ethylene ions, (by a factor of 5).
2. The ion profiles tended to peak further downstream than the ion found in F1.
3. Some ion profiles exhibited multiple peaks.
4. A few ions exhibited an extension into the burnt gas region.
5. Some ion profiles (notably those containing oxygen and hydrated species) have a considerable extension upstream of the flame front.

Mass, a.m.u.	Intensity ^a	% of Total Ion Current	Position in Flame, mm ^b
16	37.40	1.65	-0.025
24	73.60	3.47	-0.025
25	62.60	3.12	-0.015
32	36.90	1.84	-0.035
34 ^c	16.00	0.80	-
35	21.20	1.06	0.00
36	11.80	0.59	-0.010
37	8.00	0.40	-0.020
41	18.00	0.90	-0.110
43	41.50	2.07	-0.150
45	630.0	31.42	-0.070
46	11.00	0.55	-0.090
50 ^c	17.00	0.85	-
51	5.80	0.29	0.050
53	7.50	0.37	0.00
60	14.80	0.74	-0.030
61	5.10	0.25	-0.015
63	12.40	0.62	-0.125
64	10.00	0.50	-0.050
73	437.5	21.82	-0.110
74	37.40	1.86	-0.115
75	64.50	3.22	-0.130
76	16.80	0.84	-0.100

/contd.

Mass, a.m.u.	Intensity ^a	% of Total Ion Current	Position in Flame, mm ^b
78	85.90	4.28	-0.150
79	30.80	1.54	-0.150
81	19.50	0.97	-0.115
87	23.00	1.14	-0.075
90	17.90	0.89	-0.160
91	105.6	5.27	-0.150
92	64.00	3.19	-0.160
96	31.50	1.57	-0.20
97	42.00	2.09	-0.170

Table 3. Intensities and Positions of Negative Ions
Observed in the Flame with Acetylene as Additive.

Notes for Table 3.

- a). Intensity is in arbitrary units only.
- b). Position in flame has been taken with 0.00 being the downstream edge of the reaction zone, thus the negative figure implies that the profile peaked upstream of this point.
- c). Some ion signals were so small and noisy that an exact location of the peak top was impossible.

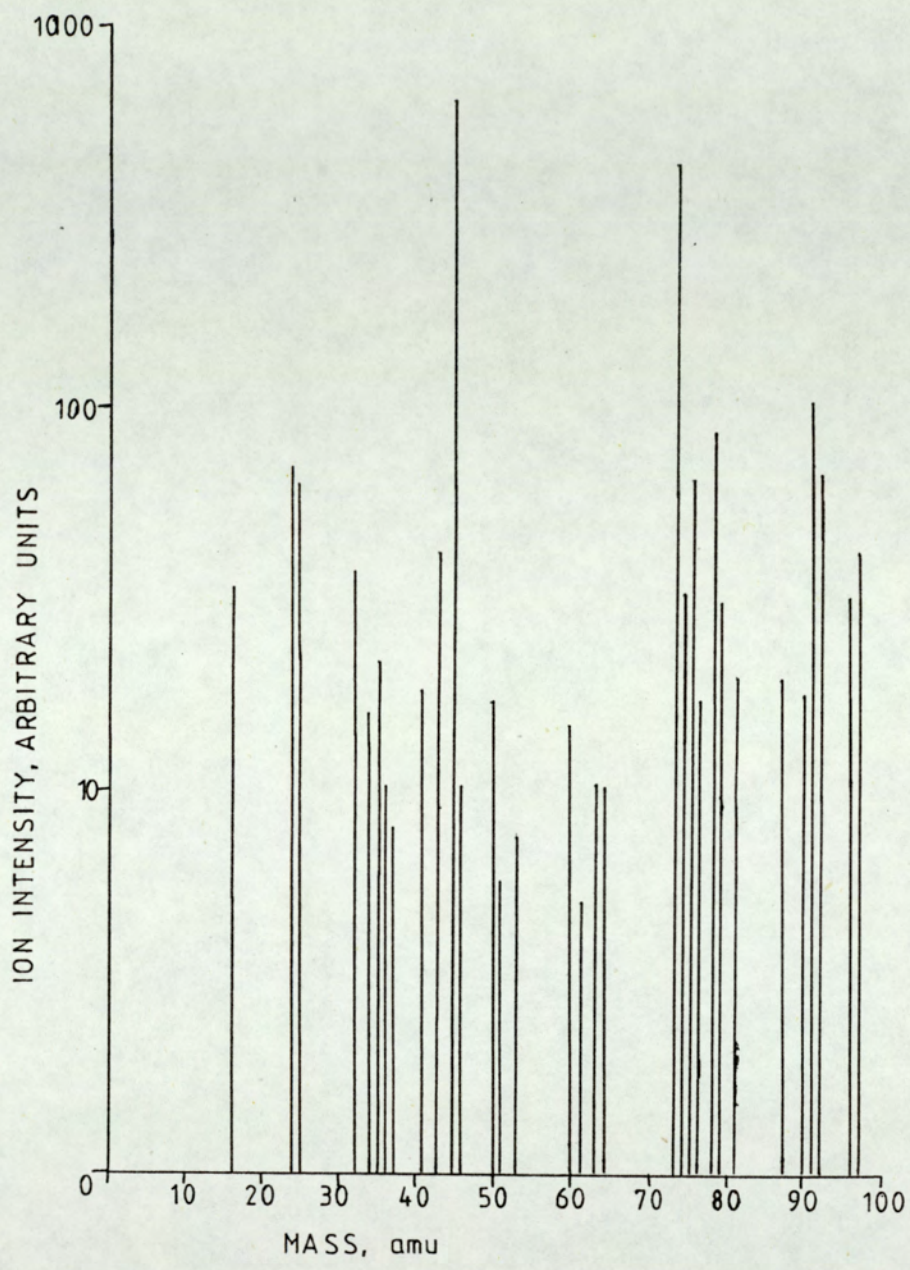


Figure 22. Stick Spectrum of the Negative Ions Found in the Acetylene Flame.

Flame	Ion Intensity, Arbitrary Units, for Each Mass.								
Distance, mm.	16	24	25	32	34	35	36	37	41
0.20		6	10		12	11	10	11	4
0.175		8	10		14	9	10	10	5
0.15		6	9		13	9	10	8	2
0.125		4	8		11	10	10	9	2
0.10	0	5	8	0	12	13	9	9	1
0.075	2	6	20	1	13	22	13	10	1
0.05	5	14	34	2	12	25	17	11	2
0.025	14	40	50	8	12	28	21	16	2
0.00	29	67	67	25	12	31	21	14	6
-0.025	32	74	70	40	11	29	17	10	9
-0.05	27	65	55	36	11	19	13	5	11
-0.075	15	43	41	30	12	17	10	6	15
-0.10	7	25	30	23	15	14	9	6	18
-0.125	2	14	17	16	17	11	6	3	17
-0.15	0	7	11	12	16	8	8	0	11
-0.175		1	7	8	14	16	5		6
-0.20		0	5	4	9	2	3	4	3
-0.225			1	3	4	2	3	4	3
-0.25			1	2	2	0	0	5	3
-0.275			2	2	0	1	0	5	2
-0.30			0	2	2	0		9	3
-0.325				0	0				0

Table 4. Continued

Flame	Ion Intensity, Arbitrary Units, for Each Mass.									
Distance, mm.	43	45	46	50	51	53	60	61	63	
0.20	6			2	5	10	5	12		
0.175	7			4	3	6	2	13		
0.15	5			2	4	6	5	14		
0.125	2		0	3	6	7	4	14	0	
0.10	1	0	3	2	6	8	4	16	1	
0.075	0	2	3	0	7	9	4	13	0	
0.05	0	2	3	3	9	8	3	13	0	
0.025	3	14	3	12	8	9	6	15	0	
0.00	3	128	4	5	7	13	11	17	1	
-0.025	9	406	8	4	6	12	16	14	1	
-0.05	13	596	12	5	5	7	17	12	5	
-0.075	21	626	14	11	3	7	13	13	5	
-0.10	25	545	12	14	2	3	10	8	8	
-0.125	40	426	12	17	0	3	8	6	12	
-0.15	40	311	9	15	1	2	4	5	12	
-0.175	35	219	7	10	1	2	2	2	11	
-0.20	25	152	6	9	2	5	2	1	5	
-0.225	17	109	3	12	5	0	2	0	3	
-0.25	13	74	2	12	5		0	2	5	
-0.275	14	52	1	12	6			3	1	
-0.30	8	31	0	10	4			2	2	
-0.325	5	18		10	0			0	0	
-0.35	4	5		6						
-0.375	1	5		5						
-0.40	0	0		6						

Table 4. Continued

Flame	Ion Intensity, Arbitrary Units, for Each Mass.								
Distance, mm.	64	73	74	75	76	78	79	81	87
0.20									3
0.175									3
0.15									4
0.125	0	0	0	0	0	0	0	0	5
0.10	0	0	4	0	2	3	0	0	5
0.075	0	2	4	0	0	3	0	0	2
0.05	0	1	0	1	4	1	1	1	5
0.025	4	1	1	2	2	0	3	2	4
0.00	5	19	4	3	3	3	5	3	4
-0.025	8	83	6	10	5	8	5	3	14
-0.05	10	190	21	29	9	20	8	7	22
-0.075	8	354	26	41	12	39	15	12	23
-0.10	2	369	38	57	17	61	22	18	22
-0.125	2	434	37	64	13	73	25	18	18
-0.15	0	345	31	62	8	86	29	13	12
-0.175	4	251	26	55	9	81	31	10	13
-0.20	3	193	21	43	7	75	28	7	13
-0.225	1	137	15	31	3	62	28	5	11
-0.25	0	102	12	22	5	49	23	3	8
-0.275		74	12	12	3	38	17	2	5
-0.30		49	8	9	4	28	16	2	4
-0.325		36	4	6	0	21	11	0	3
-0.35		28	4	5		14	11		4
-0.375		22	1	0		18	11		4
-0.40		21	0			11	8		0

Table 4. Continued

Flame Distance, mm.	Ion Intensity, Arbitrary Units, for Each Mass.				
	90	91	92	96	97
0.20	0				
0.175	1				0
0.15	2	0		0	4
0.125	0	3		0	5
0.10	0	3	0	1	2
0.075	1	5	0	0	3
0.05	0	5	0	0	0
0.025	4	3	0	1	4
0.00	3	4	2	4	0
-0.025	0	9	7	3	4
-0.05	7	21	15	6	6
-0.075	11	51	19	10	13
-0.10	13	82	42	12	27
-0.125	17	100	60	24	33
-0.15	17	106	64	29	41
-0.175	13	99	63	31	39
-0.20	16	96	54	32	40
-0.225	15	78	44	27	34
-0.25	11	63	35	20	30
-0.275	9	52	26	16	20
-0.30	10	42	20	16	20
-0.325	6	34	15	14	15
-0.35	5	22	12	13	18
-0.375	4	14	5	9	11
-0.40	0	15	0	5	9

Table 4. Continued

Table 4. Experimental Data for the Ion Profiles in the Acetylene
Flame.

IV. DISCUSSION.

IV.1. INTRODUCTION.

The discussion will consider the results from ethylene and acetylene in parallel, with due consideration being given to the results of other workers in this field. Where appropriate the differences and similarities of the two flames will be discussed in detail. The assignments of the ions for each flame are given in Tables 5. and 6. The assignments are based on carbon, oxygen and hydrogen, some peaks being attributable to isotopic satellites. Some of the ions were unidentified.

Mass, a.m.u.

Assignment.

16	O^-
17	OH^-
24	C_2^-
25	C_2H^-
32	O_2^-
33	HO_2^-
35	$^{35}Cl^-; OH^- \cdot H_2O$
36	C_3^-
37	$^{37}Cl^-; C_3H^-$
41	C_2HO^-
43	$C_2H_3O^-$
45	$CO_2H^-; C_2H_5O^-$
46	$^{13}CO_2H^-; ^{13}CCH_5O^-$
49	$HO_3^-; C_4H^-$
50	$O_2^- \cdot H_2O$
51	$HO_2^- \cdot H_2O$
53	$OH^- \cdot 2H_2O$
60	$CO_3^-; C_5^-$
61	$HCO_3^-; C_5H^-; ^{13}CO_3^-; ^{13}CC_4^-$
62	$H^{13}CO_3^-; ^{13}CC_4H^-$
63	$CO_2H^- \cdot H_2O$
64	$O_4^-; ^{13}CO_2H^- \cdot H_2O$
65	$CH_3O_2^- \cdot H_2O$

/contd.

Mass, a.m.u.	Assignment.
66	$O_3^- \cdot H_2O$
68	$O_2^- \cdot 2H_2O$
69	$HO_2^- \cdot 2H_2O$
71	$OH^- \cdot 3H_2O$
72	C_6^-
73	C_6H^-
76	CO_4^-
78	$CO_3^- \cdot H_2O$
79	$HCO_3^- \cdot H_2O$
84	$O_3^- \cdot H_2O$; C_7^-
85	$HO_3^- \cdot 2H_2O$; C_7H^- ; $^{13}CC_6^-$
87	$C_4H_7O_2^-$
88	?
90	?
92	?
94	$CO_4^- \cdot H_2O$
96	C_8^- ; $CO_3^- \cdot 2H_2O$
97	C_8H^- ; $HCO_3^- \cdot H_2O$; $^{13}CC_7^-$; $^{13}CO_3 \cdot 2H_2O$
105	$C_4H_7O_2^- \cdot H_2O$

Table 5. Assignments of Ions in the Ethylene Flame.

Mass, a.m.u.

Assignment.

16	O^-
24	C_2^-
25	C_2H^-
32	O_2^-
34	$O^- \cdot H_2O$
35	$OH^- \cdot H_2O$
36	C_3^-
37	C_3H^-
41	C_2HO^-
43	$C_2H_3O^-$
45	$CO_2H^-; C_2H_5O^-$
46	$^{13}CO_2H^-; ^{13}CCH_5O^-$
50	$O_2^- \cdot H_2O$
51	$HO_2^- \cdot H_2O$
53	$OH^- \cdot 2H_2O$
60	$CO_3^-; C_5^-$
61	$HC\dot{O}_3^-; C_5H^-$
63	$CO_2H^- \cdot H_2O$
64	$O_4^-; ^{13}CO_2H^- \cdot H_2O$
73	C_6H^-
74	?
75	?
76	CO_4^-

/contd.

Mass, a.m.u.	Assignment.
78	$\text{CO}_3^- \cdot \text{H}_2\text{O}$
79	$\text{HCO}_3^- \cdot \text{H}_2\text{O}$
81	$\text{CO}_2\text{H}^- \cdot 2\text{H}_2\text{O}$
87	$\text{C}_4\text{H}_7\text{O}_2^-$
90	?
91	?
92	?
96	$\text{C}_8^-; \text{CO}_3^- \cdot 2\text{H}_2\text{O}$
97	$\text{C}_8\text{H}^-; \text{HCO}_3^- \cdot 2\text{H}_2\text{O}$

Table 6. Assignment of Ions in the Acetylene Flame.

IV.2. THE PRESENCE OF CHLORINE IN THE ETHYLENE FLAME.

The two ions which occur at 35 a.m.u. and 37 a.m.u. are attributable to chlorine, which forms a very stable negative ion, Cl^- . Although these two ions could be entirely attributable to the two ions, $\text{OH}^- \cdot \text{H}_2\text{O}$ and C_3H^- , the signals observed from both are too large to be produced from the related neutrals of these species. Both profiles peak at a similar place in the flame, (0.15 - 0.175 mm upstream of the reaction zone) and the proportions of signal strength at 0.025 mm intervals along each profile result in the correct isotopic abundance for the two chlorine isotopes ^{35}Cl and ^{37}Cl of 67.5% and 32.5% respectively. However, this still leaves a small signal for m/e 35, which can be attributed to $\text{OH}^- \cdot \text{H}_2\text{O}$, Fig. 23.

Before the experiments on ethylene were run, some dilute sodium chloride solution had been aspirated into the flame in order to check the calibration of the mass spectrometer for negative ions, (at 35 a.m.u. and 37 a.m.u.). It is probable that some of this solution was deposited on the inner surface of the burner, thus interacting at a later stage to produce the two strong signals reported. To allow for this, the signal intensities of these two ions has^{ve} been omitted for the calculations of the relative ion currents for the individual ions.

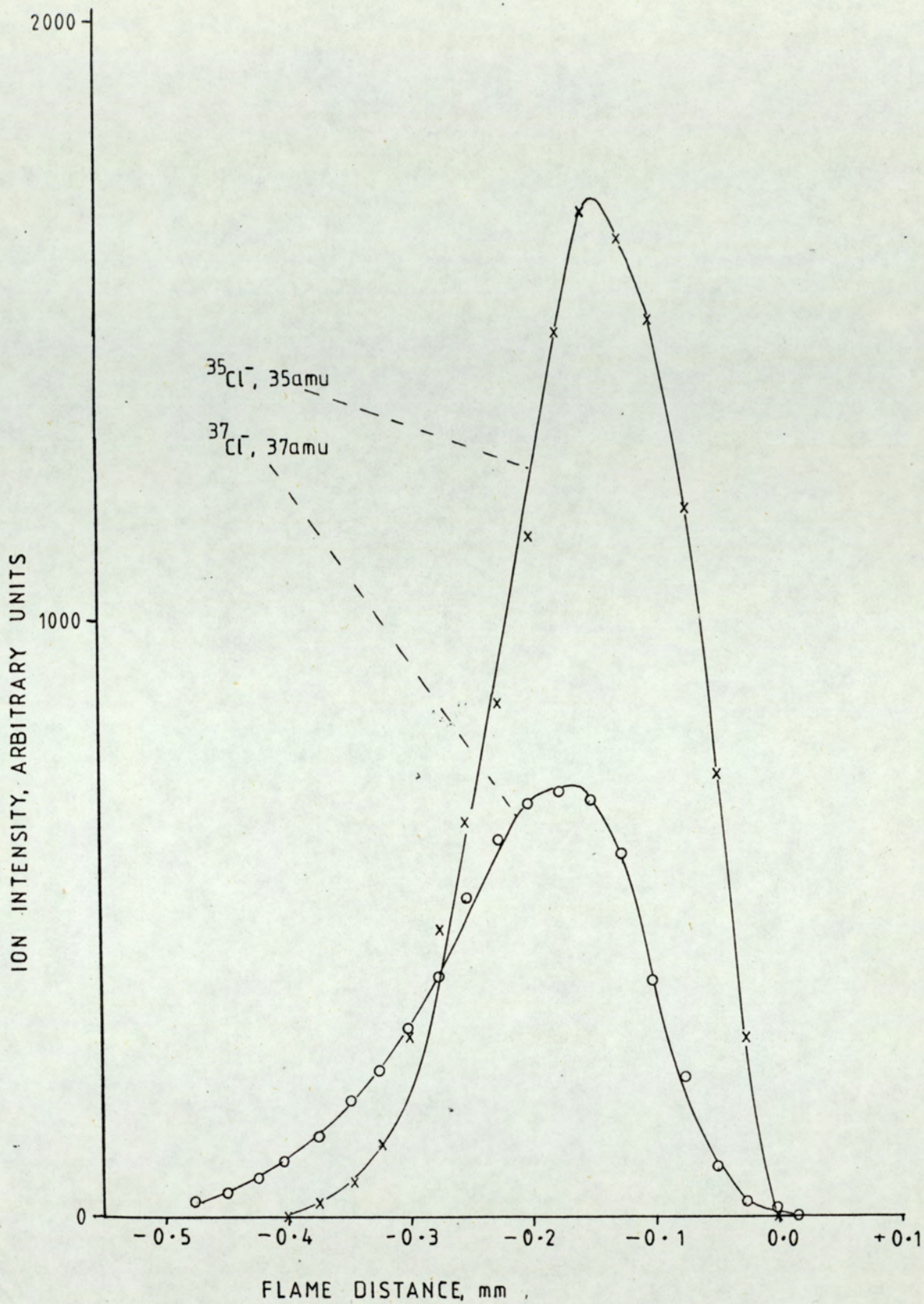


Figure 23. Ion Profiles for 35 a.m.u. and 37 a.m.u. in Flame F1

IV.3. THE DIFFERENCE BETWEEN THE ION INTENSITIES OF THE TWO
FLAMES

The most notable feature of the flame containing acetylene was that the intensity of the ion signals was greatly reduced when compared to the flame containing ethylene, by a factor of 5, for example, for m/e 45. This marked difference can be traced to the fact that chlorine was identified in flame F1. The large peaks at 35 a.m.u. and 37 a.m.u. are absent in flame F2, thus the strongly electronegative chlorine may have been a primary ion for the other ions observed. However, most of the ions observed in the ethylene flame have been reported previously, (6), also nearly all the ions found in flame F2 were seen in the experiments for flame F1, so the presence of Cl^- does not prejudice the results and discussion to a great extent.

Some of the ions which would be expected to be formed in flame F2 are absent; this is probably due to the much lower total ion current for this flame. However, by comparison with the ethylene flame and with particular regard to possible hydrates, most of the parent ions can be discussed, although they may be absent.

Some of the profiles in flame F2 have peculiar shapes, peaking at more than one position in the flame. The weakness of some of these signals results in a low signal to noise ratio, and the averaging technique as previously described becomes inaccurate. Therefore the positions of these species can

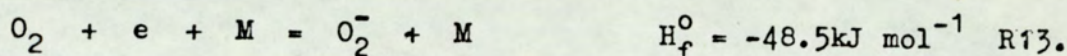
only be regarded as tentative.

IV.4. O₂⁻ FORMATION.

The primary negative ion in flame chemistry is O₂⁻, (32 a.m.u.) O₂⁻ is formed by attachment of most of the free electrons to O₂, which is in high concentration, at least in the cool upstream region of the reaction zone. The ion chemistry commences upstream with the reaction



O₂⁻ is formed by the three-body process:-



The CHO⁺ and O₂⁻ are formed in a neutral-rich regime, with which they can react. O₂⁻ can react in several different ways with neutral species:-

1. Charge transfer of electrons will occur for neutrals of increasing electron affinity.
2. Proton transfer reactions may occur to produce negative ions whose base strength is lower than that of O₂⁻.
3. O₂⁻ may also undergo rearrangements with other neutrals in other processes.
4. O₂⁻ will form cluster ions by three-body attachment reactions.
5. Associative detachment reactions can also occur, whereby a neutral and an electron are formed.

Examples of these modes of reaction for O₂⁻ are to be found in Table 5. Thus O₂⁻ reacts with many neutrals in the flame regime. O₂⁻ peaks relatively late in the reaction zone, (Figs.24 and 25), (-0.15 mm for ethylene and -0.05 mm for acetylene). This

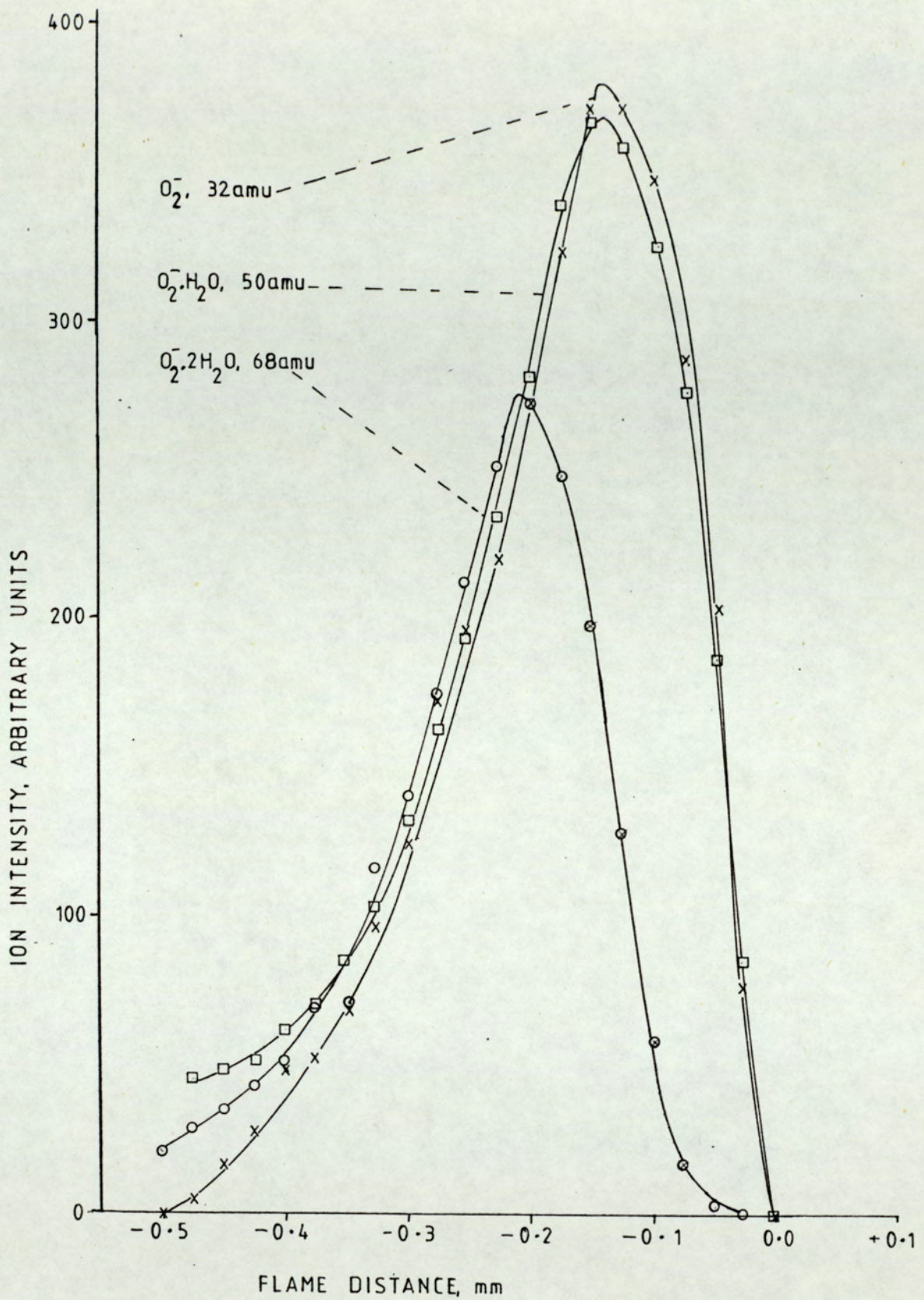


Figure 24. Ion Profiles for 32 a.m.u., 50 a.m.u. and 68 a.m.u. in Flame F1.

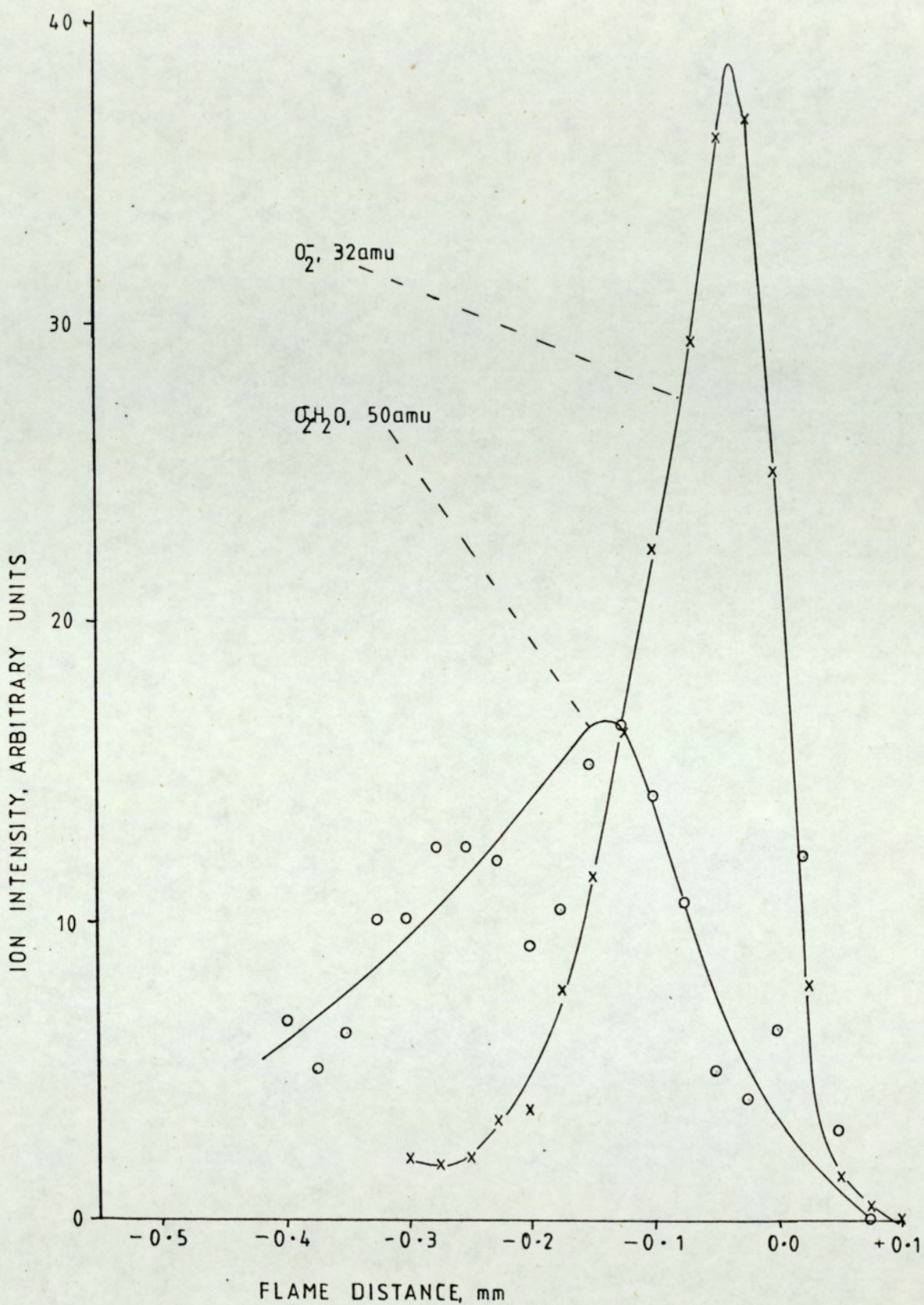


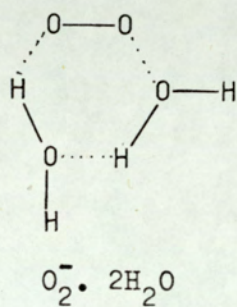
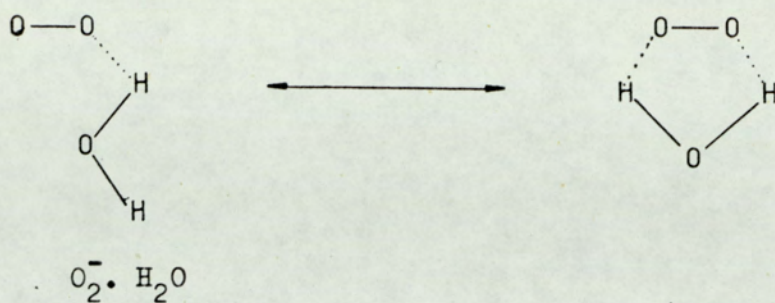
Figure 25. Ion Profiles for 32 a.m.u. and 50 a.m.u. in Flame F2

reflects the ready consumption of O_2^- for many chemi-ionization reactions with neutrals earlier in the flame. The O_2^- concentration was 3% of the total for flame F1, and 1% for flame F2.

Comparison of the different concentrations is difficult, since acetylene may favourably form neutral species with which O_2^- can react, in different concentrations to these same reactions for ethylene.

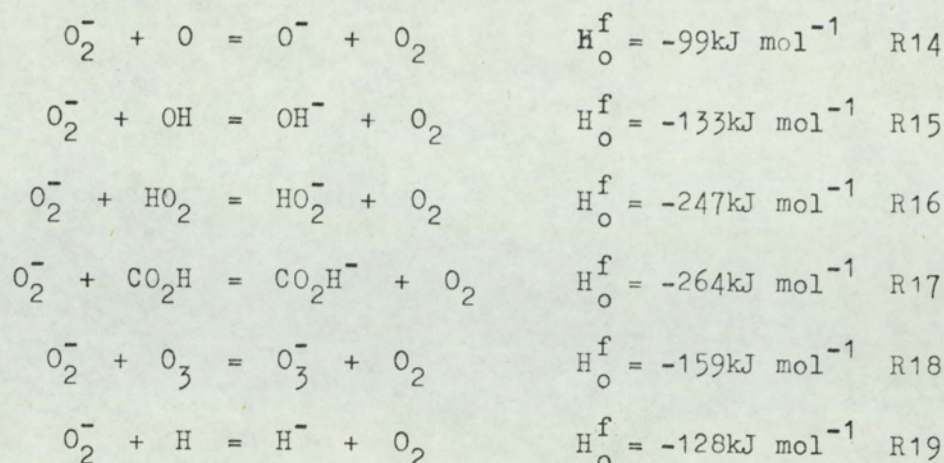
O_2^- appears to form hydrates, the ions at 50 a.m.u. and 68 a.m.u. corresponding to the monohydrate for both flames and the dihydrate for flame F1. Evidence for these ions being hydrates can be attributed to their similarities with the parent ion in peak shape and to the characteristic upstream extension of their ion profiles, suggesting water attachment is favoured at lower temperatures. For the ethylene flame, the first hydrate is as intense as the parent ion; this suggests that a large proportion of the O_2^- is stabilised by hydrate formation at the cooled surfaces of the system. However, for the acetylene flame, the monohydrate signal is half as intense as that for the parent ion. This may indicate that O_2^- formed in this instance is formed at a hotter position in the flame, the possibility of interaction with the cooler, sampling surfaces being less likely. This may be further exemplified by the fact that the dihydrate is not seen for flame F2. For F1, the dihydrate is less intense, and peaks further upstream in the reaction zone. This indicates that it is likely to be formed on a cooled surface, the possibility of formation decreasing as the reaction zone temperature increases.

The hydrated ions may be drawn:-

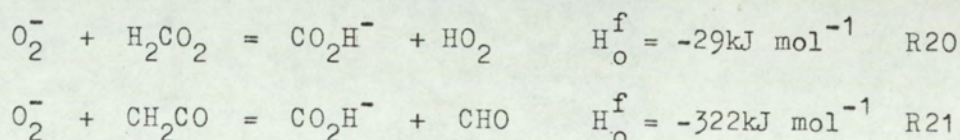


It seems plausible that the ring structures could occur on hydrate formation. If so, they help to explain why the hydrated forms of the parent ion are stable.

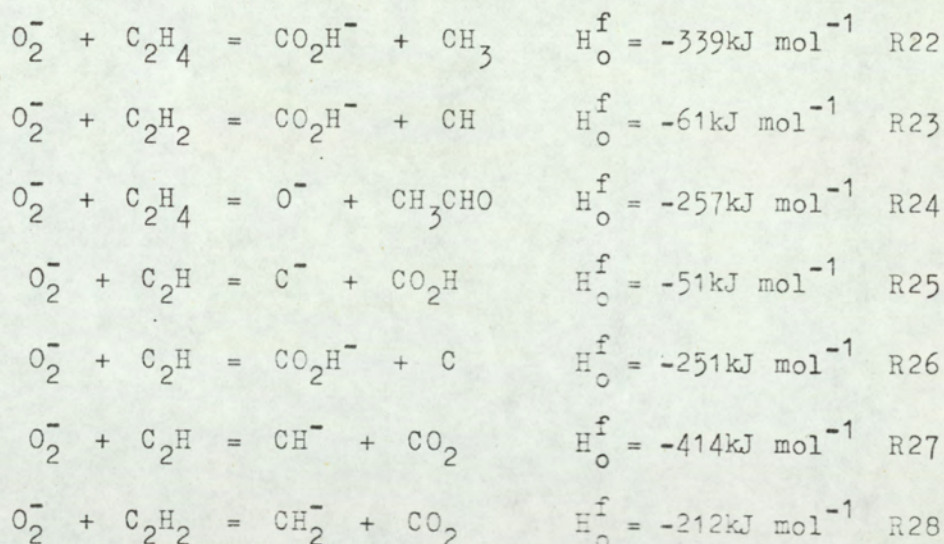
Charge Transfer Reactions.



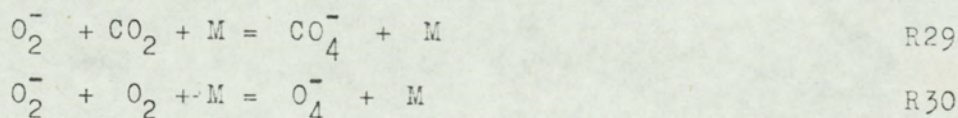
Proton Transfer Reactions.



Rearrangement Reactions.



Clustering Reactions.



Associative Detachment Reactions.

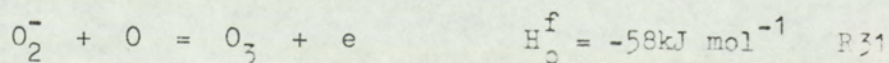


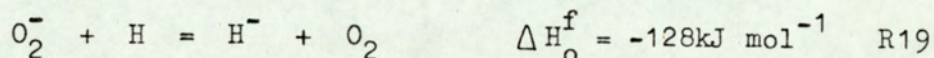
Table 7. Modes of Formation of Negative Flame Ions With O_2^- as the Primary Ion.

IV.5. IONS FORMED BY CHARGE TRANSFER OF NEUTRALS WITH O_2^- .

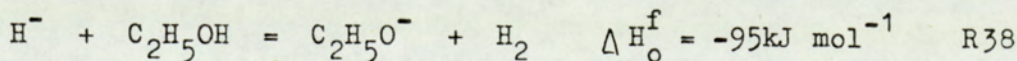
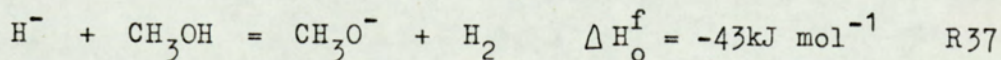
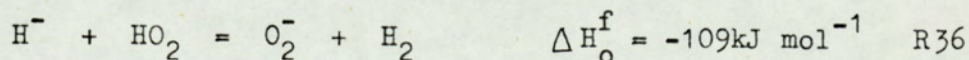
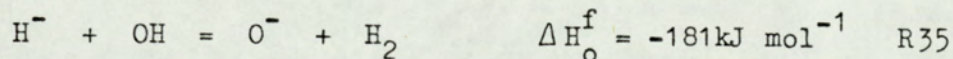
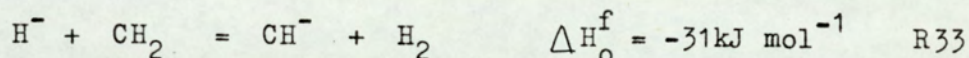
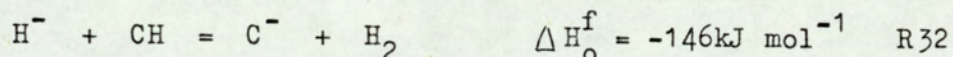
Neutrals whose electron affinity is larger than that of O_2 will form negative ions on reaction with O_2^- by charge transfer processes. Table 8 gives electron affinities of neutrals, and standard heats of formation of negative ions.

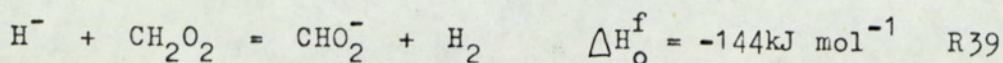
IV.5.i. H^- , 1 a.m.u.

Although H^- was detected, and quite large signals measured, it cannot be unambiguously suggested as an ion found in flames. This is due to the inability of diffusion pumps to completely remove hydrogen from the pump oil. However the reaction

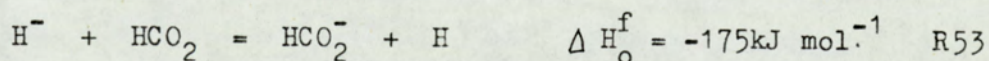
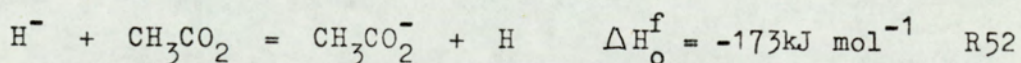
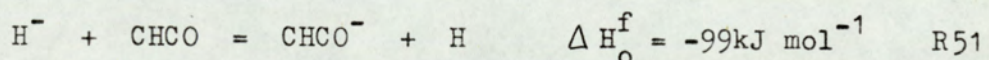
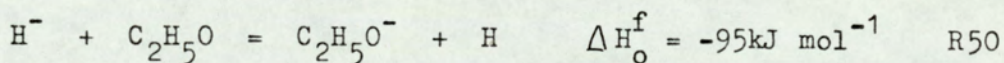
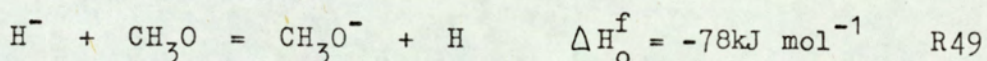
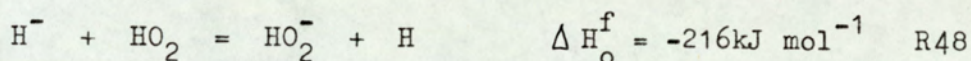
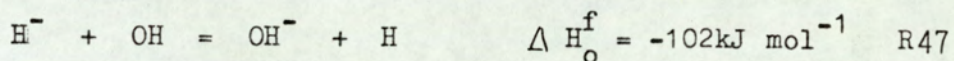
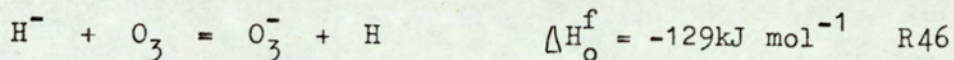
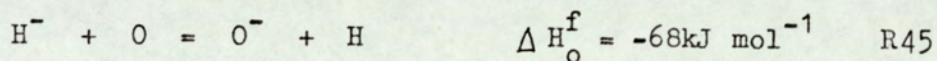
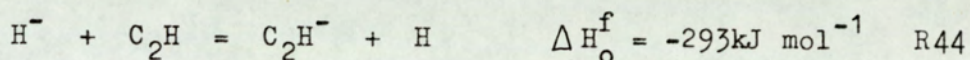
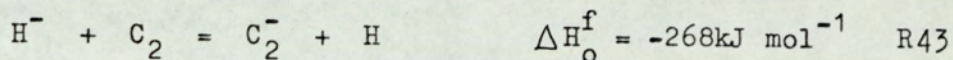
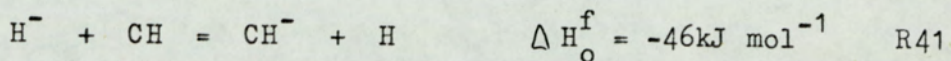
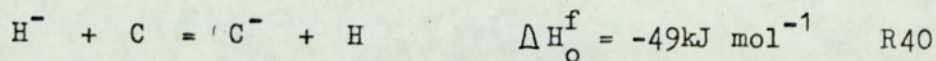


is thermodynamically favourable and quite plausible as a flame reaction. H^- would be expected to disappear by proton transfer reactions with a variety of species, e.g.

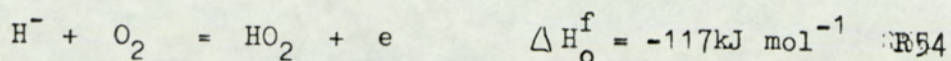




or by charge transfer reactions with neutrals whose electron affinities are higher than that of H :-



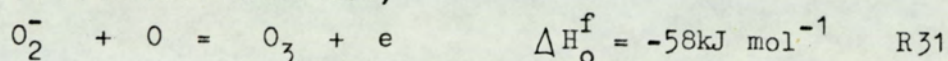
Finally, H^- could decay by virtue of associative detachment reactions such as:-



IV.5.ii O^- , 16 a.m.u.

O^- peaks fairly late in the reaction zone, (0.1mm upstream for both flames) and has rather a small profile (Fig. 26.).

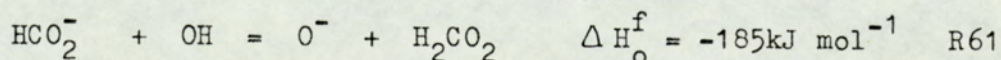
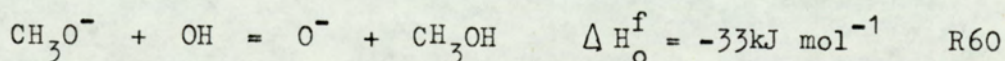
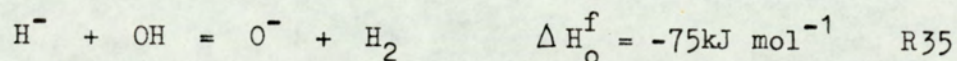
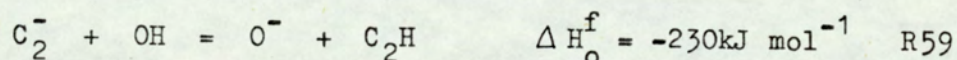
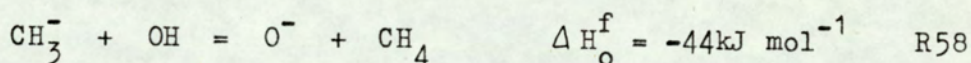
Formation by reaction R14, Table 7, is possible although the associative detachment reaction,



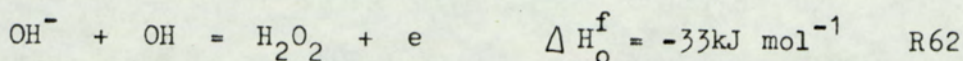
for which $k = 2 \times 10^{-10} \text{cm}^3 \text{mol}^{-1} \text{sec}^{-1}$ at 300K (33), is

predominant at room temperatures.

O^- could also be produced by proton abstraction of OH by several ionic species of stronger basicity than O^- , e.g.

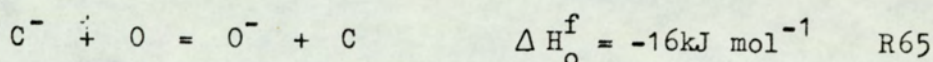
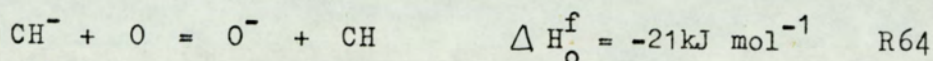
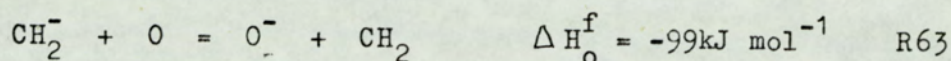


These reactions may predominate at higher temperatures, although associative detachment reactions such as



may predominate at lower temperatures. Table 9 gives the base strengths of a number of flame ions.

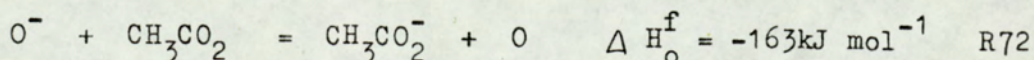
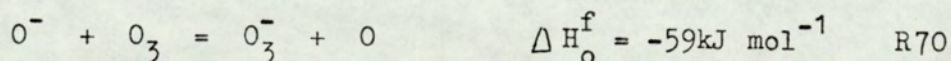
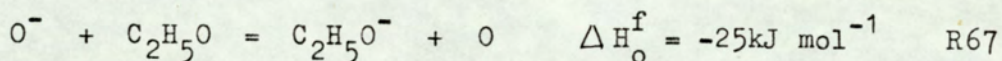
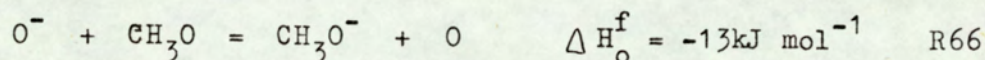
Since the electron affinity of O^- is quite low, only a few flame ions would be expected to produce O^- by charge transfer:-

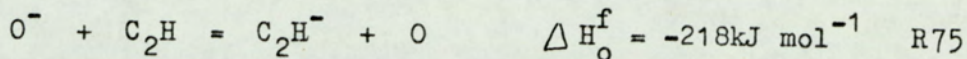
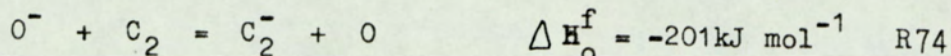
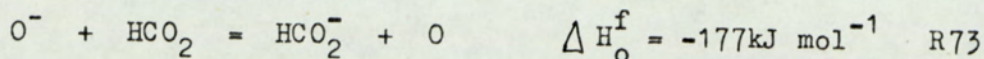


Thus O^- may be formed from the two neutrals, O and OH.

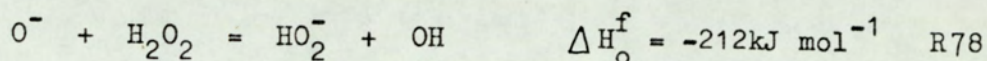
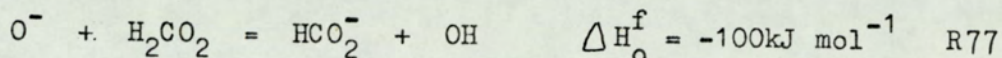
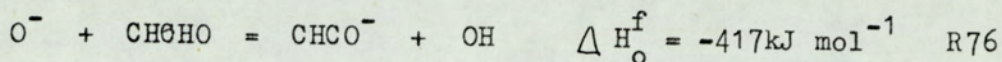
Most of the proton abstraction reactions would occur at the hotter region of the reaction zone, this partly explaining the late peaking of the profile. Loss of O^- by reaction with other neutrals would also show a reduction in the observed profile.

Charge transfer reactions may occur:-

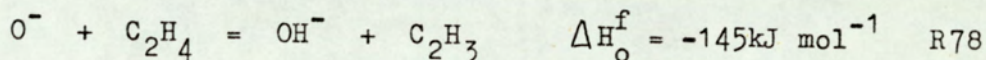




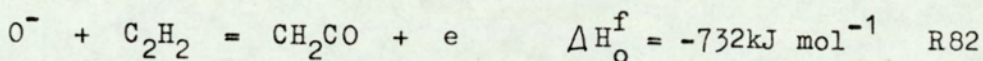
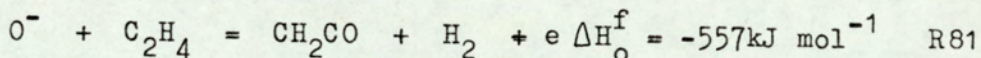
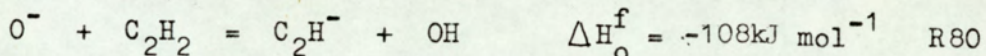
or proton transfer reactions:-



O^- may react directly with the two hydrocarbon fuels:-



$$k = 10^{-10} \text{ cm}^3 \text{ mol}^{-1} \text{ sec}^{-1} \text{ at } 300K, (33)$$



Ethylene can react with O^- , giving the hydroxyl ion. However, this reaction is not possible with acetylene, being endothermic, R79.

The dissociative attachment reactions, R81 and R82 are both possible however, and these reactions may contribute to the lowering of the intensity of the O^- ion profile. Also, since the rearrangement reaction, (R78), favours ethylene, the ion profile in flame F2 would be expected to be larger, which it is.

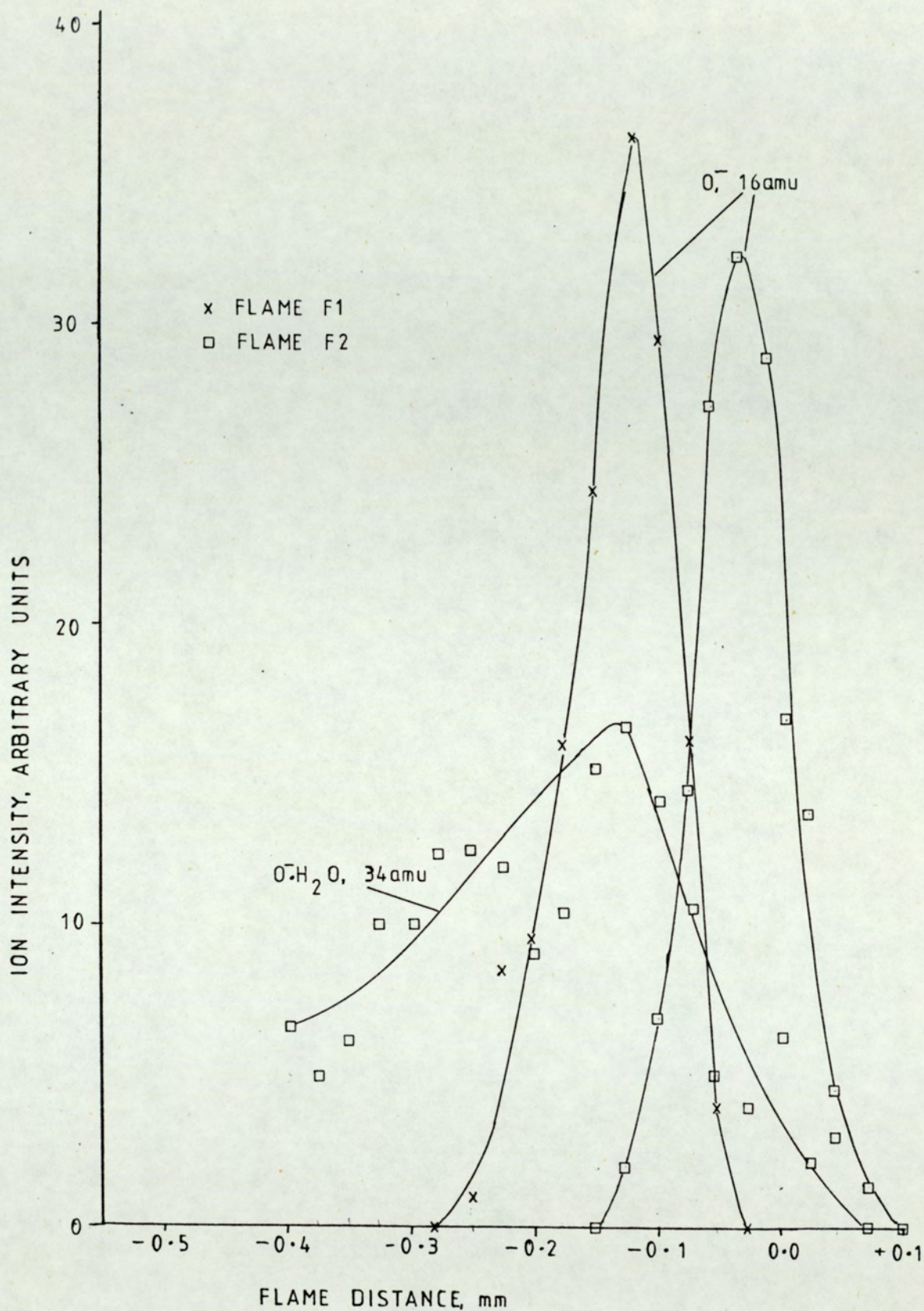


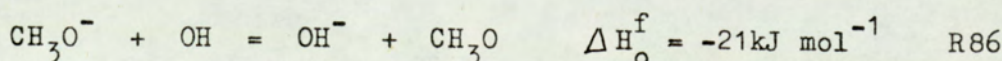
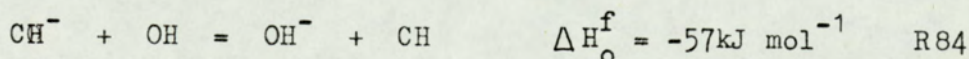
Figure 26. Ion Profiles for 16 a.m.u. and 34 a.m.u.

A very weak profile was noted at 34 a.m.u. in flame F2, this is probably due to the hydrated ion $O^{\cdot-}.H_2O$. This profile cannot be discussed satisfactorily because much of the signal is lost in background noise. Therefore it is simply noted that $O^{\cdot-}$ may form a hydrate.

IV.5.iii. $OH^{\cdot-}$, 17 a.m.u.; $OH^{\cdot-}.H_2O$, 35 a.m.u.; $OH^{\cdot-}.2H_2O$, 53 a.m.u.;
 $OH^{\cdot-}.3H_2O$, 71 a.m.u.

For flame F1 the intensity of the ion profile related to $OH^{\cdot-}$ is rather small. For flame F2, this profile was non-existent, (Fig. 27.). A reasonable profile was obtained for the first hydrate in the acetylene flame, but the profile for the second hydrate was so weak that sensible interpretation is impossible. It is better to interpret the $OH^{\cdot-}$ formed with reference to flame F1, although further complications arise because the bulk of the peak at 35 a.m.u. is due to $^{35}Cl^{\cdot-}$.

$OH^{\cdot-}$ may form by charge transfer with $O_2^{\cdot-}$, reaction R15. The ion profile peaks at or near the downstream edge of the reaction zone, and it is possible that other charge transfer reactions may occur, since it would be expected that these ions would have already formed. Thus,



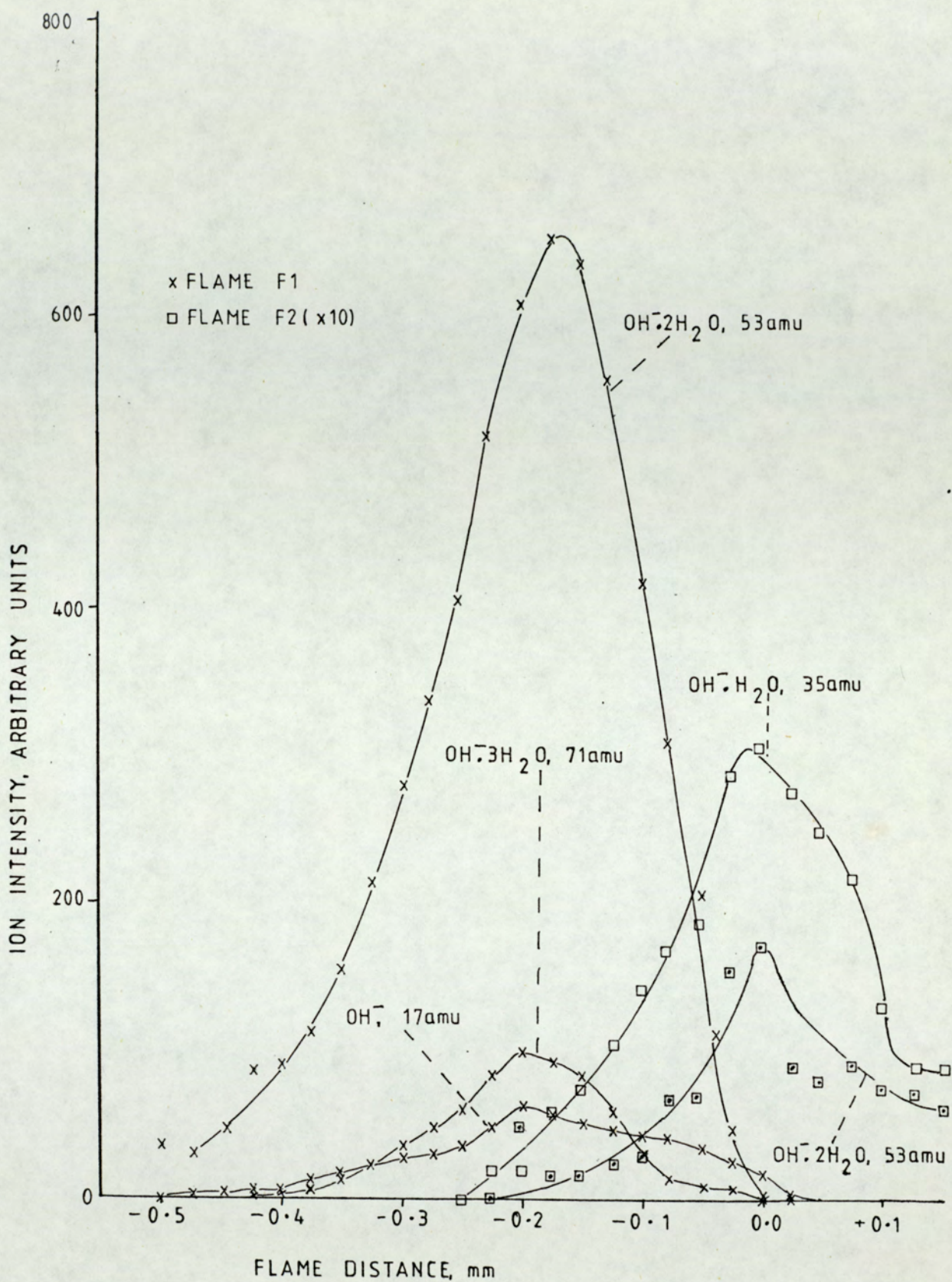
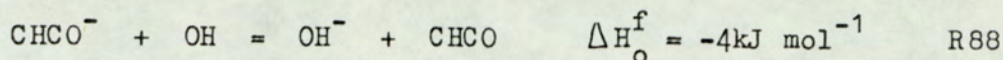
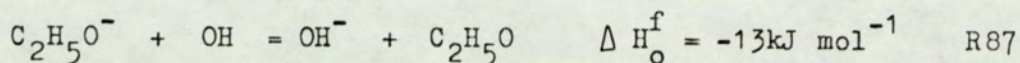
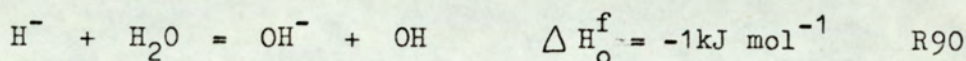
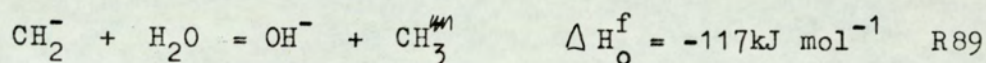


Figure 27. Ion Profiles for 17 a.m.u., 35 a.m.u., 53 a.m.u. and 71 a.m.u.

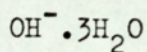
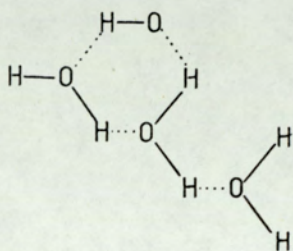
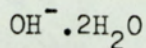
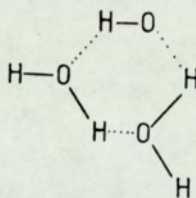
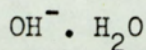
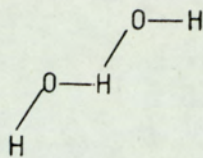


OH^- may also be formed by reactions involving the abstraction of protons from water by sufficiently strong basic negative ions. For example, ions such as CH_2^- , H^- , CH_3^- , C_2H_3^- , and C_2H_5^- are stronger bases than OH^- , and could produce OH^- , e.g.



However, with the possible exception of H^- , none of these ions were observed in either flame. This does not preclude their existence, since they are certainly reactive and may take part in other reactions (discussed later). As mentioned in the previous section, OH^- may be formed by reaction of O^- with ethylene, but not with acetylene; this could be a possible reason for the weaker signal obtained in flame F2.

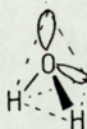
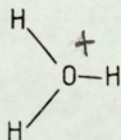
Several hydrates may be envisaged for OH^- . For flame F1 the stablest hydrate was the dihydrate, whereas the monohydrate was stablest for flame F2. This indicates that quite a large proportion of OH^- is stabilised via hydrate formation, and more secondary reactions occur for the ethylene flame. The dihydrate can presumably form a ring structure, thus delocalising the negative charge.



The first hydrate has recently been isolated in complexes containing sulphur and hydroxyl groups (34). It appears that the proton is placed symmetrically between two hydroxyl groups.

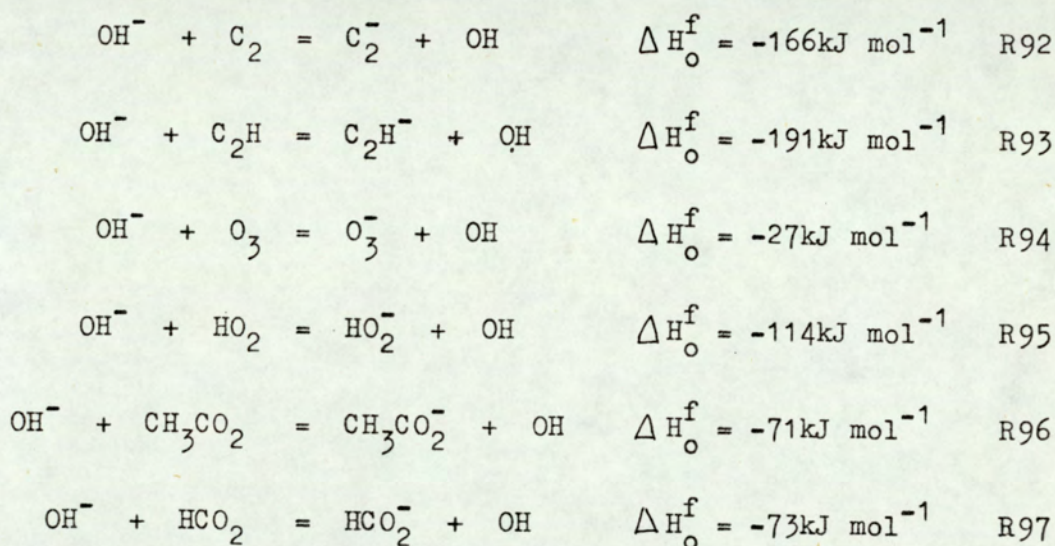
Crystallographic studies show that the distance between the oxygen atoms is 2.29 nm.

Various spectroscopic techniques (35) have also shown that the hydronium ion H_3O^+ exists as a planar ion, rather than having the same geometry as water, which is tetrahedral:-

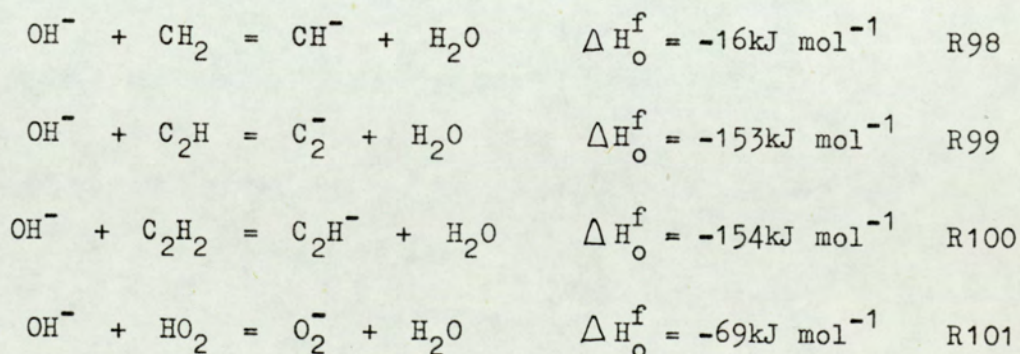


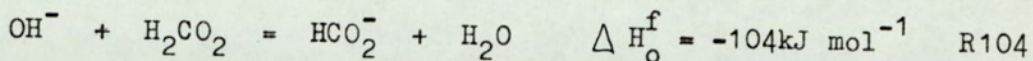
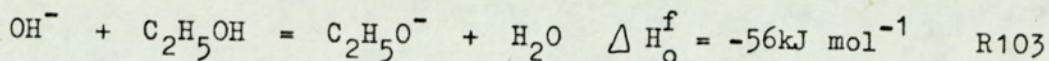
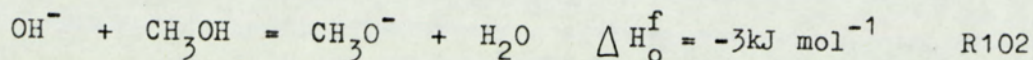
If this is the case, it seems plausible that hydrates may be formed, (for both positive and negative ions) and that reasonable structures can be assigned to them. Thus, for OH^- , the dihydrate would be the most stable structure, the trihydrate being less stable due to the third water molecule having to bond onto the side of the (presumably) stable ring structure of the dihydrate.

OH^- may react in several ways to produce other negative ions; by charge transfer to neutrals of higher electron affinity than OH^- :-

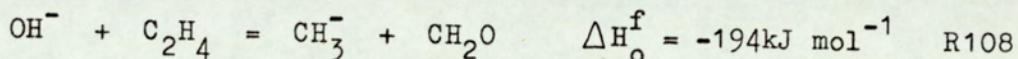
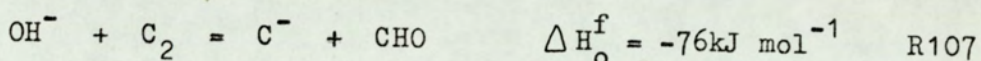
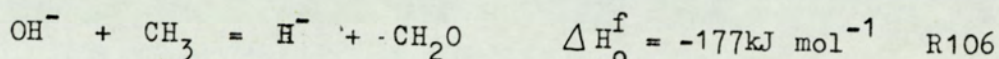
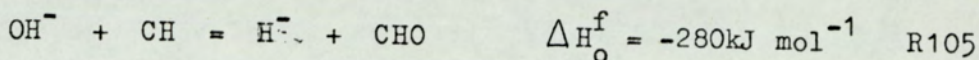


or by proton transfer:-

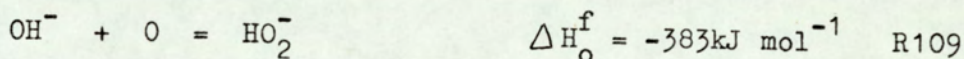




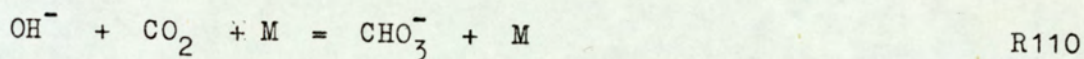
or by rearrangement processes:-



by associative attachment:-



and finally by three-body clustering:-



Many reactions are thermodynamically favourable for the consumption of OH^- , which explains its low ion profile.

IV.5.iv. HO_2^- , 33 a.m.u.; $\text{HO}_2^- \cdot \text{H}_2\text{O}$, 51 a.m.u.; $\text{HO}_2^- \cdot 2\text{H}_2\text{O}$, 69 a.m.u.

As with OH^- , little evidence of this ion is shown in the acetylene flame. No parent ion is present, and only a small amount of the supposed monohydrate is observed, (Fig. 28.).

This was the smallest ion signal observed for flame F2, and most of the discussion will consider the ethylene flame. In flame F1, HO_2^- is found upstream in the reaction zone. Other workers, (e.g. 6) report that HO_2^- is the earliest ion measured. In

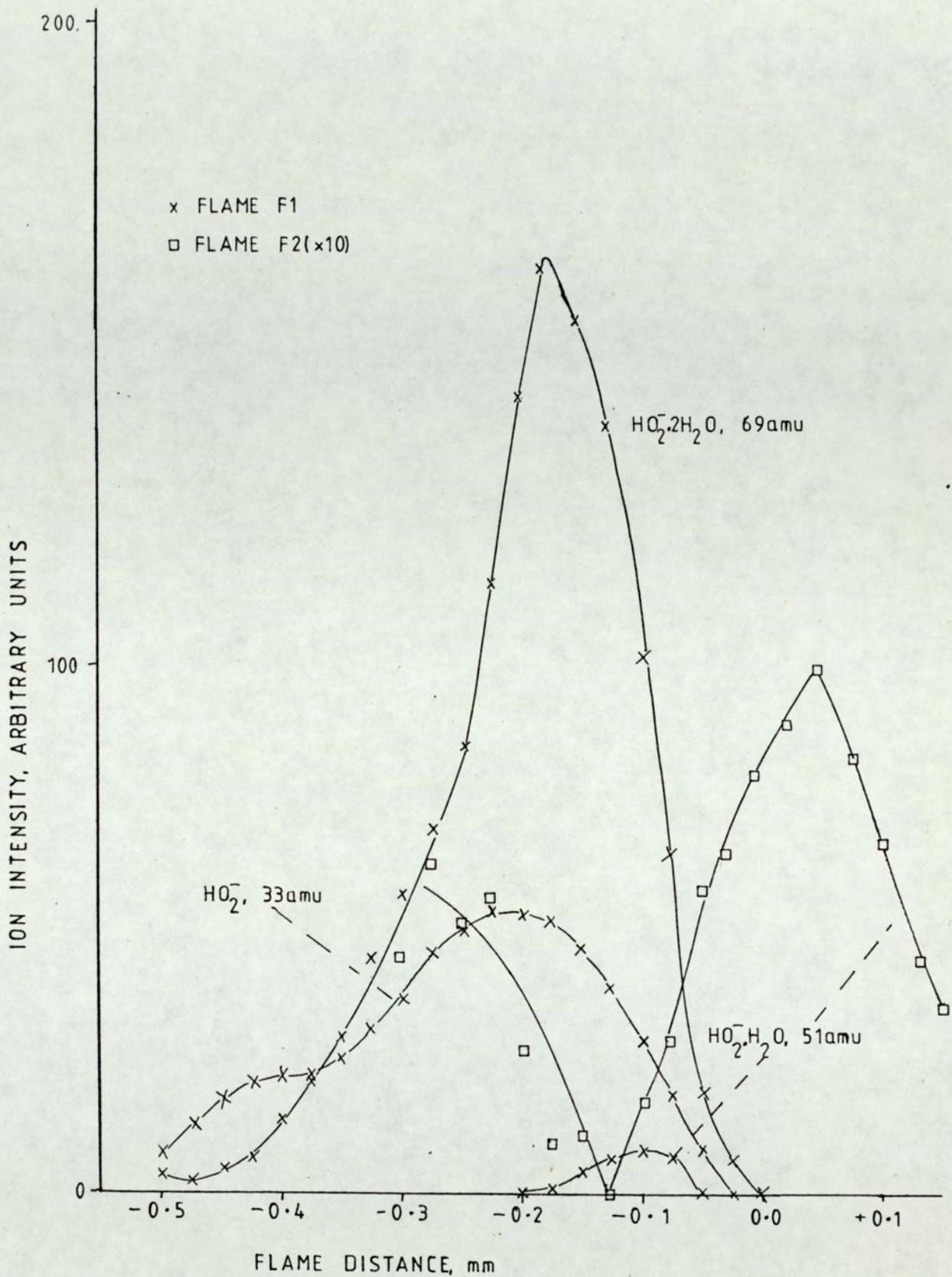
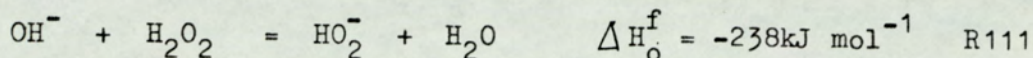


Figure 28. Ion Profiles for 33 a.m.u., 51 a.m.u. and 69 a.m.u.

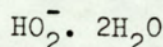
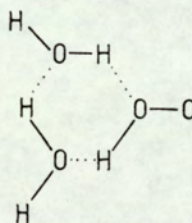
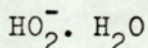
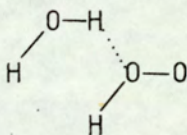
this system, other ions were found further upstream; this suggests that the sampling technique plays an important part in the formation of some of the species.

Apart from the charge transfer reaction with O_2^- , reaction R16, HO_2^- may arise from other sources, e.g. by proton transfer from H_2O_2 :-



Since HO_2^- is formed early in the flame, few other reactions for its formation are likely.

As with the other oxygenated species, HO_2^- forms hydrates. The stablest appears to be the dihydrate, in flame F2, which may be visualised as having a ring structure:-



The monohydrate is even weaker than HO_2^- itself but this would be expected since an open structure would not help to delocalise the extra electron.

HO_2 radicals could be expected to form from associative detachment reactions such as



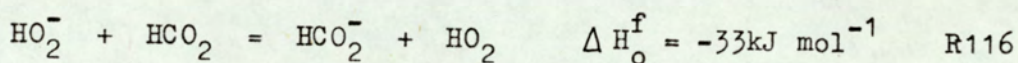
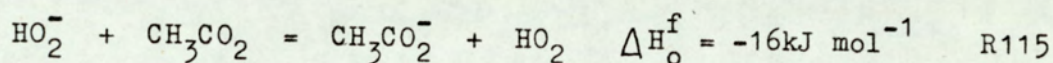
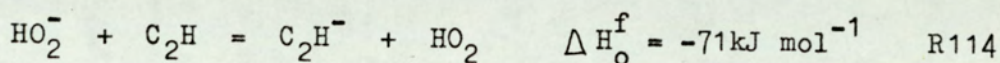
or by the slow oxidation of hydrocarbons:-



R112

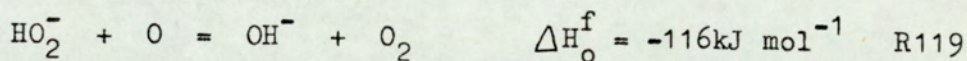
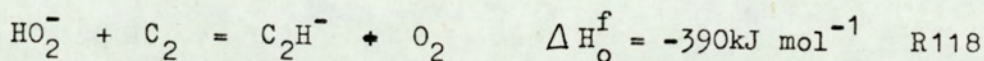
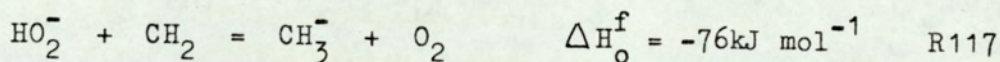
This type of reaction would presumably occur at the sampling wall since this oxidation reaction would proceed too slowly in the main reaction zone of the flame, (36).

HO_2^- is extremely electronegative and the negative ion will only undergo a few charge transfer reactions with other flame neutrals, e.g.:-



No proton abstraction reactions appear possible, whereby H is abstracted from a neutral to form hydrogen peroxide and an ion.

This is due to the low basicity of HO_2^- . A few proton transfer reactions are possible:-



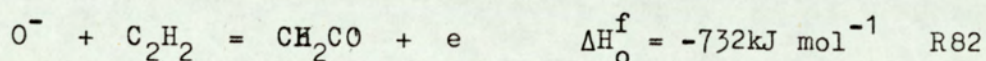
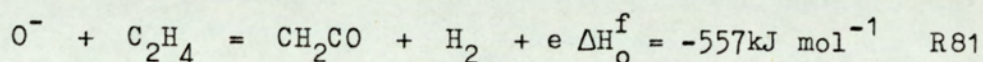
It appears therefore, that HO_2^- is a fairly stable negative ion, few reaction pathways ^{being} available for its consumption. However, little of the ion is formed, suggesting that its parent neutrals, HO_2 and H_2O_2 are in low concentration, being difficult

to form from the available negative ion species.

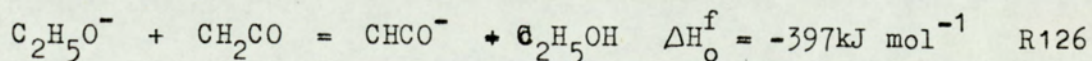
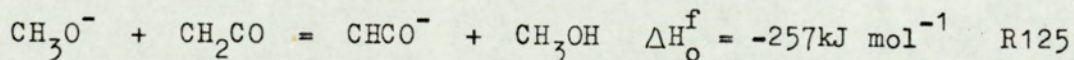
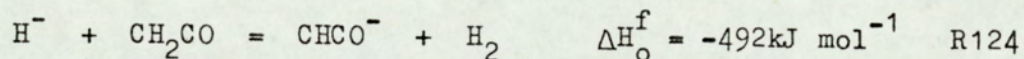
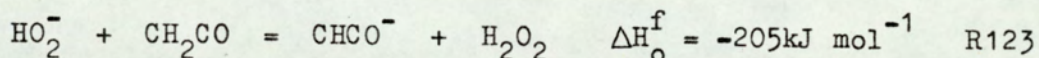
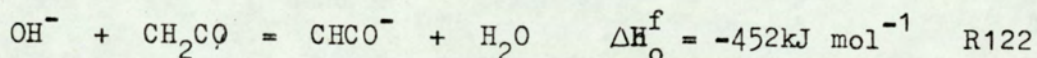
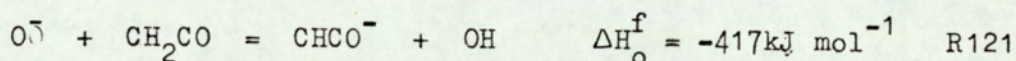
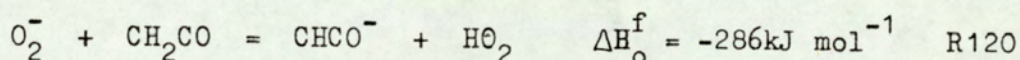
IV.4.v. C_2HO^- , 41 a.m.u.

This ion was observed in both flames (0.6%, -0.1mm for F1, 0.9%, -0.1mm for F2), Fig. 29. This ion profile is almost identical for both flames, suggesting a common mode of formation, and no particular reliance on the fuel used.

C_2HO^- is derived from ketene, $H_2C:C:O$ which could be produced by ion-molecule reactions on both ethylene and acetylene:-



Ketene itself may react to yield the negative ketylid ion by proton abstraction:-



$CHCO^-$, of course can form from the neutral $CHCO$ by charge transfer reactions, e.g.:-

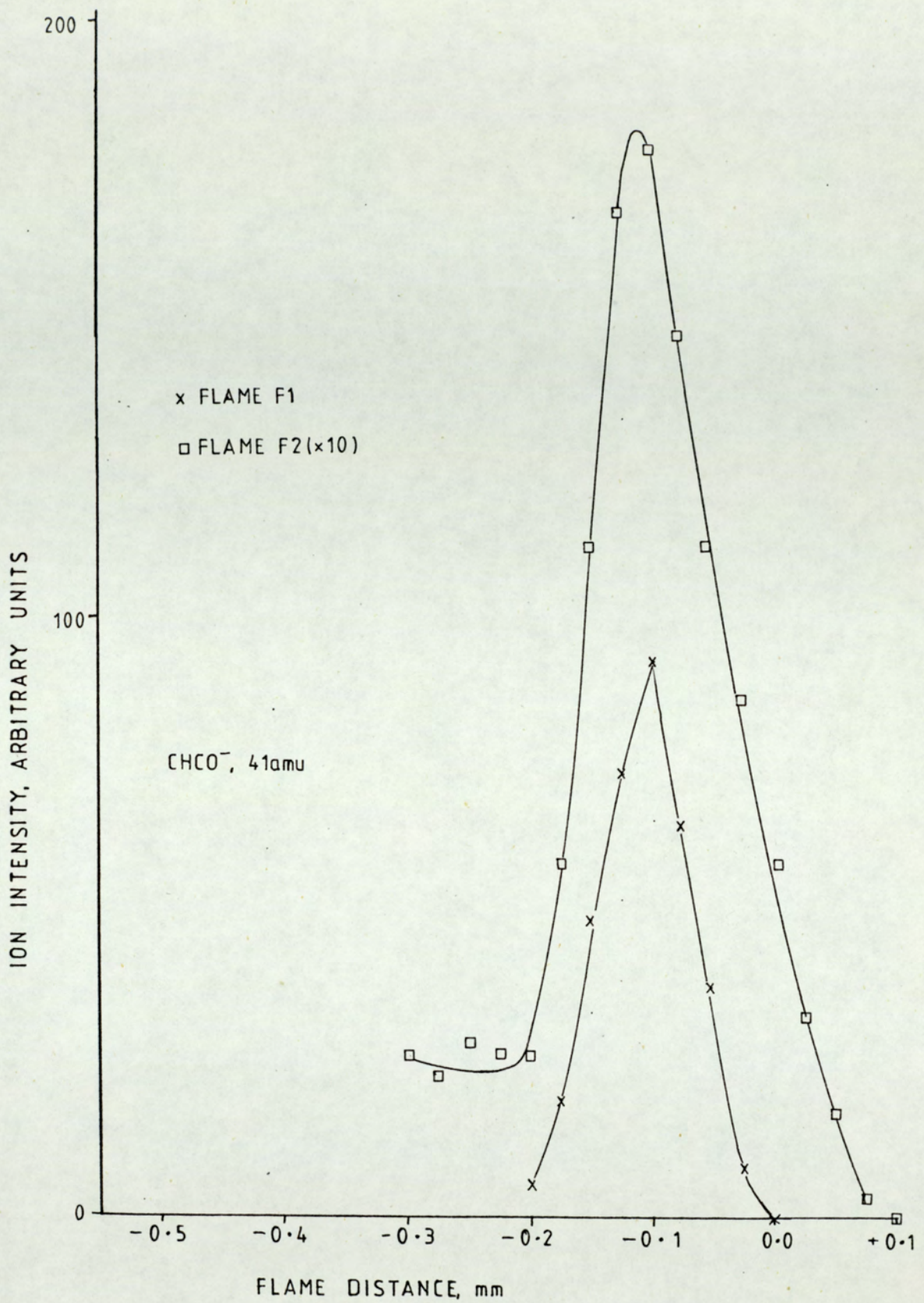
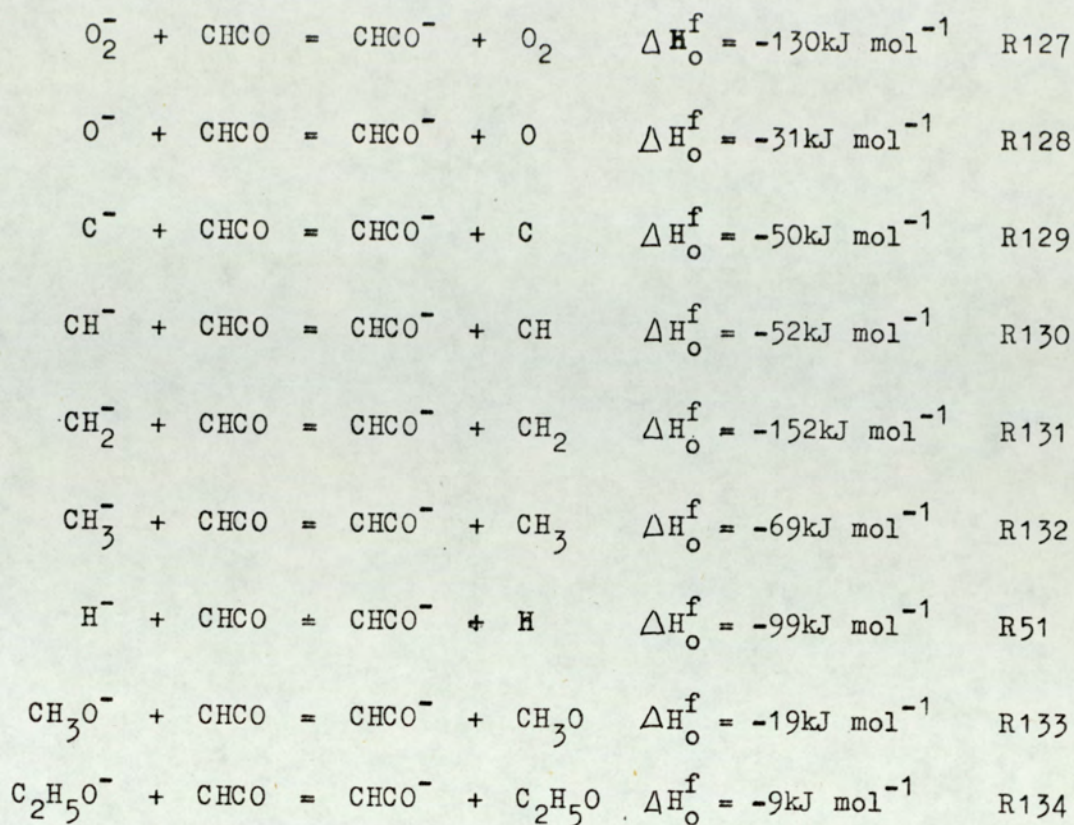
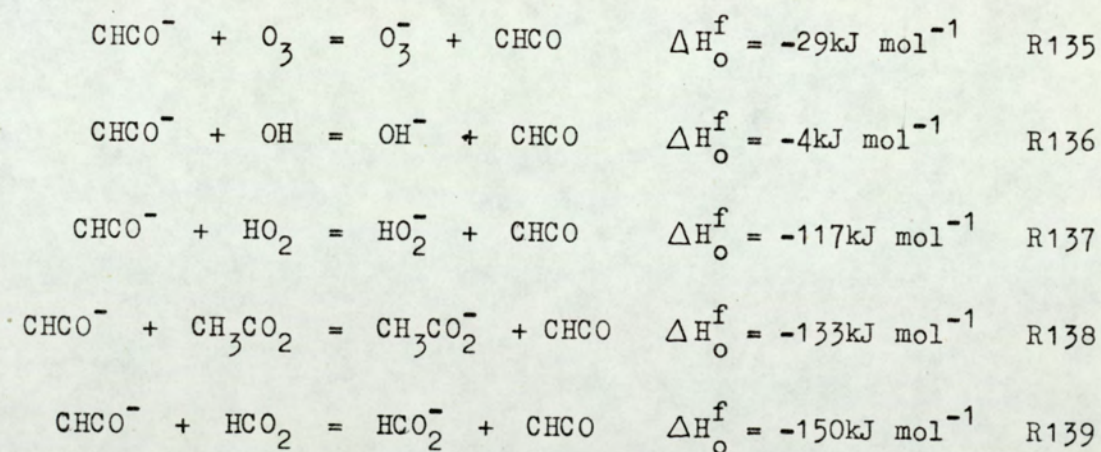


Figure 29. Ion Profiles for 41 a.m.u.

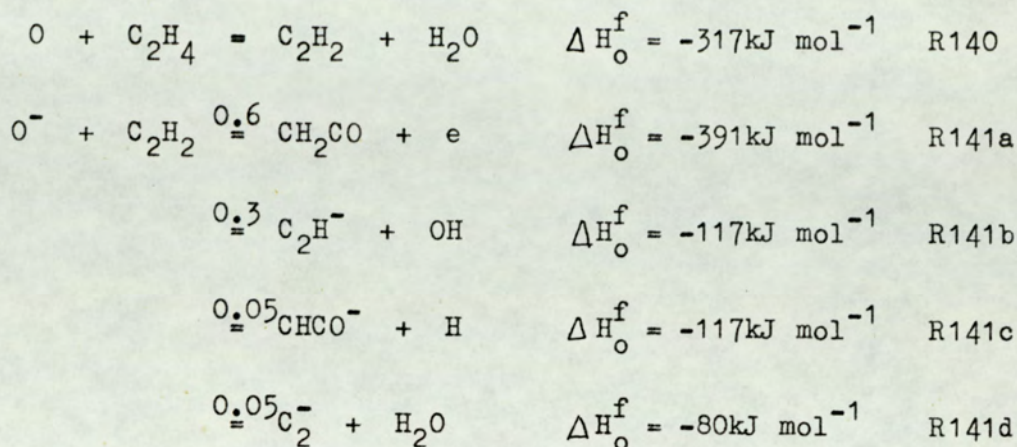


CHCO⁻ is quite strongly electronegative; its consumption precludes many charge transfer reactions, but a few are feasible:-



Proton transfer reactions, whereby the neutral, ketene is reformed are unlikely to occur, due to the endothermicity of ketene, ($\Delta H_{\text{O}}^{\text{f}} = +328\text{kJ mol}^{-1}$). Thus, once formed CHCO⁻ is quite a stable negative ion, few reactions being thermodynamically

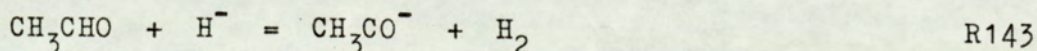
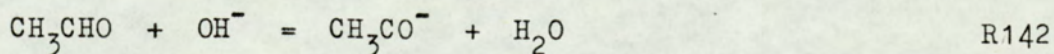
favourable for its consumption. However, little appears to be formed, probably because ketene formed from the hydrocarbon fuel competes with other reactions, e.g.:-



These proportions have been measured at room temperature, (37).

IV.5.vi. $\text{C}_2\text{H}_3\text{O}^-$, 43 a.m.u.

This ion was formed in both flames, (F1, 1%, -0.05 mm from the downstream edge of the reaction zone; F2, 2%, -0.14 mm) $\text{C}_2\text{H}_3\text{O}^-$ peaks at different places for the two flames, (Fig.30.)- this makes it difficult to decide whether this ion is a true flame ion or a spurious ion produced by collision on the sampling wall. No thermodynamic or kinetic information is known for this ion, but its neutral would presumably be fairly strongly electronegative, of the same order as $\text{C}_2\text{H}_5\text{O}$, 163kJ mol^{-1} . Thus the neutral, $\text{C}_2\text{H}_3\text{O}$ would react by charge transfer with most of the flame ions to yield $\text{C}_2\text{H}_3\text{O}^-$. Also, it would probably form from acetaldehyde by proton transfer reactions, e.g.:-



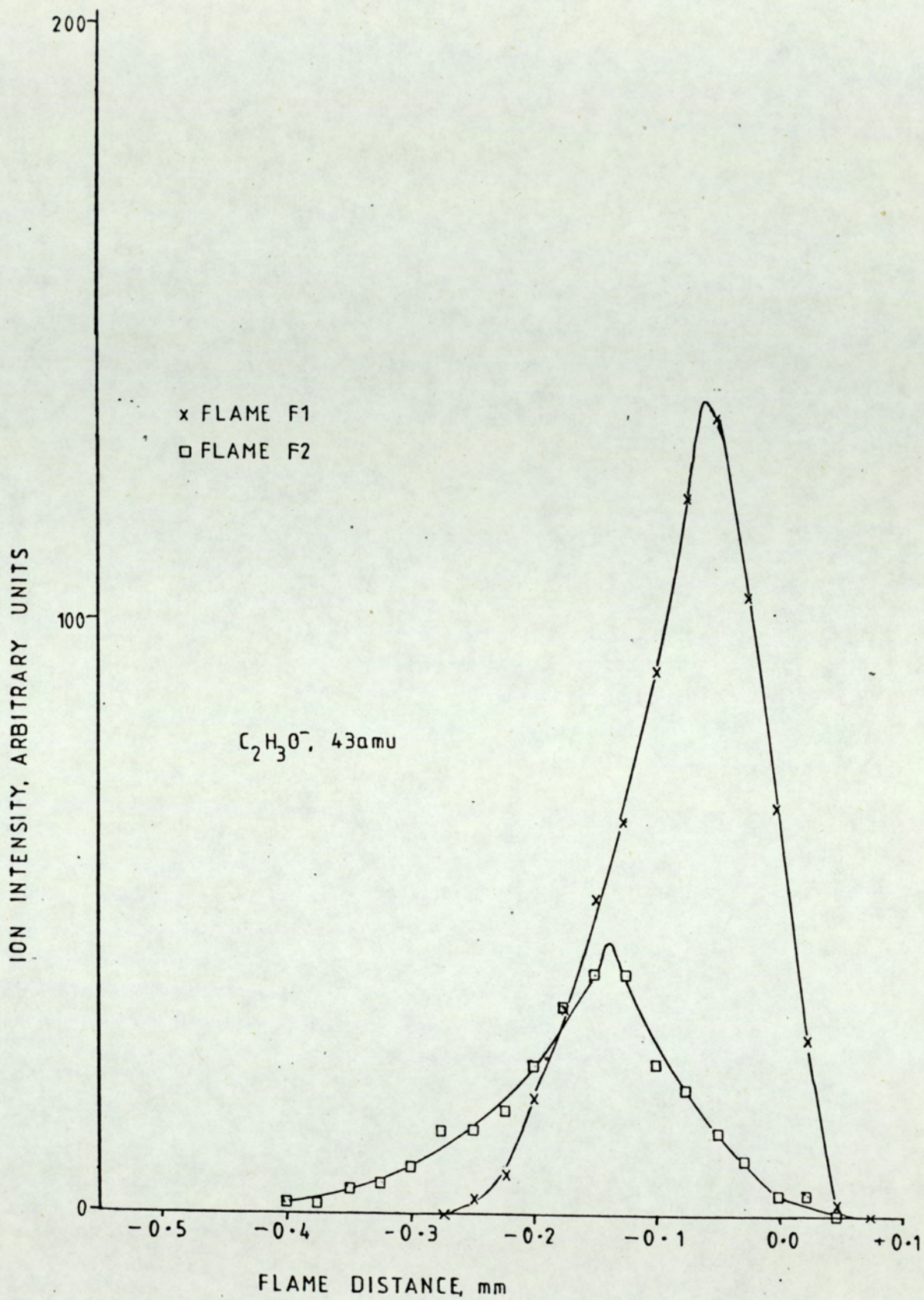


Figure 30. Ion Profiles for 43 a.m.u.



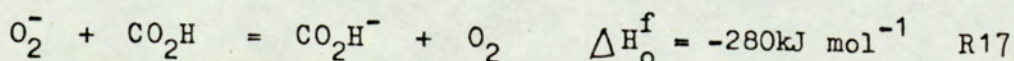
R144

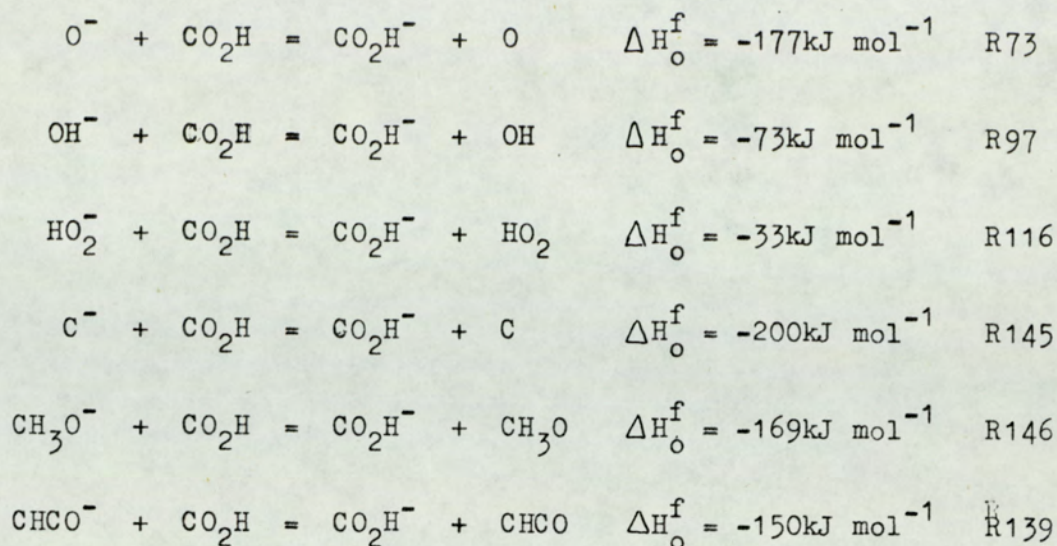
It would be expected that this ion would form hydrates and there are ions at 61, 79, and 97 a.m.u. which could correspond to the respective three hydrates. However, these ions peak earlier in the flame, and could be hydrates of the ion at 61 a.m.u., HCO_3^- , whose profile they resemble. That CH_3CO^- has a small profile can be explained by its probable rapid reaction with acetaldehyde to form 3-hydroxybutanal, (discussed later).

IV.5.vii. CO_2H^- , 45 a.m.u.; $^{13}\text{CO}_2\text{H}^-$, 46 a.m.u.; $\text{CO}_2\text{H}^- \cdot \text{H}_2\text{O}$, 63 a.m.u.

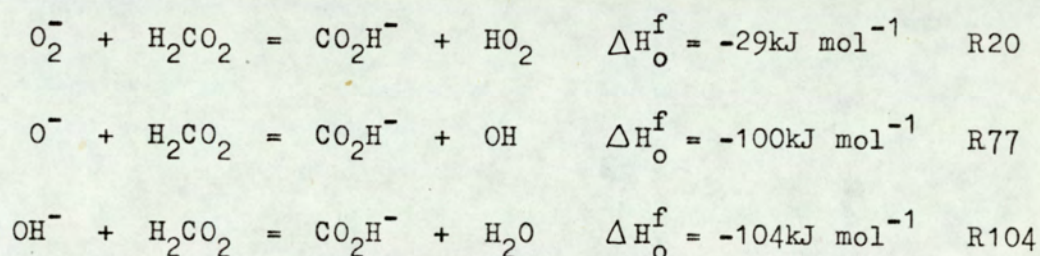
The ion observed at 45 a.m.u. is the largest negative ion profile measured in lean flames. For the ethylene flame, the parent ion exhibits a broad plateau, indicating its formation throughout the reaction zone, by reactions in the flame and also on the cooler surfaces of the sampling system. In the acetylene flame, the ion peaks at an intermediate position (0.07mm upstream) suggesting that, for this flame, the bulk of the CO_2H^- is formed in the flame itself. However, the hydrate peaks at an earlier position (0.13 mm upstream) suggesting that some of CO_2H^- is formed by cooler reaction processes. The peak at 46 a.m.u. for both flames is a ^{13}C isotope of the parent ion, (Figs. 31,32).

The electron affinity of CO_2H is the largest measured for radicals in flame chemistry. Thus, charge transfer reactions with almost all of the flame ions will occur, e.g.:-

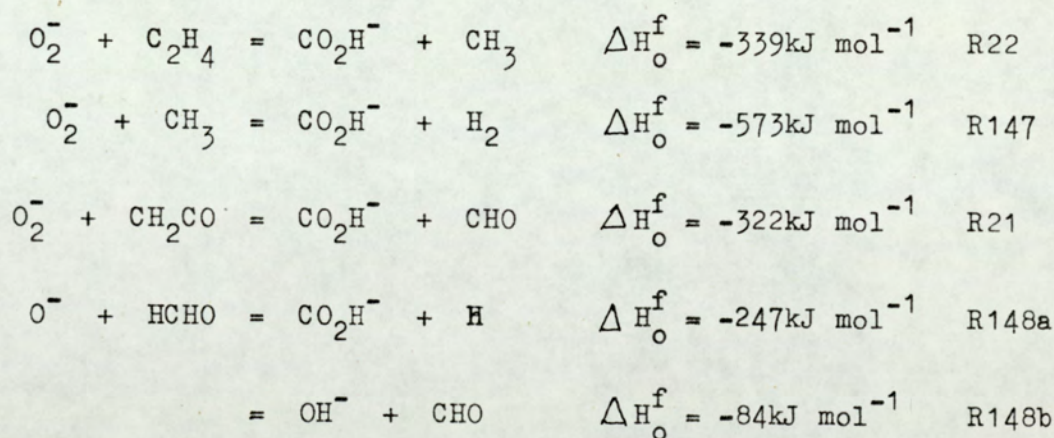




The CO_2H^- ion can be produced by proton transfer reactions from many flame ions since its base strength is low:-



A number of rearrangement reactions can occur:-



Proton abstraction from ethanol would also give the same mass number, the ion being $\text{C}_2\text{H}_5\text{O}^-$. The profile at 45 a.m.u. is

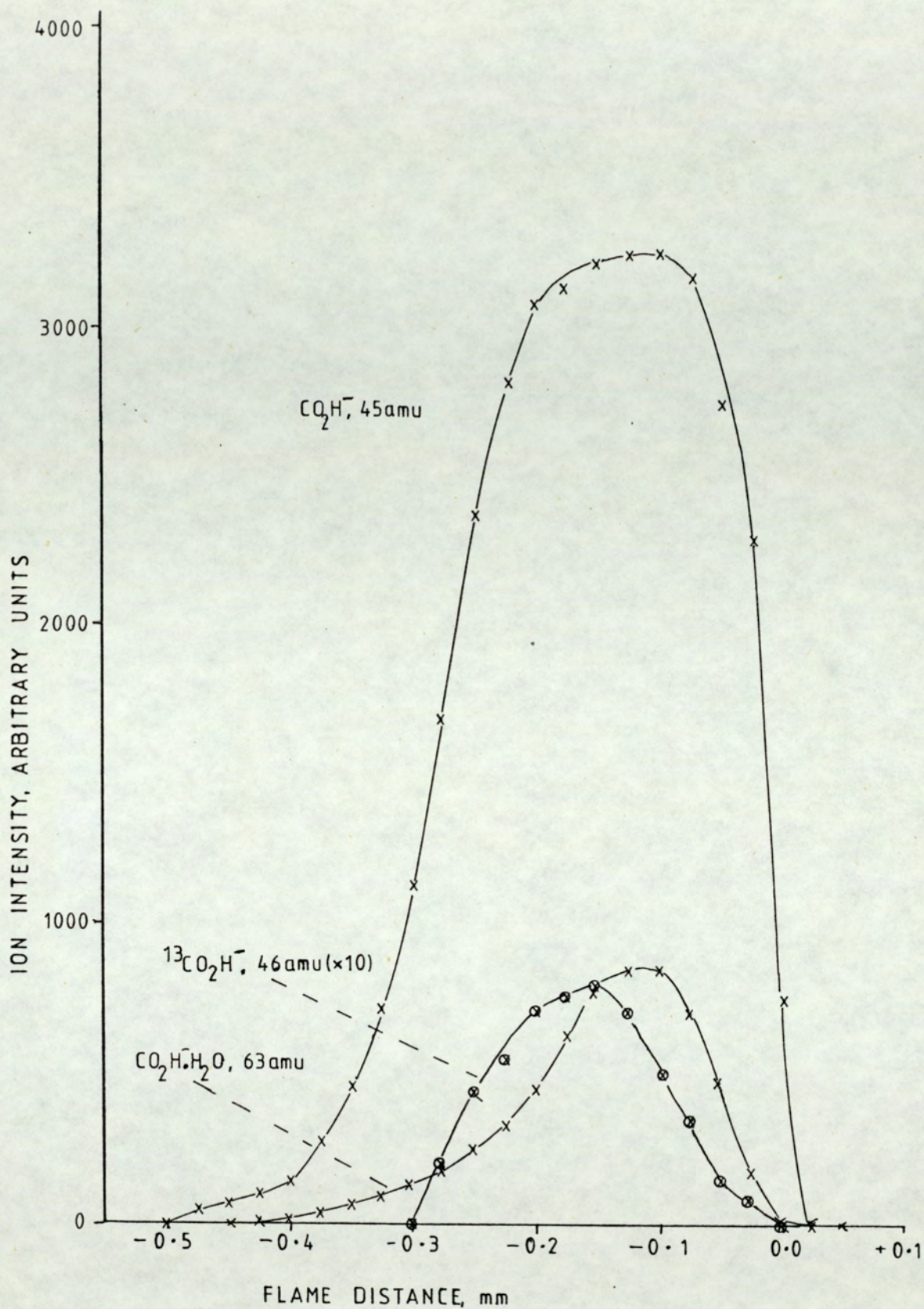


Figure 31. Ion Profiles for 45 a.m.u., 46 a.m.u. and 63 a.m.u. in Flame F1.

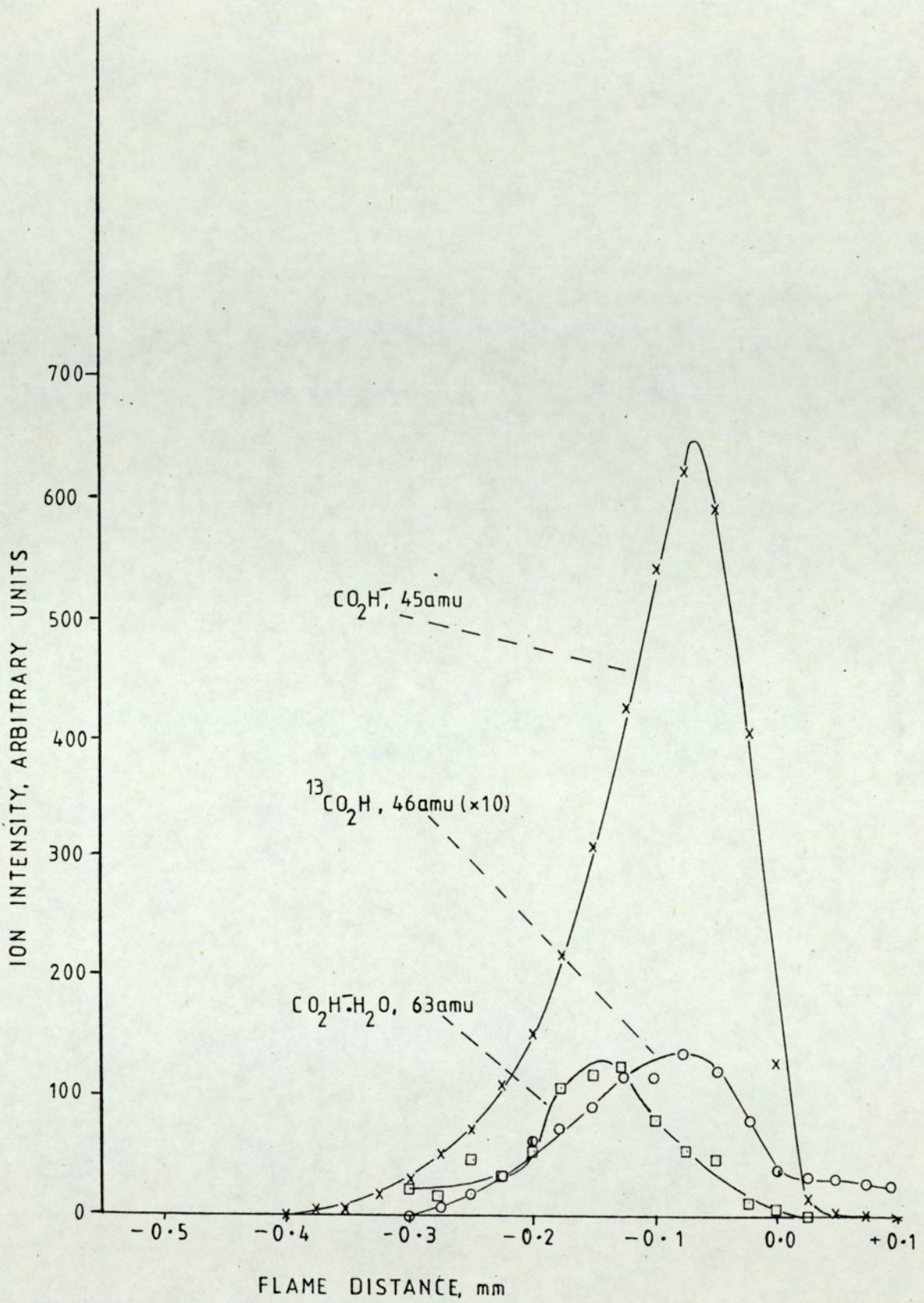
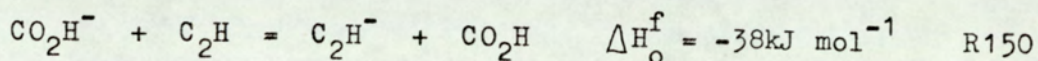
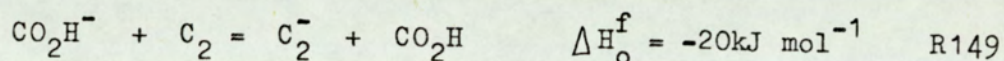


Figure 32. Ion Profiles for 45 a.m.u., 46 a.m.u. and 63 a.m.u. in Flame F2.

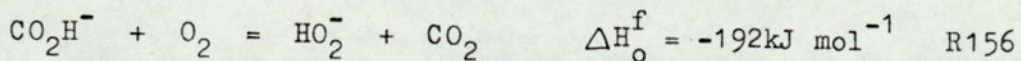
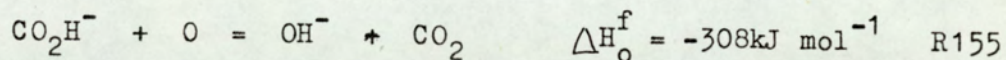
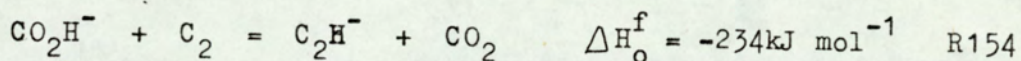
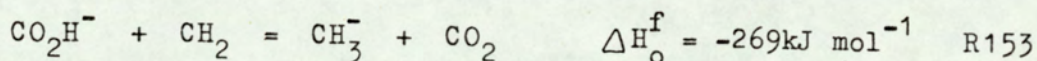
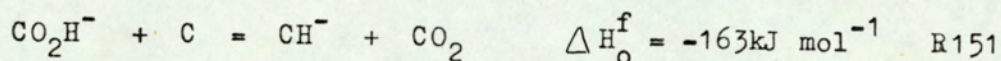
probably due to both these ions, many neutral species contributing to the profile.

The peak at 46 a.m.u. is due to the ^{13}C isotope of the 45 a.m.u. profile. As would be expected, the formide ion forms a hydrate at 53 a.m.u. If the ion were $\text{C}_2\text{H}_5\text{O}^-$, this would also be expected to form a hydrate.

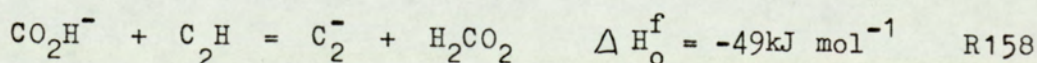
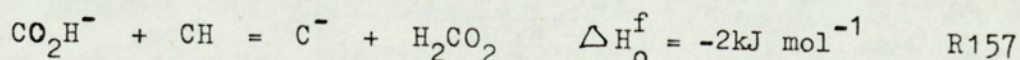
Once formed, CO_2H^- is a stable ion, its electron affinity precluding most charge transfer reactions to produce other ions except possibly:-

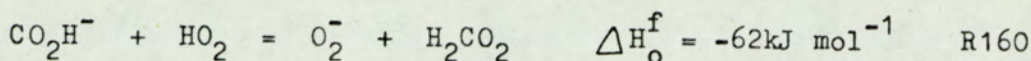
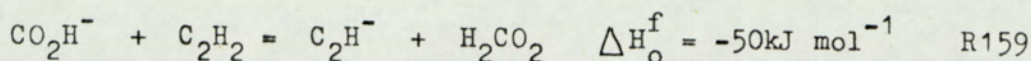


Proton transfer reactions may occur:-



thus providing a means for CO_2 formation in the flame, or by proton abstraction reactions:-





IV.5.viii. O_3^- , 48 a.m.u.; $\text{O}_3^- \cdot \text{H}_2\text{O}$, 66 a.m.u.; $\text{O}_3^- \cdot 2\text{H}_2\text{O}$, 84 a.m.u.

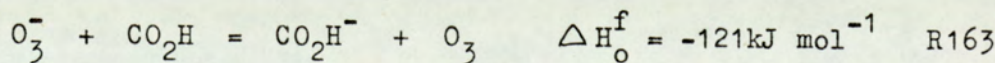
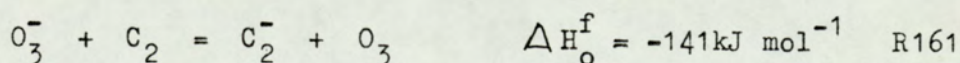
None of these ions were observed in the acetylene flame. Even for flame F1, the ion signals were extremely weak, Fig.33., that at 48 a.m.u. (corresponding to the parent ion), being so small that it was impossible to locate the peak in the profile. Discussion will be confined to flame F1, noting that this ion is probably present in undetectable quantities in flame F2.

The peak at 66 a.m.u. is a hydrate, indicated by the upstream extension of this profile. The peak at 84 a.m.u. may be attributable to a dihydrate, or to another species, C_7^- . It is difficult to envisage structures for the hydrates of O_3^- .

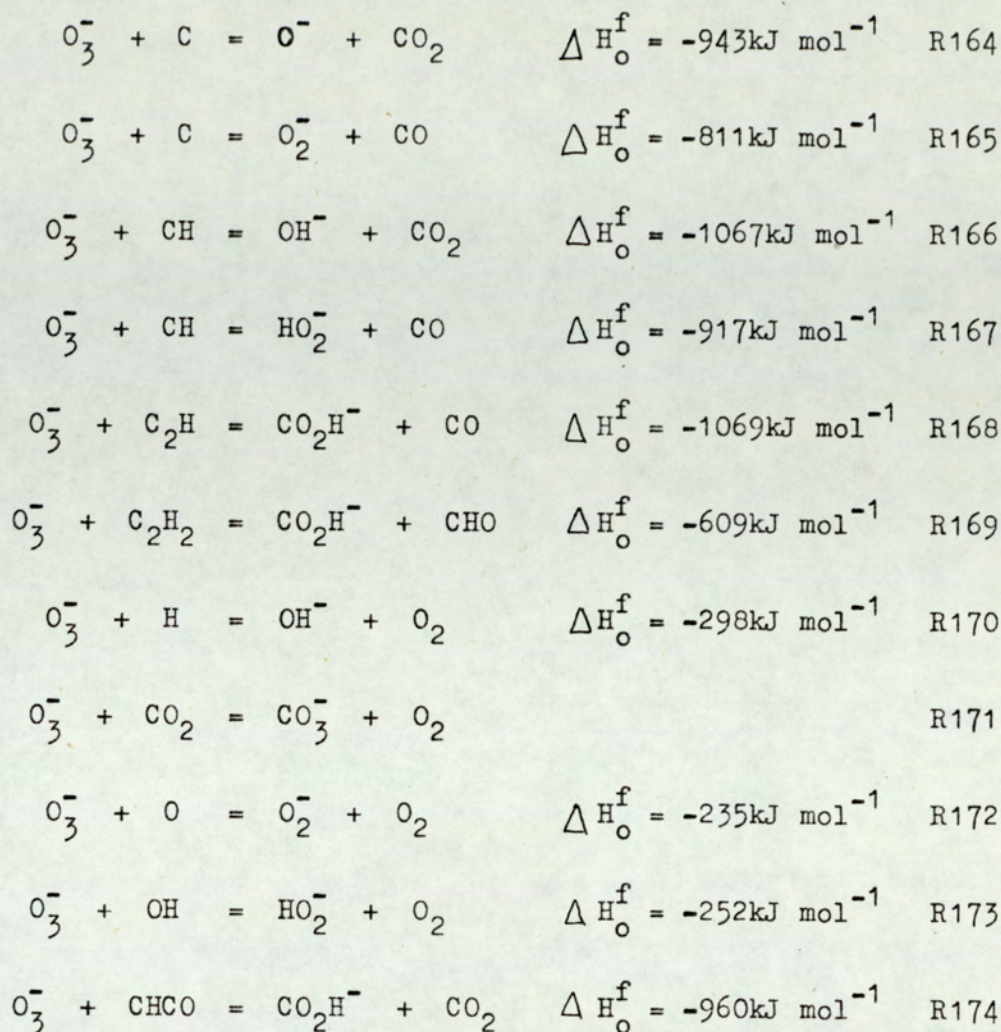
Ozone has a high electron affinity: it would be expected to react readily with flame ions by charge transfer. However, the position of the profiles for O_3^- (and its hydrates) suggests that few negative ions would have been formed with which ozone could react. The profiles peak at an early position upstream probably only enabling O_2^- to react:-



O_3^- may react by charge transfer:-



or by several rearrangement reactions:-



$$k_{\text{R170}} = 8.4 \times 10^{-10} \text{cm}^3 \text{mol}^{-1} \text{sec}^{-1} \quad (38).$$

$$k_{\text{R171}} = 4 \times 10^{-10} \text{cm}^3 \text{mol}^{-1} \text{sec}^{-1} \quad (38).$$

As can be seen from these reactions, O_3^- is extremely reactive, especially on the formation of CO_2 and CO . This may explain why the profile is so small for O_3^- .

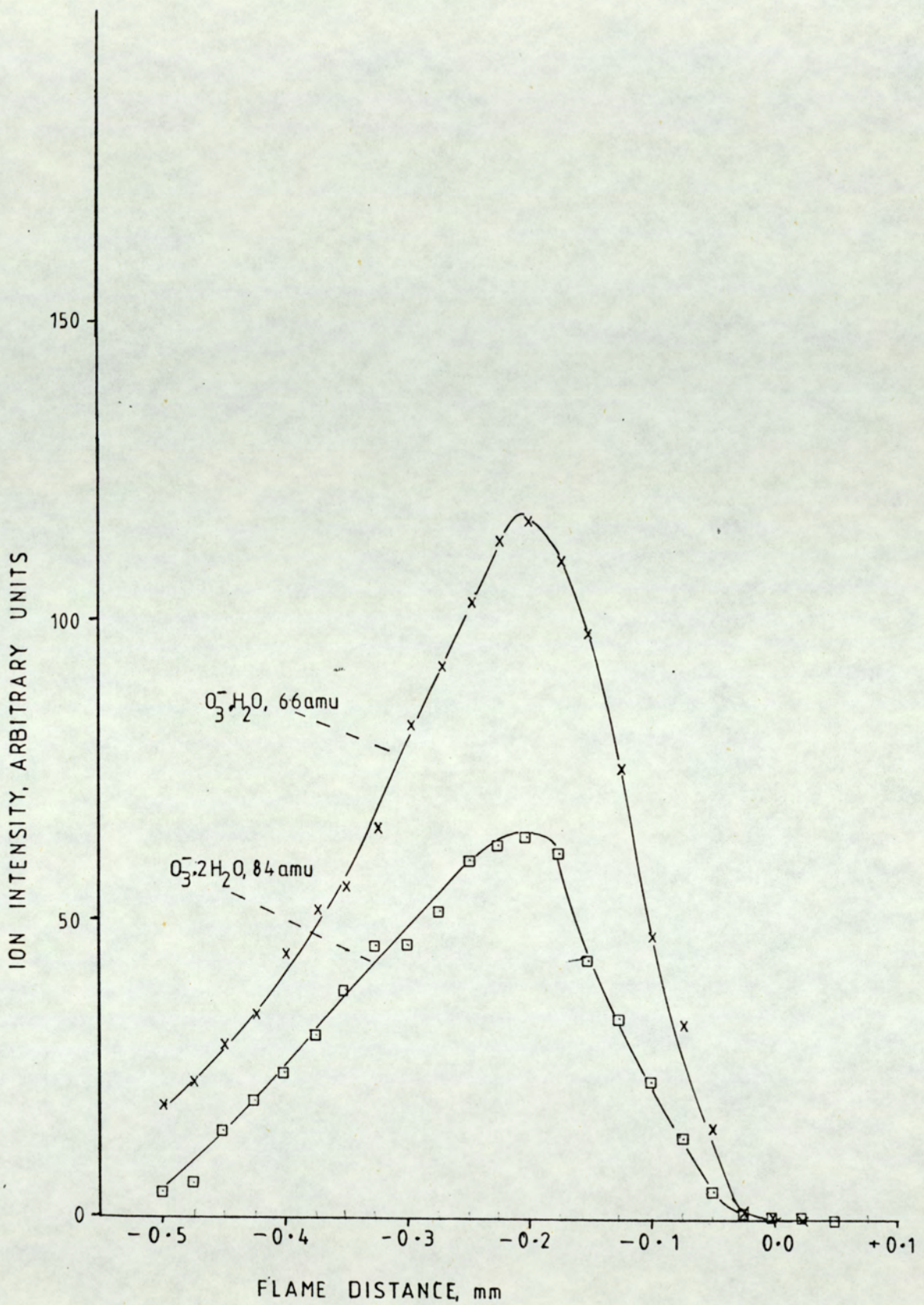


Figure 33. Ion Profiles for 66 a.m.u. and 84 a.m.u. in Flame F1.

Neutral Species, X	$H_0^f(X)$, kJ mol ⁻¹	Electron Affinity E.A., kJ mol ⁻¹	$H_0^f(X)^-$ kJ mol ⁻¹	a
C	715	122	587	b
CH	594	120	469	b
CH ₂	385	20	360	b
CH ₃	142	103	33	d
CH ₄	-74	-	-	d
C ₂	838	342	490	b
C ₂ H	544	360	172	b
C ₂ H ₂	227	-	-	d
C ₂ H ₃	285	-	-	d
C ₂ H ₄	52	-	-	d
O	249	141	102	b
O ₂	0	42	-49	b
O ₃	145	-201	-63	b
HO	39	176	-143	b
HO ₂	19	289	-276	b
H	218	73	139	b
CH ₃ O	15	154	-142	b
CH ₃ OH	-238	-	-	e
C ₂ H ₅ O	-18	163	-192	b
C ₂ H ₅ OH	-236	-	-	e
CHCO	153	172	-25	b
CH ₃ CO ₂	-208	305	-460	b
CO ₂ H	-223	322	-477	b
CH ₂ O ₂	-472	-	-	f

/contd.

Neutral Species, X	$H_0^f(X)$, kJ mol ⁻¹	Electron Affinity E.A., kJ mol ⁻¹	$H_0^f(X)^-$ kJ mol ⁻¹	a
CH ₂ O	-317	-	-	f
CO ₂	-393	-	-	e
CO	-110	-	-	e
H ₂ O	-242	-	-	e
CH ₃ CO	-24	-	-	d
CHO	32	-	-	d
CH ₂ OH	-18	-	-	d
CH ₃ CHO	-24	-	-	f
C ₂ H ₂ O	328	-	-	f
CO ₃	-	172	-	c
CO ₃ ·H ₂ O	-	201	-	c
C ₂ H ₂ O ₂	-593	-	-	f
H ₂ O ₂	-128	-	-	f

Table 8. Electron Affinities, and Heats of Formation of Possible Flame Neutrals.

a). The standard heat of formation at 298K for a negative ion X⁻ is calculated from the expression

$$H_0^f(X)^- = H_0^f(X) - EA(X) - 6.216 \text{ kJ mol}^{-1},$$

where the last term represents 5/2 RT for the electron.

- b). Values obtained from reference (6).
c). Values obtained from reference (43).
d). Values obtained from reference (44).
e). Values obtained from reference (45).
f). Values calculated from bond enthalpies, (45).

Negative Ion.	Proton Affinity, kJ mol^{-1} (298K)
CH_2^-	1756
H^-	1682
CH_3^- , C_2H_3^- , C_2H_5^-	> 1680
OH^-	1642
CH^-	1625
O^-	1605
CH_3O^-	1600
C_2HO^-	≤ 1596
$\text{C}_2\text{H}_5\text{O}^-$	> 1583
C_2^-	> 1554
C^-	1535
C_2H^-	> 1487
O_2^-	1474
CHO_2^-	1445
HO_2^-	1403

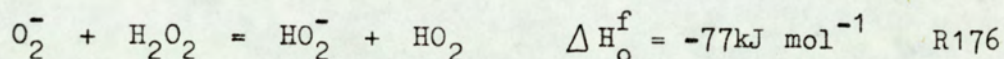
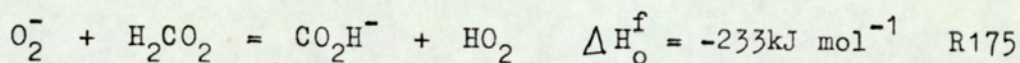
Table 9. Proton Affinities of Negative Flame Ions in Order of Decreasing Base Strength, (6).

IV.6. IONS FORMED FROM O_2^- BY PROCESSES NOT INVOLVING CHARGE TRANSFER.

All neutral species whose electron affinity is greater than that of oxygen will form a negative ion by charge transfer. In the case of flame ions, most of the neutrals meet this criterion. However, O_2^- may still react with some neutrals by processes other than charge transfer to produce negative ions.

IV.6.i. Proton Transfer Reactions Involving O_2^- .

Few flame neutrals have a low enough proton affinity to allow abstraction of H^+ by O_2^- . In Table 9 only CO_2H^- and HO_2^- are less basic than O_2^- , these being the only ions that may be formed from their corresponding neutrals by proton transfer:-



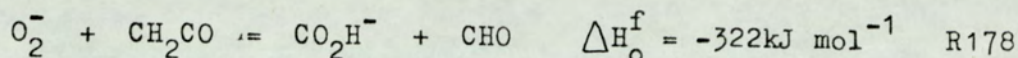
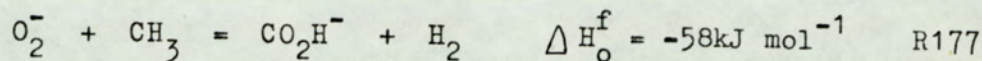
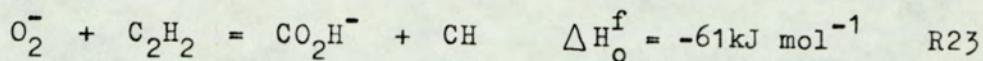
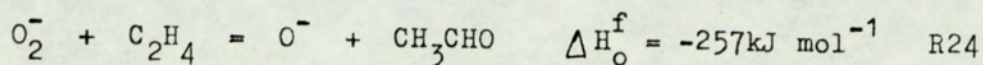
These reactions may be considered as alternatives for the formation of CO_2H^- and HO_2^- .

Of course, other negative ions may be found in flames by proton transfer of neutrals with ions other than O_2^- : this possibility has been discussed for each individual ion in the preceding section.

IV.6.ii. Rearrangement and Clustering Reactions Involving O_2^- .

Several ions already discussed can be formed by

rearrangement reactions e.g.:-

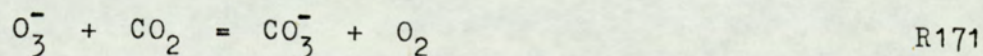


Product ions may also be formed from negative ions apart from O_2^- by these rearrangement processes; this has been discussed for the individual ions formed from charge transfer reactions with O_2^- in the preceding section.

Some of the ions which appear above 51 a.m.u. in the mass spectrum of the two flames can be shown to be formed by rearrangement processes. However it is possible that these ions may also be formed by three-body clustering reactions, it being difficult to decide which mode of formation is more likely.

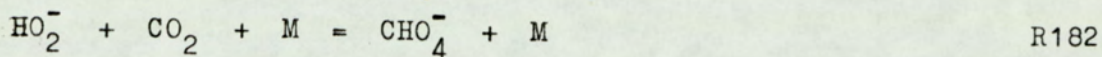
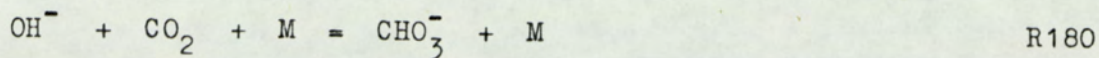
IV.6.ii.a. CO_3^- , 60 a.m.u.; $\text{CO}_3^- \cdot \text{H}_2\text{O}$, 78 a.m.u.; $\text{CO}_3^- \cdot 2\text{H}_2\text{O}$, 96 a.m.u.

The profiles at these three masses can again be attributable to more than one negative ion species. The peaks at 60 a.m.u. and 96 a.m.u. could be attributable to the polyacetylide species C_5^- and C_8^- respectively. However it is known from the chemistry of the ionosphere that ions such as CO_3^- and HCO_3^- are highly stable (39). Reactions such as:-



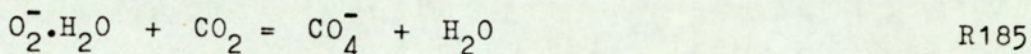
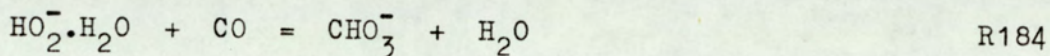
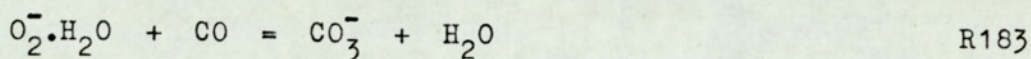
may occur, or three body clustering reactions such as:-



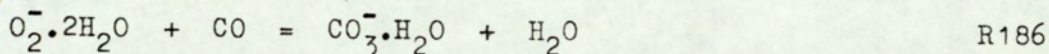


The latter ion, CHO_4^- was not observed in either flame, but has been identified by others as a possible flame ion (40).

These ions may also be formed by three-body association followed by switching reactions:-



These reactions could account for the fate of some of the hydrates, and it may be possible that hydrates of CO_3^- may be formed from dihydrates:-



The possible structure of such hydrates is difficult to visualise.

The peak at 60 a.m.u. is sharp and maximises at 0.1mm upstream for flame F1. For F2 this profile peaks at 0.03 mm upstream, Figs. 34,35. The peak at 78 a.m.u., although slightly less intense, has a very broad peak, maximising at a position further upstream in both flames than the parent ion. Because of the obvious differences between the shapes of these peaks, it seems likely that the bulk of the peak at 60 a.m.u. is due to a polyacetylide ion for the ethylene flame, and all for the acetylene

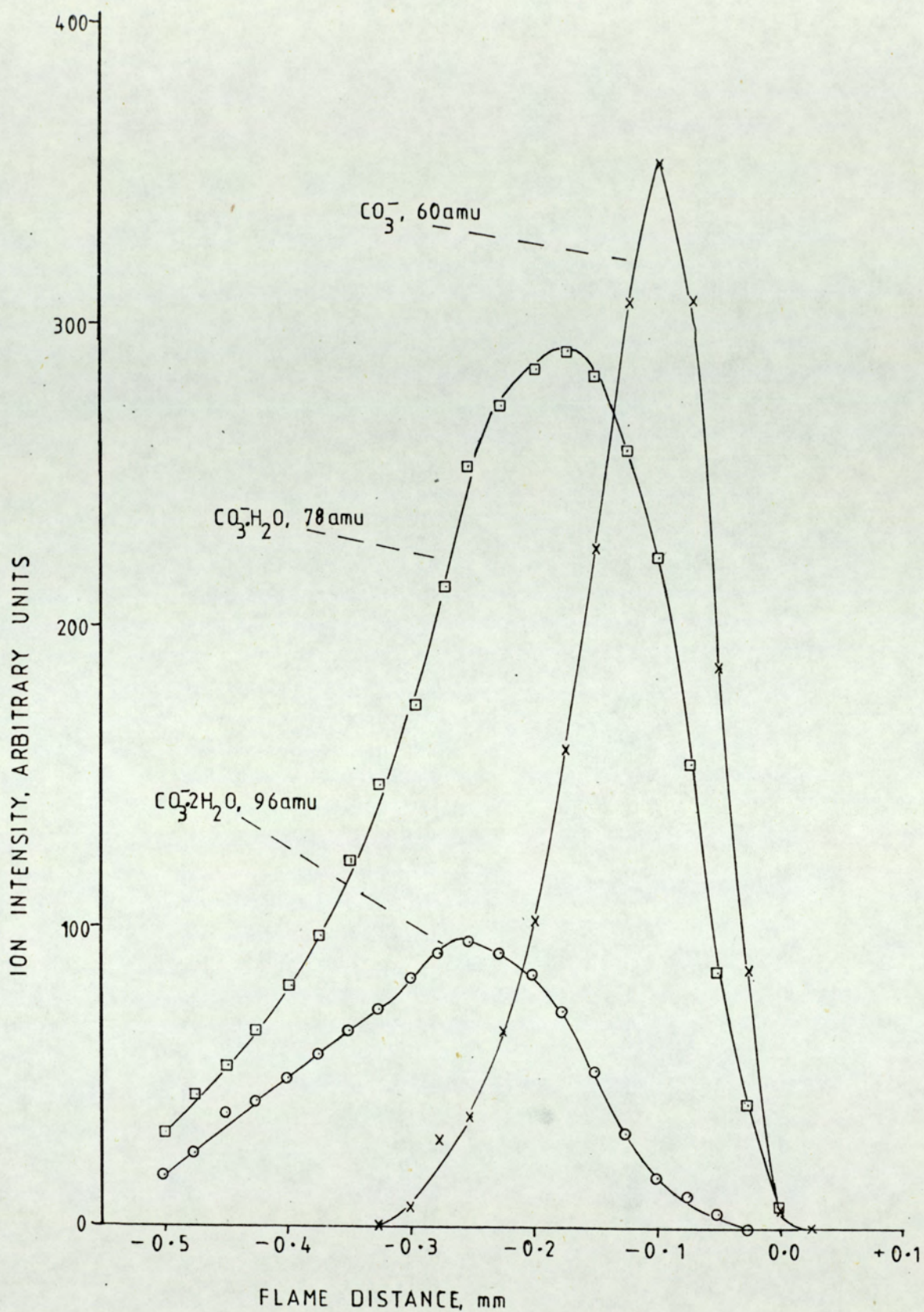


Figure 34. Ion Profiles for 60 a.m.u., 78 a.m.u. and 96 a.m.u. in Flame F1.

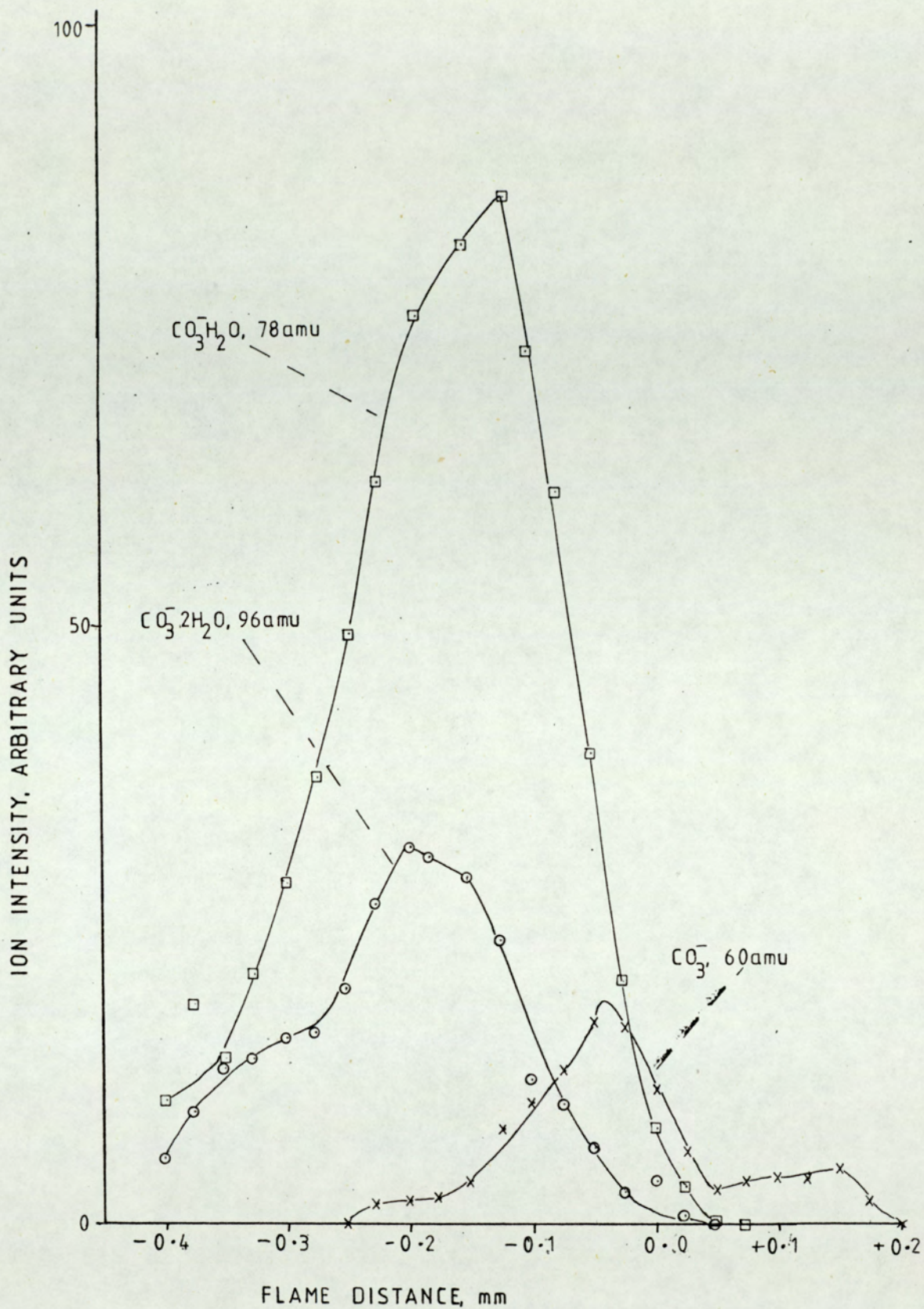


Figure 35. Ion Profiles for 60 a.m.u., 78 a.m.u. and 96 a.m.u. in Flame F2.

flame. Thus the peak at 78 a.m.u. probably represents the stablest form of the ion, that is the monohydrate. The peak at 96 a.m.u. poses a similar problem, there is almost certainly some contribution from the polyacetylide ion C_8^- , but again because of the characteristic upstream extension of the profile a hydrate is suggested. This broad peak maximises slightly further upstream of the monohydrate, the conclusion being that to a certain extent the broadness and shift of the peaks is due to the contribution from the polyacetylide ions C_5^- and C_8^- , the true position of the peak being for the monohydrated carbonate ion.

IV.6.ii.b. HCO_3^- , 61 a.m.u.; $HCO_3^- \cdot H_2O$, 79 a.m.u.; $HCO_3^- \cdot 2H_2O$, 97 a.m.u.

As previously mentioned these ions are produced by reactions similar to those for the formation of CO_3^- . Again it is difficult to make positive identifications of the ions and ion profiles. 61 a.m.u. and 97 a.m.u. could be regarded as the polyacetylide species C_5H^- and C_8H^- . These profiles are generally the same as the corresponding profiles for CO_3^- , Figs. 36, 37. However, for flame F1 the monohydrate peak is much larger (by a factor of 2) than the $CO_3^- \cdot H_2O$ peak. Also it is much sharper and it has to be concluded that this peak must also be due to some other, unknown species. For flame F2 the monohydrate peak is smaller than that for $CO_3^- \cdot H_2O$, but much larger than the parent ion HCO_3^- . This indicates that the ion profile at 79 a.m.u. for the acetylene flame is probably the true hydrate.

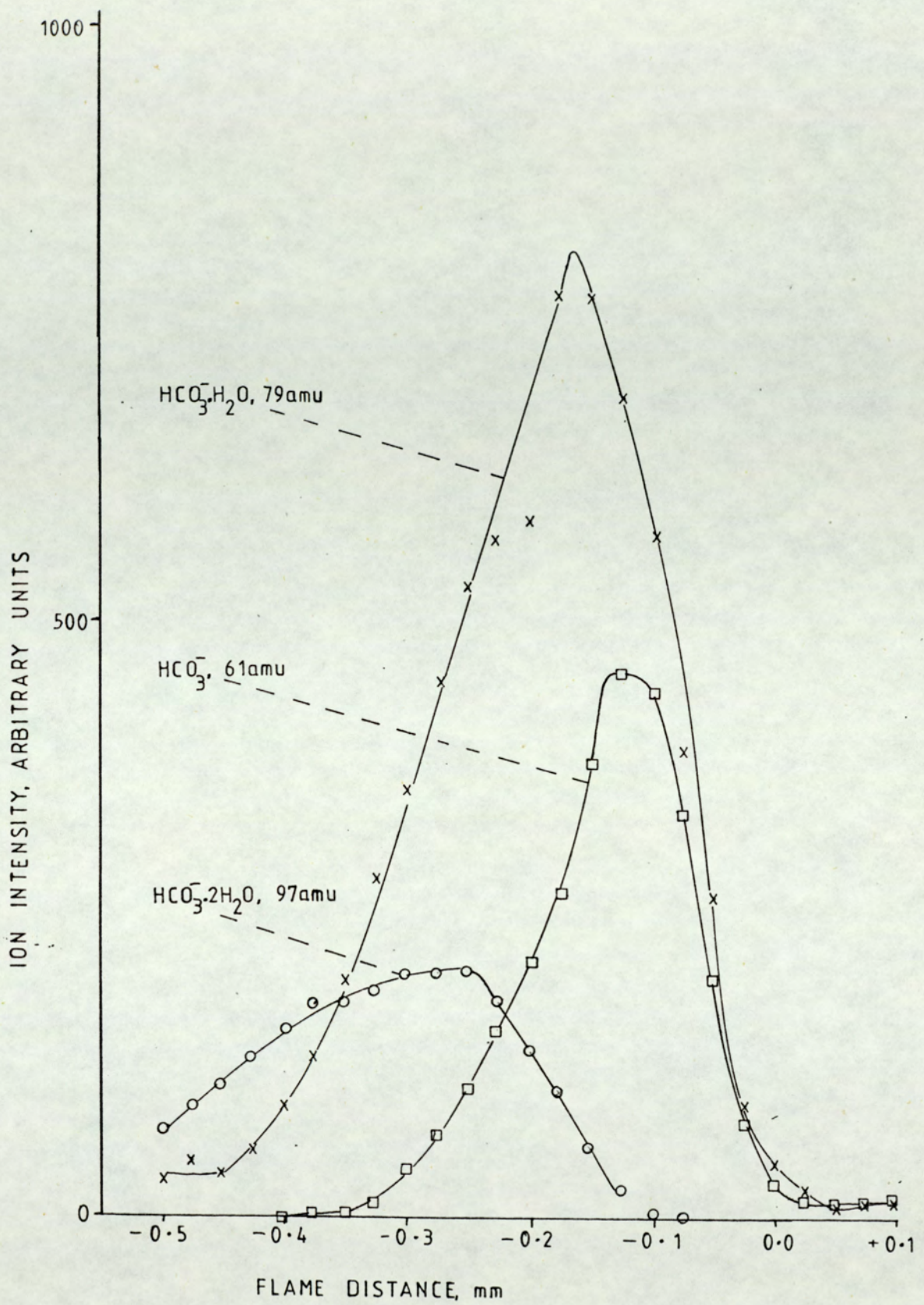


Figure 36. Ion Profiles for 61 a.m.u., 79 a.m.u. and 97 a.m.u. in Flame F1.

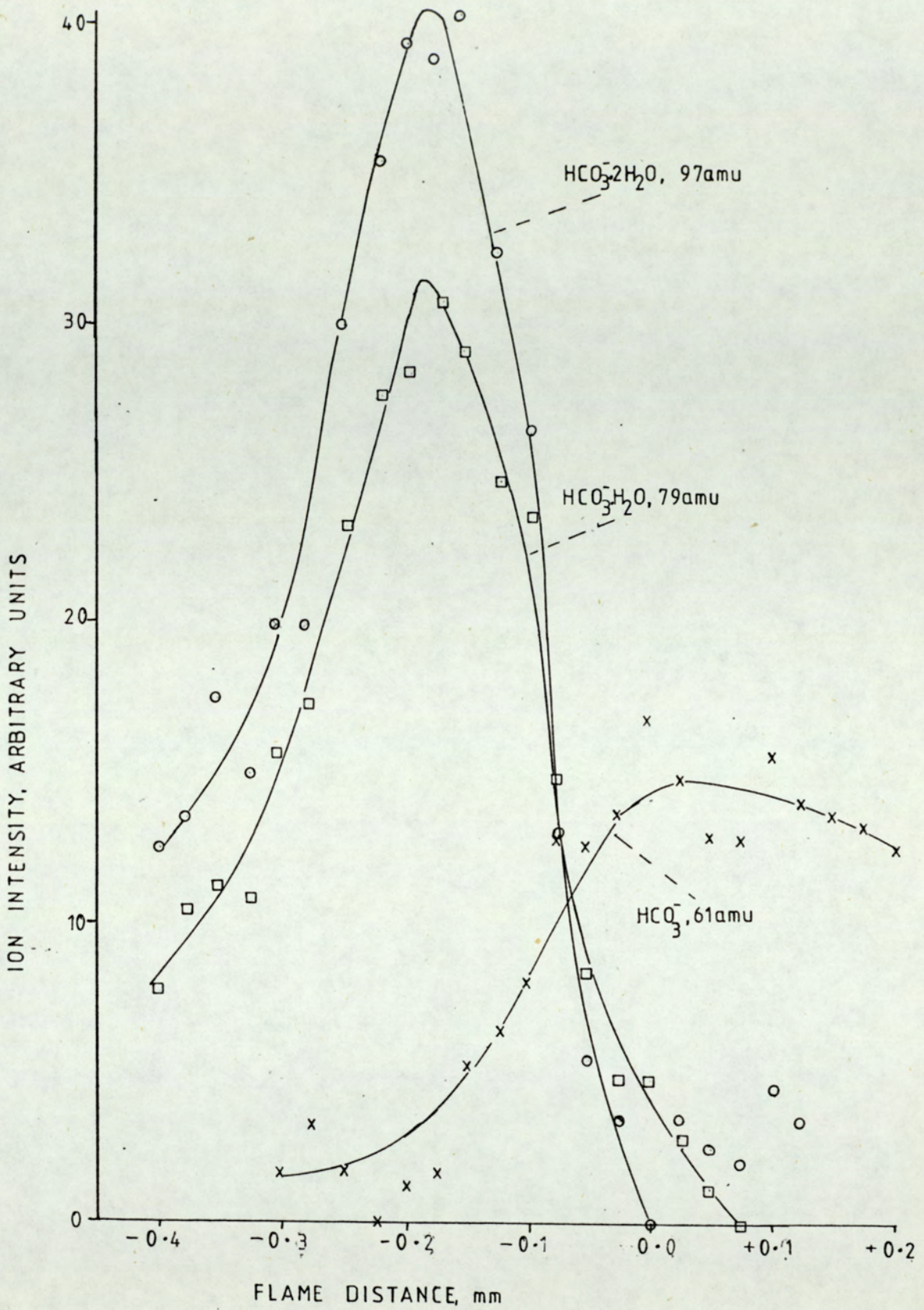


Figure 37. Ion Profiles for 61 a.m.u., 79 a.m.u. and 97 a.m.u. in Flame F2.

IV.6.iii.c. CO_4^- , 76 a.m.u.; $\text{CO}_4^- \cdot \text{H}_2\text{O}$, 94 a.m.u.

CO_4^- is formed by similar processes to CO_3^- and HCO_3^- , as mentioned previously. The peak at 76 a.m.u. is rather weak, peaking at 0.125mm upstream of the reaction zone front, Fig.38. The peak at 94 a.m.u. is extremely weak for flame F1, and non-existent for flame F2, and is inconclusive as being a hydrate.

These three ions, CO_3^- , HCO_3^- and CO_4^- provide evidence for the formation (and consumption) of carbon monoxide and carbon dioxide in the flame.

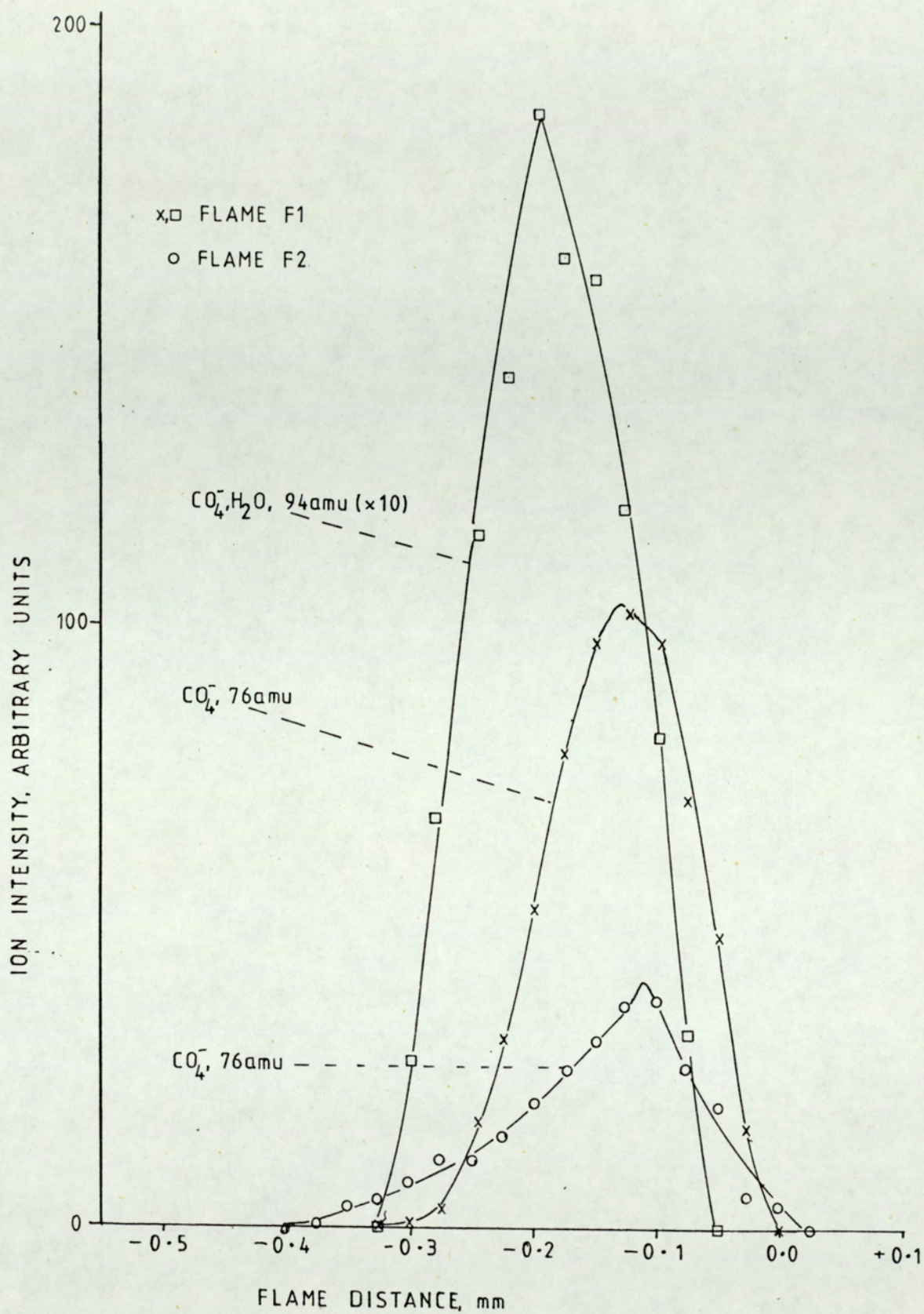
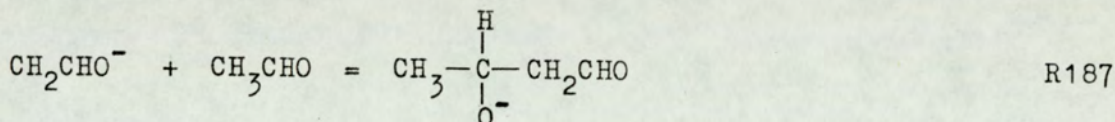
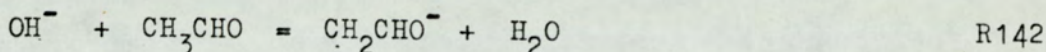


Figure 38. Ion Profiles for 76 a.m.u. and 94 a.m.u.

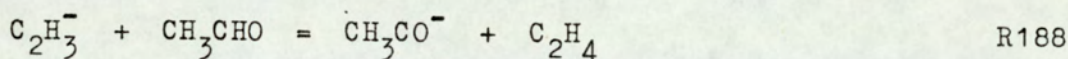
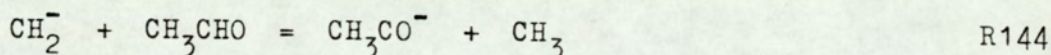
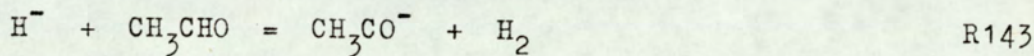
IV.7. OTHER OXYGENATED SPECIES OBSERVED IN THE FLAMES.

IV.7.i. $C_4H_7O_2^-$, 87 a.m.u.; $C_4H_7O_2^- \cdot H_2O$, 105 a.m.u.

The profile at 87 a.m.u. is probably due to the 3-hydroxybutanal (aldol) negative ion. This may be formed by the reaction of acetaldehyde with OH^- :-



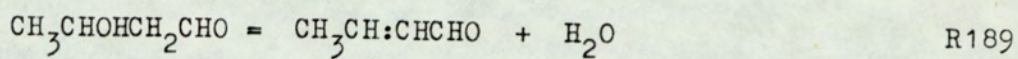
It may be possible that this reaction may also occur with negative flame ions of stronger basicity than OH^- :-



Thus it appears possible for 3-hydroxybutanal to be formed from several flame ions, with acetaldehyde as the precursor neutral. This would also explain the fairly weak profile at 43 a.m.u., since CH_2CHO^- would be used up in aldol formation.

The peak at 105 a.m.u. is certainly a hydrated species possibly of $C_4H_7O_2^-$, Fig. 39. However evidence for this is inconclusive since it peaks further upstream than the parent ion in flame F1; in flame F2 this profile is non-existent. It may be that the hydrate is stabler than the parent ion at lower temperatures, (and therefore peaking at an earlier position in the flame), since the neutral,

3-hydroxybutanal would be expected to form hydrates. It is also possible for 3-hydroxybutanal to lose water to produce 2-butenal:-



but whether this type of reaction would occur in a flame regime is uncertain.

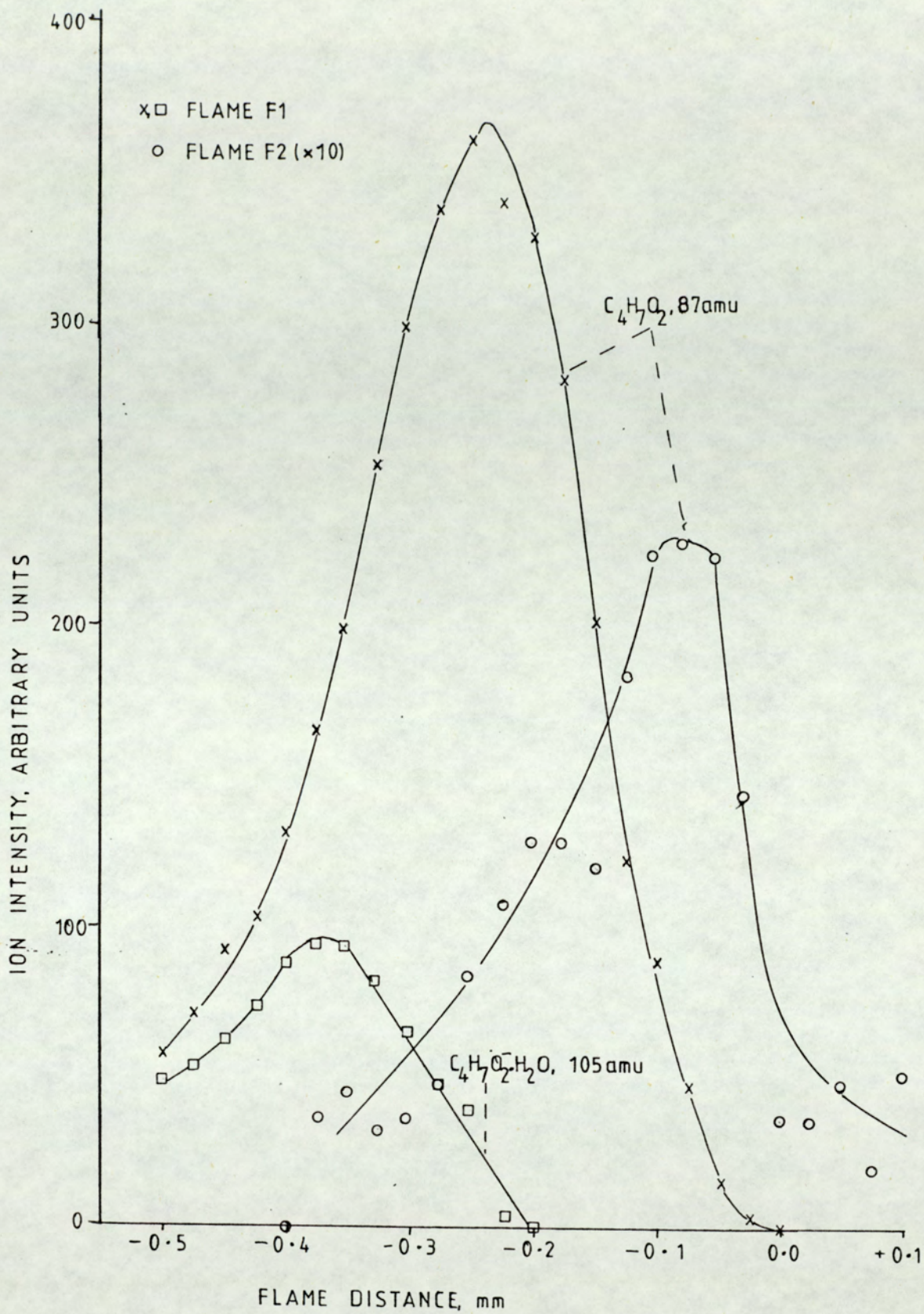
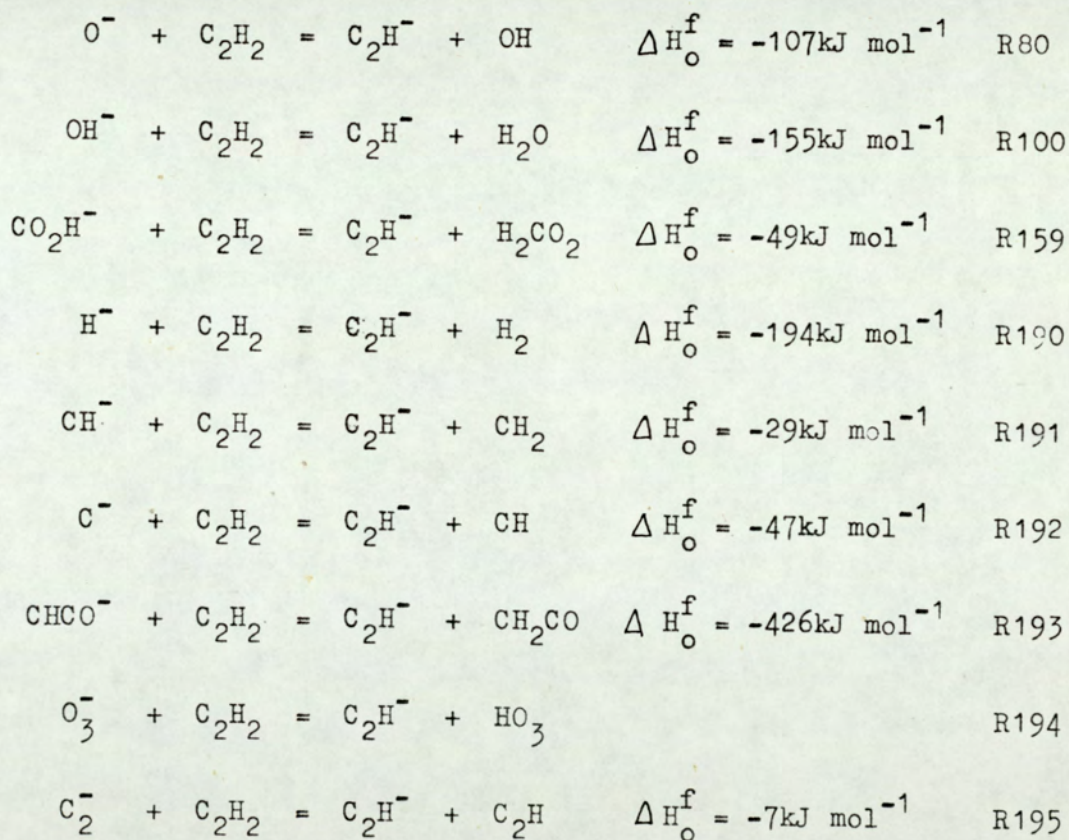


Figure 39. Ion Profiles for 87 a.m.u. and 105 a.m.u.

IV.8. CARBONACEOUS SPECIES.

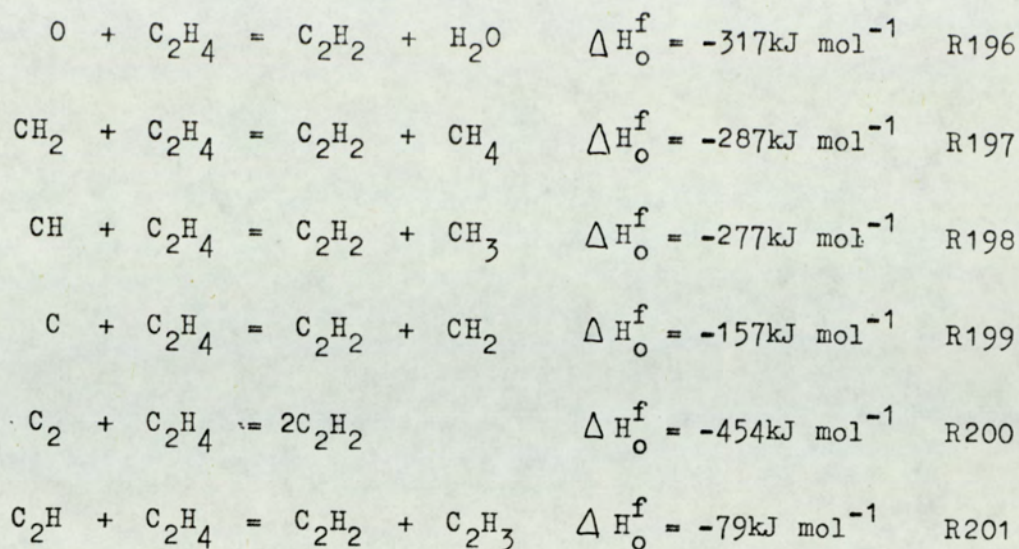
The acetylene flame produces two intense peaks at 24.a.m.u. and 25 a.m.u., peaking near the hotter end of the reaction zone, Figs. 40,41. For ethylene, these two peaks are weak, after allowing for the general increase of the signal intensity for the other flame ions, Fig. 43. These two ions are attributable to C_2^- and C_2H^- respectively, and the difference in the intensities can be explained by consideration of the reactions which produce them.

For acetylene, C_2H^- may be formed as follows:-



However, these reactions are not available for ethylene.

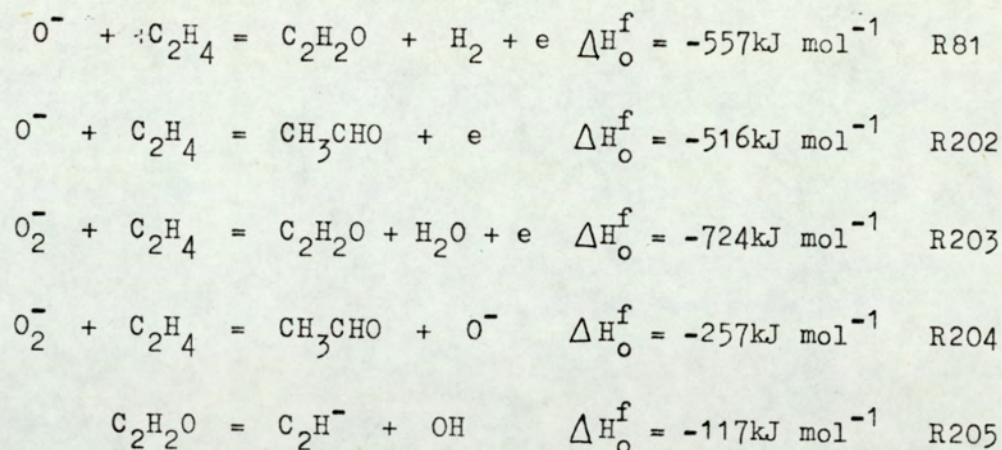
Ethylene may react by radical reactions to produce acetylene, and thence form C_2H^- :-



then



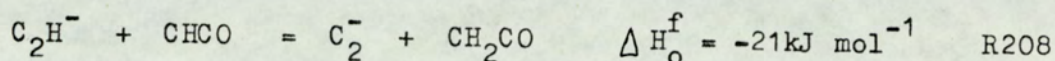
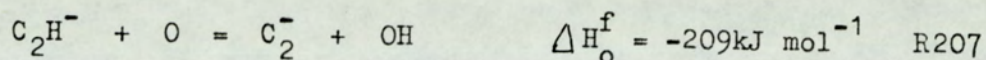
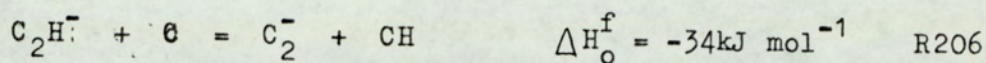
etc. as described previously. Also, it is possible that O^- and O_2^- can react directly with C_2H_4 to form $\text{C}_2\text{H}_2\text{O}$, which may then react further to yield C_2H^- :-



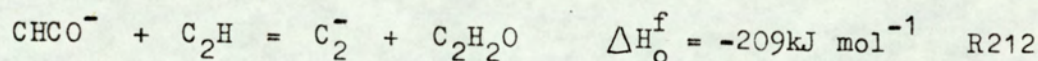
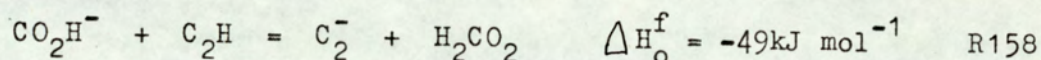
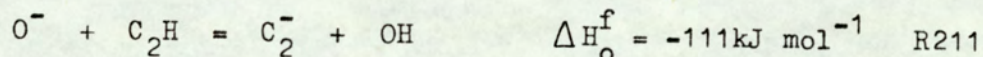
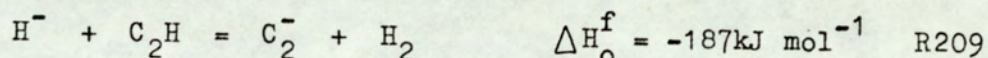
Thus there are several avenues open for the conversion of ethylene to C_2H^- . However, the concentration of neutral species capable of forming acetylene from ethylene may be inadequate to ensure a large concentration of C_2H^- . Also as can be seen from reactions R81, R202, R203, R204 above, competitive reactions

occur to produce either ketene or acetaldehyde. Acetaldehyde is unlikely to be able to react further to produce C_2H^- .

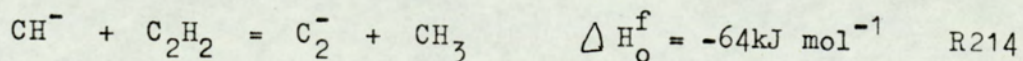
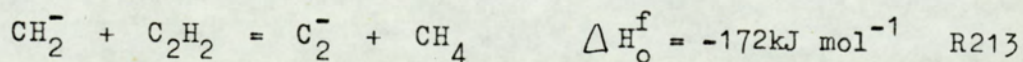
C_2H^- may now react further to produce C_2^- , by proton transfer reactions involving some of the flame neutrals:-



C_2^- may also be formed by reaction of the neutral radical C_2H with several negative flame ions:-

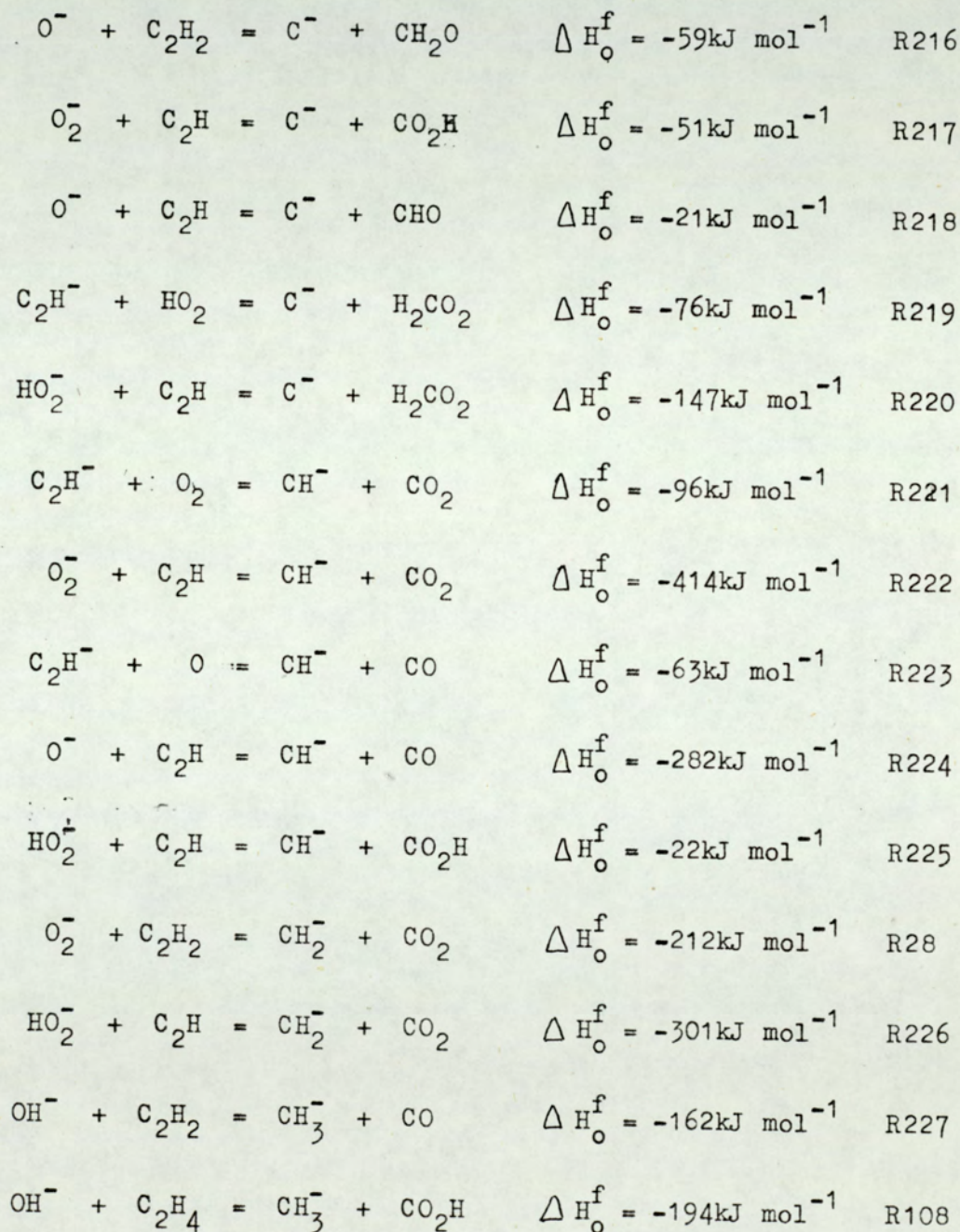


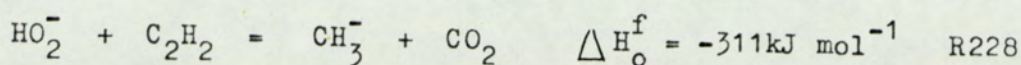
CH_2CO may also react to form, among other ions, C_2^- , as mentioned in section IV.5.5. Acetylene may also react by rearrangement processes to form C_2^- :-



Thus there are more possible reaction pathways where acetylene may form C_2H^- and C_2^- than for ethylene and this may explain the higher concentration of these species in flame F2.

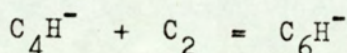
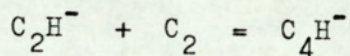
Single carbon species may also form, although none were detected, possibly due to their high reactivity. Some of these species may then be available for the build up of polyacetylides.



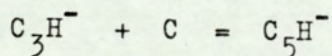
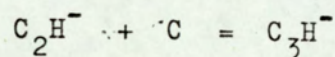


Thus several reactions are thermodynamically possible for the formation of single carbon species. These ions are presumably lost by formation of higher carbon species, and by charge transfer reactions to produce other negative ions. Most of the above reactions are thermodynamically possible for acetylene: few are possible for ethylene, therefore it is likely that the CH_m^- species ($m = 0, 1, 2, \text{ or } 3$) would be formed in higher concentrations in the acetylene flame.

If it is assumed that the above species can be formed in both flames, then the precursors for polyacetylide formation are present. For example:-



etc., or:-



etc., or by single carbon species to form C_3^- , C_4^- , C_5^- etc. by these methods. This process of polyacetylide formation is rapid enough only when the radical concentration is high, i.e. in the oxidation zone of the flame (41). Thus any polyacetylide species should be detected in the reaction zone. For the ethylene flame, C_2^- and C_2H^- were observed, C_2H^- being in greater concentration. A large peak is seen at 36 a.m.u. which could correspond to C_3^- . However much of the intensity of this peak is probably attributable

to overlap of the two chloride peaks at 35 a.m.u. and 37 a.m.u. The C_4^- and C_4H^- ion profiles were not observed (at 48 a.m.u. and 49 a.m.u.), so any C_4^- negative ions formed are probably unstable. Peaks were observed at 60 a.m.u. and 61 a.m.u., possibly showing the presence of C_5^- and C_5H^- , but as mentioned previously, these two masses are mostly attributable to the oxygenated species CO_3^- and HCO_3^- . A large peak was found at 72 a.m.u., which would correspond to C_6^- , no other interfering species being likely. The small peak at 73 a.m.u. is possibly C_6H^- . C_7^- and C_7H^- possibly form at 84 a.m.u. and 85 a.m.u. but the shapes of both these peaks are broad, and both could arise from hydrated species, $O_3 \cdot 2H_2O$ and $HO_3 \cdot 2H_2O$. This is also true of the peaks at 96 a.m.u. and 97 a.m.u. - these being attributable to C_8^- and C_8H^- , or more likely, because of the peak shape to $CO_3 \cdot 2H_2O$ and $HCO_3 \cdot 2H_2O$ respectively.

Therefore the only significant carbonaceous species found in flame F1 are C_2^- , C_2H^- , and C_6^- . The low concentrations of the carbonaceous species can be explained by the relative incapability of ethylene to form C_2^- , C_2H^- and the single-carbon species as explained previously. The profile at 72 a.m.u., C_6^- may be stabilised by virtue of some ring-closure process, although if this is the case, it would be difficult to decide if the resultant ring was aromatic or aliphatic in nature.

For flame F1, small upstream peaks were noted for 36 a.m.u. and 37 a.m.u., suggesting that C_3^- and C_3H^- are formed. Again, no significant peaks were found at 48 and 49 a.m.u. indicating the unlikelihood of the formation of C_4^- and C_4H^- . At 60 a.m.u. and 61 a.m.u. the downstream position of the peaks indicates the possibility

of C_5^- and C_5H^- formation along with the formation of the ions CO_3^- and HCO_3^- . The odd shape of these peaks confirm this dual assignment. No peak was observed at 72 a.m.u., indicating the absence of C_6^- . However a large peak was found at 73 a.m.u., this being the second largest peak observed in the acetylene flame experiments, showing that C_6H^- is formed. This peak will be discussed later. No peaks were found that corresponded to C_7^- and C_7H^- at 84 a.m.u. and 85 a.m.u., suggesting that any $C_nH_m^-$ species (n odd, $m = 0,1$) do not form for $n > 5$, because of a low concentration of single-carbon species. Peaks were observed at 96 a.m.u. and 97 a.m.u. which are possibly due to C_8^- and C_8H^- , but these could also be assigned to the hydrated species, $CO_3^- \cdot 2H_2O$, and $HCO_3^- \cdot 2H_2O$.

Acetylene forms more polyacetylides than ethylene, one reason being the greater ease with which acetylene can form the precursor ions C^- , CH^- , C_2^- and C_2H^- . The two flames differ in one other major aspect, in that ethylene forms mostly C_6^- , whereas acetylene exclusively forms C_6H^- . A possible explanation for this behaviour is that ethylene may preferentially form an aromatic ring structure for C_6^- , whilst acetylene retains its aliphatic character to form the polyacetylide C_6H^- . The sp^2 hybridisation for the ethylene molecule may be retained in some way when C_2^- reacts with C_2 radicals thus forming a benzenoid structure. Acetylene, which has sp hybridisation may be unable to lose enough of this character to preferentially form an aromatic ion, C_6^- .

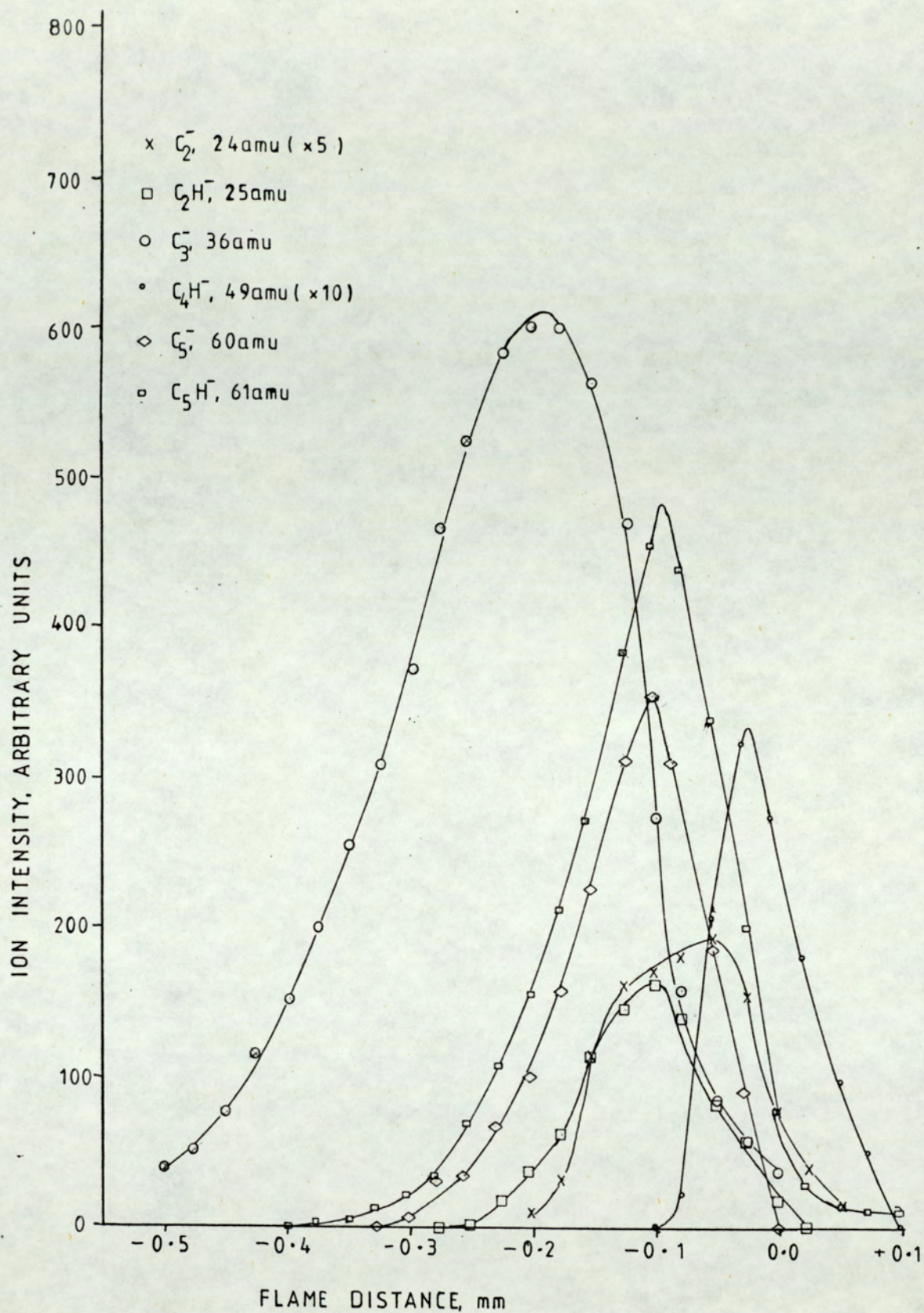


Figure 40. Ion Profiles for 24 a.m.u., 25 a.m.u., 36 a.m.u., 49 a.m.u., 60 a.m.u. and 61 a.m.u. in Flame F1.

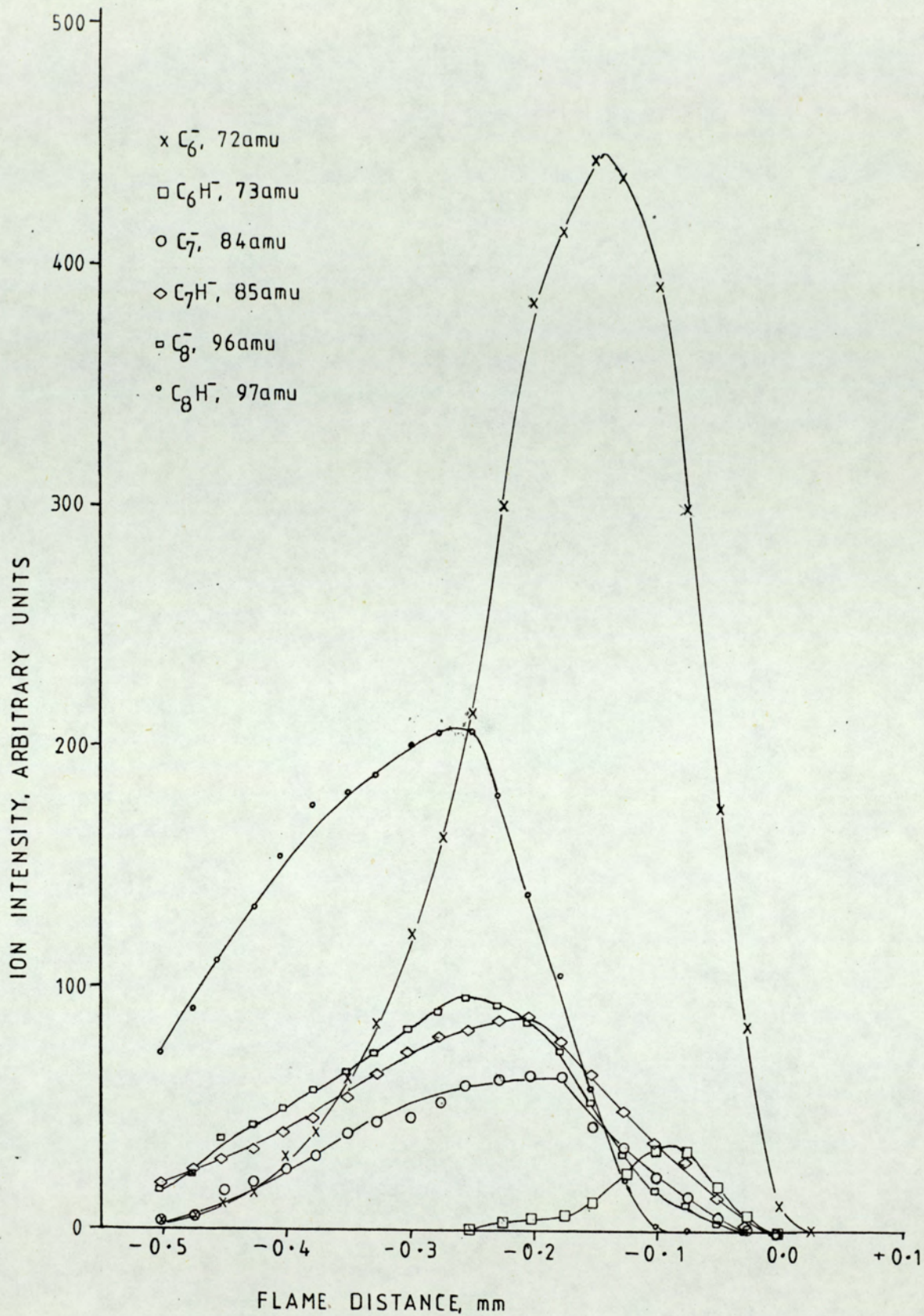


Figure 41. Ion Profiles for 72 a.m.u., 73 a.m.u., 84 a.m.u., 85 a.m.u., 96 a.m.u. and 97 a.m.u. in Flame F1

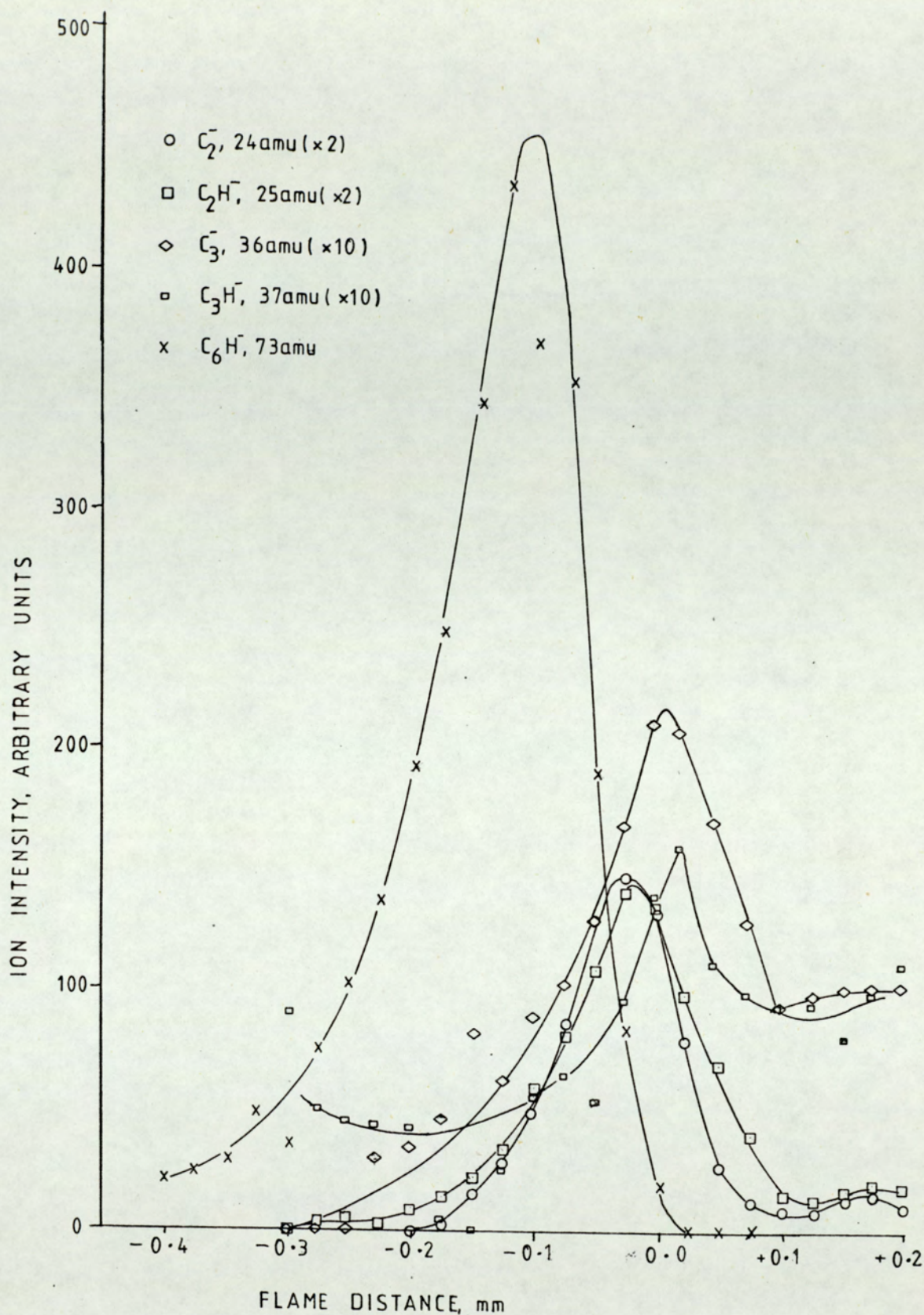


Figure 42. Ion Profiles for 24 a.m.u., 25 a.m.u., 36 a.m.u., 37 a.m.u. and 73 a.m.u. in Flame F2.

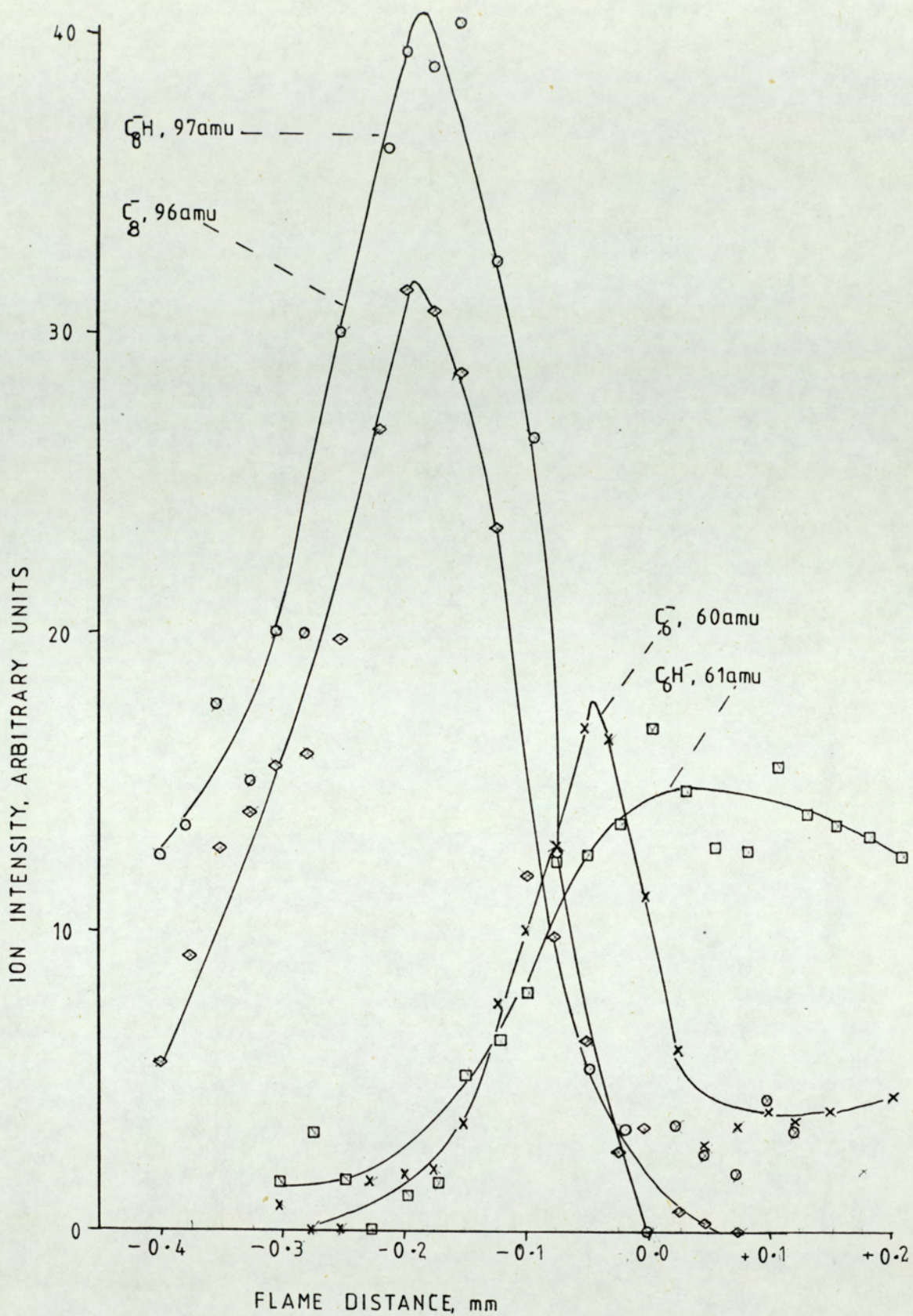
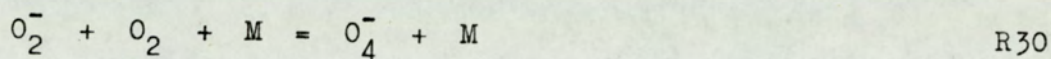


Figure 43. Ion Profiles for 60 a.m.u., 61 a.m.u., 96 a.m.u. and 97 a.m.u. in Flame F2.

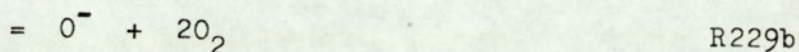
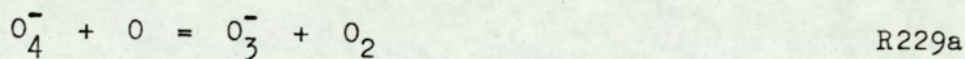
IV.9. UNASSIGNED ION PROFILES.

IV.9.1. 64 a.m.u.

This ion was observed in both flames, being fairly weak, and peaking at a position towards the hotter part of the reaction zone, Fig. 44. This ion would probably form by three-body clustering reactions such as:-



Little information is available for this ion, making it difficult to discuss thermodynamically. However a reaction for its consumption has been observed:-



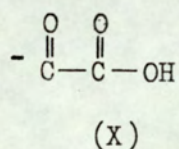
for which $k_{R229} = 4 \times 10^{-10} \text{ cm}^3 \text{ mol}^{-1} \text{ sec}^{-1}$ at 300 K, (39).

Thus it appears probable that this ion may form, it being expected that it would have some hydrates associated with it. Unfortunately none were observed.

IV.9.ii. 73 a.m.u.

A large peak at this mass was observed in the acetylene flame, a smaller one in the ethylene flame. As previously mentioned, this ion could be assigned to the polyacetylide species C_6H^- . However closer examination of this ion in the acetylene flame reveals the possibility of other identities for this ion. It is in a position upstream of the reaction zone tip, a position

occupied by oxygen containing species. The other polyacetylide species peak later in the reaction zone. Also it has a marked extension upstream, at the lower temperature end of the reaction zone. again suggesting the presence of oxygen. More proof of an oxygenated species is provided by a large, broad peak at 91 a.m.u., again with an upstream extension, Fig. 45. The peak at 91 a.m.u. therefore, is likely to be a hydrate of the ion at 73 a.m.u. Since no polyacetylides have been found to have hydrates, it must be concluded that part of the peak at 73 a.m.u. is due to an oxygenated species, the only structure which can be envisaged being that of the glyoxide ion, CHOCOO^- , (X):-



Little information is available for this ion. However, the standard heat of formation for the parent molecule, (CHOCOOH) is $\Delta H_{\text{O}}^{\text{f}} = -320 \text{kJ mol}^{-1}$. It is probable that $\Delta H_{\text{O}}^{\text{f}}$ for the radical CHOCOO is also negative, and thus presumably $\Delta H_{\text{O}}^{\text{f}}$ for the negative ion would also be negative. Thus this ion would form readily and react with ease.

A further complication to the assignment are smaller peaks at 74 a.m.u. and 75 a.m.u. The ion at 75 a.m.u. could be due to CHOHCOO^- , (XI):-

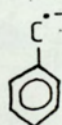


This ion would be expected to form a hydrated ion at 93 a.m.u.;

however, this ion is absent. The peak at 74 a.m.u. may be due to an isotopic satellite. This peak is positioned at the same place as that at 73 a.m.u., and is 8.5 % of the intensity. If the peak at 73 a.m.u. were due to C_6H^- , the isotope $^{13}CC_5H^-$ would be 6.6 % of the parent ion peak. Alternatively, if this ion were $CHOCOO^-$, the ^{13}C peak would be 2.2 % of the parent ion. No conclusions can be drawn as to the true identity of this ion except that it is probably a mixture of the two species, C_6H^- and $CHOCOO^-$.

IV.9.iii. 90 a.m.u. and 92 a.m.u.

Two peaks were completely unidentifiable in both flames, at 90 a.m.u. and 92 a.m.u. These two peaks have similar intensities and profiles, Fig.46. Several empirical formulae could be written for these species. All the aliphatic formulae would have to be negative molecular ions, and these either do not appear in the flame, or are rapidly changed into radical species. If it is possible for aromatic species to form, then these two ions could be considered as:-



(XII)



(XIII)

It is known (42) that benzene has a positive electron affinity (e.a. > 0), implying that a negative ion will form. It is possible that ions such as XII and XIII could be produced, the excess negative charge being accommodated by the aromatic ring.

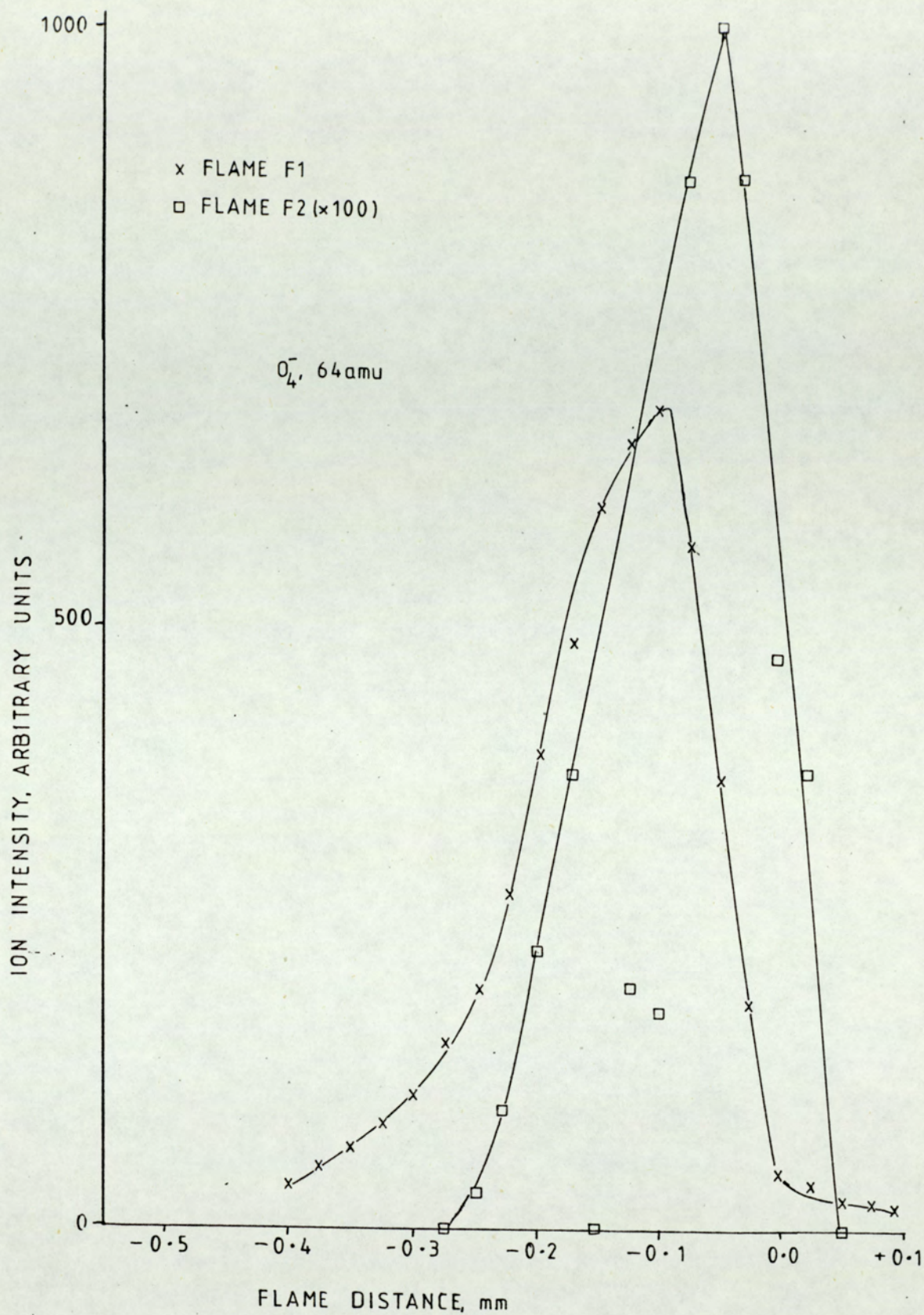


Figure 44. Ion Profiles for 64 a.m.u.

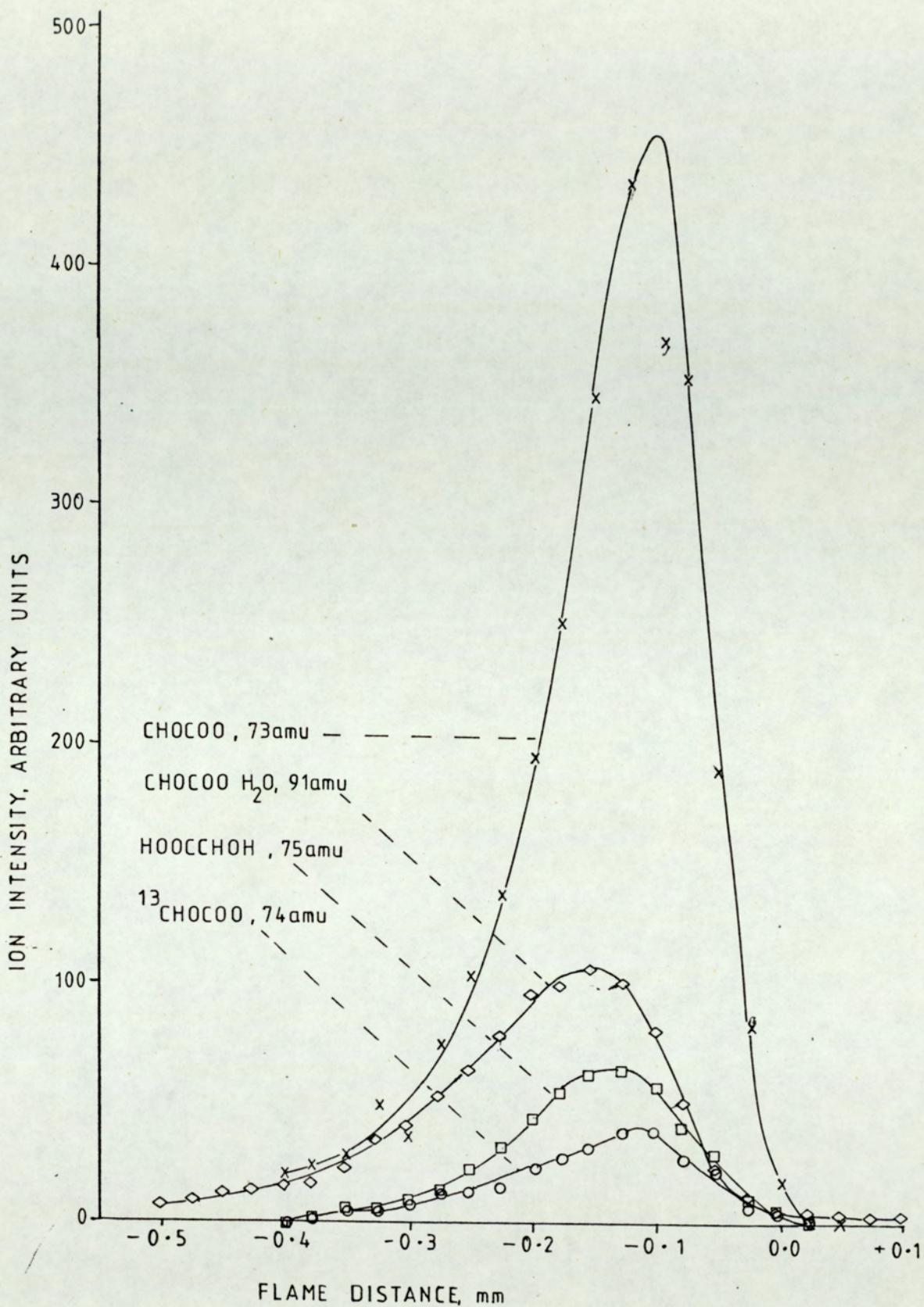


Figure 45. Ion Profiles for 73 a.m.u., 74 a.m.u., 75 a.m.u. and 91 a.m.u. in Flame F2.

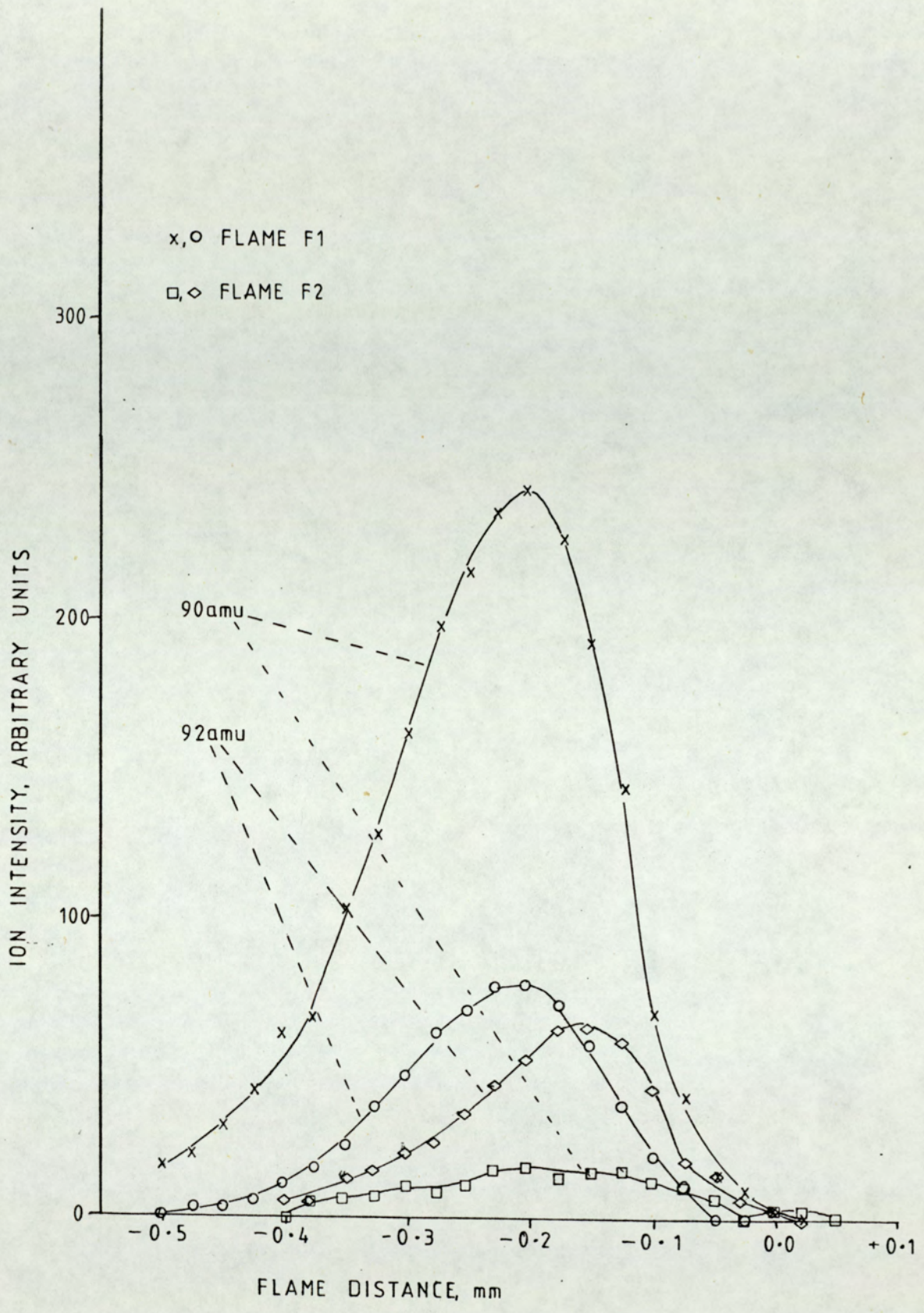


Figure 46. Ion Profiles for 90 a.m.u. and 92 a.m.u.

V. CONCLUSIONS.

1. In an oxy-hydrogen laminar flame in which small quantities of hydrocarbon fuels have been added many negative ions are formed.
2. For non-sooting flames there are two distinct regions in the reaction zone where ion formation takes place. In the position upstream of the reaction zone tip, cooler reactions take place to produce species containing either oxygen and hydrogen or oxygen, hydrogen and carbon. In the hotter region of the flame, near the reaction zone edge, ions containing carbon and hydrogen are formed, these being attributable to polyacetylides, and possibly to some unsaturated aromatic species.
3. Ethylene and acetylene containing flames are similar in that the same types of ion are formed. However for acetylene more polyacetylide ions form, due to the more facile formation of C_2^- , C_2H^- and single-carbon ions and neutrals.
4. Many oxygenated species form hydrates, some up to three water molecules. It is evident that hydrates tend to stabilise the parent ion.
5. Some of the oxygenated species are formed on the wall of the sampling nozzle where cooler reactions may take place.
6. Using a fairly simple basic quadrupole mass spectrometer and detection system, flame chemistry can be studied with relative ease.

VI. SUGGESTIONS FOR FURTHER WORK.

1. One of the main problems was assigning a particular mass to a specific ion. The resolution of the mass spectrometer was typically 100. At this low resolution it is impossible to discriminate between ions of integral number. A resolution of 1000 would be sufficient to resolve many of the ions. Unfortunately, the transmission at this resolution would be very low. A redesign of the ion optics may improve transmission sufficiently to allow a higher resolution. Alternatively, by using isotope doped fuels, and deuterium instead of hydrogen it would be possible to at least discriminate between the polyacetylides and the oxygenated species.
2. The negative ion measurements were made using a Faraday cup. A better detection system would have been to use a multiplier set up for positive ion detection, and a conversion dynode to convert the negative signal into a positive one. This would eliminate problems caused by high floating potentials and allow a phase-sensitive detector to be used.
3. The lens system in the pre-quadrupole region was fabricated from aluminium. Over a short period of time this became oxidised. Gold plating of the lens would considerably reduce this effect.
4. Only one inlet nozzle was used in these experiments. Studies of ion concentrations and ion types versus inlet nozzle diameter may be useful to sort out which ions are

true flame ions, and which are formed by the sampling process.

5. Experiments with other hydrocarbons such as methane and ethane may be useful in helping to corroborate the findings in this work. Methane would be useful since it may then be possible to find single-carbon species.
6. Some kinetic work is necessary on negative flame ions to obtain data on reaction rates and types.

REFERENCES.

1. Eltenton, G.C. J.Chem.Phys., 15, 474, (1947).
2. Calcote, H.F. Ninth Symp. (Int.) Combustion, 622, Academic Press, New York, (1963).
3. Deckers, J. and van Tiggelen, A. Combust.Flame, 1, 281, (1957).
4. Sugden, T.M. Ninth Symp. (Int.) Combustion, 607, Academic Press, New York, (1963).
5. Bohme, D.K. Interactions Between Ions and Molecules, Ed. Ausloos, Plenum Press, New York, p489, (1975).
6. Bohme, D.K., Goodings, J.M., and Ng, C. Int.J.Mass Spectrom. Ion Phys., 24, 335, (1977).
7. Sugden, T.M. Sci.Progr., Vol. LI No. 202, (1963)
8. Knewstubb, P.F. and Sugden, T.M. Nature, 196, 1312, (1962).
9. Miller, W.J. and Fontijn, A. Nature, 679, 4959, (1964).
10. Calcote, H.F. and Miller, W.J. J.Chem.Phys., 41, 4001, (1964).
11. Massey, H.W. in Negative Ions, Cambridge University Press, (1950).
12. Crittenden, B.D. and Long, R. Combust.Flame, 20, 359, (1973).
13. Homann, K.H. and Wagner, H.Gg. Eleventh Symp. (Int.) Combustion, 371, Academic Press, Pittsburg (1967).
14. Voet, A. Rubber Chem. Technol. 37, 630, (1964).
15. Homann, K.H. Angew. Chem. Int. Ed. Vol 7, 6, 421, (1968).
16. Forbes, W.F. and Robinson, J.C. Nature, 214, 80, (1967).
17. Badger, G.M., BATTERY, R.G., Kimber, R.W.L., Lewis, G.E., Moritz, A.G., and Napier, I.M. J.Chem.Soc., 2449, (1958).

18. Long, R. and Tompkins, E.E. *Nature*, 213, 1011, (1967).
19. Long, R. *Bham.Univ.Chem.Eng.* 26(2-3), 55, (1975).
20. Tesner, P.A. *Faraday Symp. Chem. Soc.*, 7, 104, (1973).
21. Paul, W. and Raether, M. *Z.Physik*, 140, 262, (1958).
22. Goodings, J.M., Jones, J.M., Parkes, D.A. and Sugden, T.M. *Proc.Combust.Inst.Eur.Symp.*, 250, (1973).
23. Harvey, R. and MacColl, A. *Seventeenth Symp. (Int.) Combustion*, (1978), in press.
24. Goodings, J.M. *Private Communication*, (1979).
25. Morley, C. *Private Communication*, (1977).
26. Burdett, N.A. and Hayhurst, A.N. *Combust.Flame*, 34, 119, (1979).
27. Green, J.A. *AGARD Combustion and Propulsion Panel*, Pisa, (1965).
28. Hayhurst, A.N. and Telford, N.R. *Proc.Roy.Soc.Lond.*, A322, 483, (1971).
29. Hayhurst, A.N. and Telford, N.R. *Combust.Flame*, 28, 67, (1977).
30. Morley, C. *Vacuum*, 24(11-12), 581, (1974).
31. Stafford, G., Reeher, J., Smith, R. and Strong, M. *Dyn.Mass Spectrom.*, 5, 55, (1978).
32. Gaydon, A.G. and Wolfhard, H.G. *Flames, Their Structure, Radiation and Temperature*. 2nd. Edition, London, Chapman and Hall, (1960).
33. Fehsenfeld, F.C. *Interactions Between Ions and Molecules*, Ed. Ausloos, P., Plenum Press, New York, (1975).
34. Raymond, K., Freyberg, D. and Abu-Dari, K. *J.Am.Chem.Soc.* 101, 3688, (1979).
35. Mateesen, G. and Benedikt, G. *J.Am.Chem.Soc.* 101, 3959, (1979).

36. Knox, J.H. and Turner, J.M. J.Chem.Soc. 3491, (1965).
37. Bohme, D.K., Mackay, G.I., Schiff, H.I. and Hemsworth, R.S. J.Chem.Phys. 61, 2175, (1974).
38. Fehsenfeld, F.C., Schmeltekopf, A.L., Schiff, H.I. and Ferguson, E.E. Planet.Space Sci. 15, 373, (1967).
39. Fehsenfeld, F.C., Ferguson, E.E. and Bohme, D.K. Planet.Space Sci. 17, 1759, (1969).
40. McAllister, T., Nicholson, A.J.C. and Swingler, D.L. Int.J.Mass Spectrom.Ion Phys. 27, 43, (1978).
41. Lahaye, J. and Prado, G. Water, Air and Soil Pollution, 3, 473, (1974).
42. Christophorou, L.G. and Goans, R.E. J.Chem.Phys. 60, 4244, (1974).
43. Franklin, J.L. and Harland, P.W. Annu.Rev.Phys.Chem. 25, 485, (1974)
44. Handbook of Chemistry and Physics, The Rubber Co.
45. Maron, S.H. and Prutton, C.F. Principles of Physical Chemistry, Fourth Edition, p141, Collier-Macmillan, New York, (1972).